The Potential Effect of Los Angeles Basin Pollution on Grand Canyon Air Quality

by
Gregory S. Poulos

Department of Atmospheric Science
Colorado State University
Fort Collins, Colorado

Roger A. Pielke, P.I.

Colorado State University

Department of Atmospheric Science

Paper No. 490

THE POTENTIAL EFFECT OF LOS ANGELES BASIN POLLUTION ON GRAND CANYON AIR QUALITY

Gregory S. Poulos

Department of Atmospheric Science
Colorado State University
Fort Collins, Colorado
Spring 1992

Atmospheric Science Paper No. 490

The funding for this research was provided by the National Park Service through Interagency Agreement #0475-4-8003 with the National Oceanic and Atmospheric Administration through Agreement #CM0200 DOC-NOAA to the Cooperative Institute for Research in the Atmosphere (Project #5-31253).

ABSTRACT

THE POTENTIAL EFFECT OF LOS ANGELES BASIN POLLUTION ON GRAND CANYON AIR QUALITY

This study presents a numerical investigation of air pollutant transport from the Los Angeles Basin to Grand Canyon National Park (GCNP). The Colorado State University Regional Atmospheric Modeling System (CSU-RAMS) is used to develop fields of different atmospheric variables. These fields are applied in a Lagrangian Particle Dispersion Model (LPDM) to simulate the advection of pollutant particles. It is found that, indeed, under the somewhat idealistic, worst case, initial conditions presented, particles released from the Los Angeles Basin will impact the Grand Canyon but only in small amounts. By comparing a flat to complex terrain simulation, the importance of the terrain features between Los Angeles and GCNP to the dispersion of Los Angeles Basin pollutants is made obvious. Mountain barriers and undulating land reduce what could otherwise be a very serious pollutant impact on GCNP. Based on these results the conclusion is made that under the southwest flow conditions existing during the Winter Haze Intensive Tracer EXperiment (WHITEX) period of February 10-13, 1987 Los Angeles Basin pollution did not contribute significantly to visibility reduction in the Grand Canyon. This supports the WHITEX conclusion that the Navajo Generating Station (NGS) was the primary contributor during this period of poor haze conditions.

Gregory S. Poulos
Department of Atmospheric Science
Colorado State University
Fort Collins, Colorado 80523

Spring 1992

ACKNOWLEDGEMENTS

Sincere gratitude is extended to Professor Roger A. Pielke for his thoughtful advising from beginning to end. In discussions throughout the development of this study, colleagues and many friends were also important including, Dr. Douglas A. Wesley, Mike Meyers, Dr. Melville E. Nicholls, Xubin Zeng, Scot Randell, and Mike Moran. In particular, I would single out Dr. Michael Weissbluth for his advice and role as a confidant. Finally, no greater thanks and appreciation can be shown than that for my Father and Mother whose inspiration, guidance, expectations, and love were by far the strongest motivation for this study. Thank you Dad and Mom. I would also like to extend my thanks to Bryan Critchfield, Tara Pielke,and Dallas McDonald for the preparation and typing of this thesis.

TABLE OF CONTENTS

LIST OF FIGURES

LIST OF TABLES

Chapter 1

INTRODUCTION

It is a well known fact that industrialization in the United States has contributed to numerous environmental pollutant problems. Among the main effects of industrialization are concentration changes in carbon monoxide (CO), ozone (O_3), carbon dioxide (CO_2), sulfur dioxide (SO_2), and its cousin, sulfate (SO_4). These changes, in turn, have created public policy issues such as stratospheric ozone layer depletion, global warming, acid precipitation production, and visibility reduction. Visibility reduction is one of these issues which affects humans on a daily basis. Aesthetically pleasing views are compromised as extinction and absorption by particles and gases increase. Accordingly, the desire to reduce the amount of pollutants in the air grows as visibility continues to degrade. This desire has been expressed in legislation enacted by Congress (United States Congress, 1990).

National Parks and large Wilderness Areas are specifically protected by congressional action through this Federal legislation. Specifically, the law requires the prevention of significant deterioration (PSD) in such areas. Grand Canyon National Park is designated as one of these areas, called Class I regions. Indeed, the vistas at Grand Canyon National Park (GCNP) are among the most picturesque and aesthetically valuable in the United States National Park system. Given the slow reduction in visibility that has been occurring in the Grand Canyon region since the mid-1950's (Trijonis and Yan, 1978) and the recent dictate from Congress that visibility degradation be prevented (for instance, in Section 169A of the Clean Air Act Amendments of 1990 where the national air quality goal for national parks is stated as, "the prevention of any future, and the remedying of any existing, impairment of visibility" – United States Congress, 1990), it is only natural to consider the sources of increased pollutant load to the Grand Canyon atmosphere. By

identifying source contributions a concerted effort can be applied to reduce those sources and maintain satisfactory visibility levels.

In the late 1960's through mid-1970's the main man-made source of pollutants in GCNP was identified as copper smelters in southern Arizona (Trijonis, 1979). In the late 1970's and 1980's the focus of potential sources shifted to a recently built coal-fired power plant in northeast Arizona which became fully operational in 1976, the Navajo Generating Station, and southern California. Numerous studies have identified southern California including the Los Angeles Basin as a likely source of pollutants (Macias et al., 1981; Hering et al., 1981; Blumenthal et al., 1981; Miller et al., 1990; Ashbaugh, 1983; Yamada et al., 1989; Ashbaugh et al., 1984; Henmi and Bresch, 1985; and Malm et al., 1990). Studies have also found that the Navajo Generating Station (NGS), located 20 km from the northern boundary of the Grand Canyon near Page, Arizona, can be a large contributor to haze conditions (Malm et al., 1989; 1990). In one of these studies, as reported in the WHITEX Report (Winter Haze Intensive Tracer EXperiment: Malm et al., 1989, a tracer (CD_4, heavy methane) was released into the Navajo Generating Station emission plume eventually implicating it as a source. Conclusions could only be made with respect to the meteorological conditions existing during the WHITEX study period. Interestingly, despite their vast emission reductions since the 1960's, southern Arizona copper smelters continue to be cited for source contributions in the Grand Canyon area (Henmi and Bresch, 1985; Ashbaugh et al., 1984; and Nochumson, 1983).

Determining which of the three main identified sources: 1) the southern California/Los Angeles Basin; 2) the Navajo Generating Station; or 3) the southern Arizona copper smelter region, is responsible for Grand Canyon visibility degradation is complicated. It is most logical to expect, and current fieldwork suggests, that different meteorological conditions would cause different sources to be a favored contributor at different times. Source attribution is further complicated by smaller sources or lesser contributors in northern California, southwest Colorado, and northern Mexico. Loading of pollutants into the airstream prior to its passage over one of the three main sources can obscure a particular source's contribution. Power plants in northern Mexico are potentially significant because pollutant controls are virtually non-existent and are not required. Generally,

the contribution from these sources is considered less either due to distance from the Grand Canyon, their smaller size, topographical barriers, or climatological meteorological conditions as supported in the WHITEX report conclusions (Malm et al., 1989).

In this study my goal is to prescribe a worst case condition representative of the poor haze period February 10-13, 1987 in the Grand Canyon in which meteorological flow through the Los Angeles Basin to the Grand Canyon during the winter season would be expected. Given this intention the Colorado State University Regional Atmospheric Modeling System (CSU-RAMS, hereafter referred to as RAMS) is used to simulate thermodynamic atmospheric conditions observed during the WHITEX period with an initially west-southwesterly (251°) wind throughout the depth of the model atmosphere. These simulated atmospheric conditions are used as input to a Lagrangian Particle Dispersion Model (LPDM). The LPDM is set up with volumetric Los Angeles Basin pollutant fields. The pollutants are advected by the LPDM according to the fields input from RAMS. The WHITEX period had poor visibility periods in the Grand Canyon.

It is important to remember that the WHITEX study determined that the major contributor to WHITEX period haze was the Navajo Generating Station. This conclusion was based on concentration measurements at Grand Canyon sites of a unique tracer (CD_4) released in the NGS plume. Because of the high economic cost of pollutant control on coal-fired power plants, the WHITEX report conclusions were questioned (NAS, 1990). One reason the conclusions were questioned was because atmospheric soundings indicated strong, upper-level west-southwesterly flow (i.e. flow from the Los Angeles area toward Grand Canyon National Park) during the WHITEX period (10-13 February 1987, see Figure 1.1). Certainly, one would expect west-southwesterly flow aloft to transport air parcels from the southwest U.S. into the Grand Canyon region, but because the results of the unique tracer experiment WHITEX are so conclusive and the importance of low-level easterlies was ignored, the EPA has already decided to force the NGS to apply appropriate pollutant control technology (EPA, 1991a, b). These controls are intended to improve the visibility in the Grand Canyon such that PSD (Prevention of Significant Deterioration) requirements of the Clean Air Acts are not violated.

SOUNDING DATE: 02/10/87 TIME: 1656

ALT MSL (M)	WIND SPD M/S	WIND DIR DEGR	TEMP (C)	RH PCT	PRES (MB)
1317	1.0	80.0	8.0	77.0	870
1513	1.8	61.0	5.8	90.0	849
1666	0.9	58.0	4.7	90.0	834
1830	0.5	8.0	3.7	92.0	817
1990	0.9	37.0	2.3	91.0	801
2146	1.9	316.0	3.1	91.0	786
2299	3.6	318.0	4.1	80.0	771
2441	3.3	311.0	3.1	80.0	758
2584	3.7	266.0	2.1	83.0	744
2729	6.7	247.0	1.4	78.0	731
2872	8.7	243.0	0.9	70.0	718
3016	9.7	244.0	0.1	68.0	706
3171	11.1	245.0	-1.7	69.0	692
3323	11.4	246.0	-2.5	71.0	679
3485	12.3	246.0	-3.9	75.0	665
3647	12.5	246.0	-5.6	84.0	652

SOUNDING DATE: 02/12/87 TIME: 1657

ALT MSL (M)	WIND SPD M/S	WIND DIR DEGR	TEMP (C)	RH PCT	PRES (MB)
1317	3.0	45.0	10.5	77.0	871
1475	2.2	92.0	9.3	77.0	854
1651	1.5	155.0	8.4	76.0	836
1804	1.9	248.0	7.1	77.0	821
1967	5.4	294.0	6.5	74.0	805
2124	5.1	283.0	5.6	74.0	790
2272	6.9	278.0	4.7	74.0	775
2417	7.5	278.0	3.6	73.0	762
2557	9.9	280.0	2.4	69.0	749
2698	8.2	277.0	1.4	69.0	736
2837	11.9	278.0	0.4	65.0	723
2971	10.5	269.0	-0.7	60.0	711
3112	10.2	277.0	-1.8	62.0	698
3181	10.1	272.0	-2.6	63.0	692

SOUNDING DATE: 02/11/87 TIME: 1657

ALT MSL (M)	WIND SPD M/S	WIND DIR DEGR	TEMP (C)	RH PCT	PRES (MB)
1317	1.0	220.0	8.1	87.0	872
1469	0.2	122.0	6.7	86.0	856
1631	2.7	57.0	5.4	87.0	839
1781	2.2	111.0	4.3	92.0	824
1932	2.1	94.0	3.1	91.0	809
2089	2.3	53.0	3.1	91.0	793
2252	2.9	334.0	3.0	91.0	777
2419	0.8	350.0	2.7	91.0	762
2569	0.9	114.0	2.4	85.0	748
2733	0.4	283.0	1.3	84.0	733
2880	0.6	44.0	0.1	91.0	719
3027	0.4	220.0	-1.4	90.0	706
3179	1.6	161.0	-2.7	90.0	693
3341	3.3	184.0	-4.0	89.0	679
3497	3.3	192.0	-5.2	89.0	665
3645	4.1	205.0	-6.3	89.0	653
3785	3.6	226.0	-7.0	88.0	641
3933	3.4	210.0	-8.0	88.0	629
4092	5.6	217.0	-9.2	88.0	616
4256	5.2	230.0	-10.4	87.0	603
4333	4.6	226.0	-10.9	87.0	597

SOUNDING DATE: 02/13/87 TIME: 1704

ALT MSL (M)	WIND SPD M/S	WIND DIR DEGR	TEMP (C)	RH PCT	PRES (MB)
1317	0.0	0.0	9.3	75.0	864
1466	1.9	69.0	7.1	86.0	848
1613	1.8	58.0	6.4	89.0	833
1756	1.8	341.0	7.4	75.0	819
1915	1.4	275.0	6.6	73.0	803
2106	6.2	220.0	6.0	72.0	785
2269	6.4	209.0	4.8	78.0	769
2434	6.4	215.0	3.4	82.0	754
2602	6.3	224.0	1.9	88.0	738
2778	8.9	238.0	0.6	91.0	722
2962	10.4	243.0	-0.9	90.0	706
3132	12.1	247.0	-2.3	90.0	691
3307	15.3	254.0	-3.6	90.0	676
3394	16.1	254.0	-4.2	89.0	669

Figure 1.1: Soundings for Page, Arizona during the poor haze period of February 10-13, 1987 at $\sim$ 1700Z each day. Note that flow aloft is from the southwest on average.

My intention is to help determine the significance of Los Angeles Basin pollution to haze problems in the Grand Canyon for a specific case. The domain for my study is depicted in Figures 1.2 and 1.3. Figure 1.2 depicts the study region from Los Angeles to

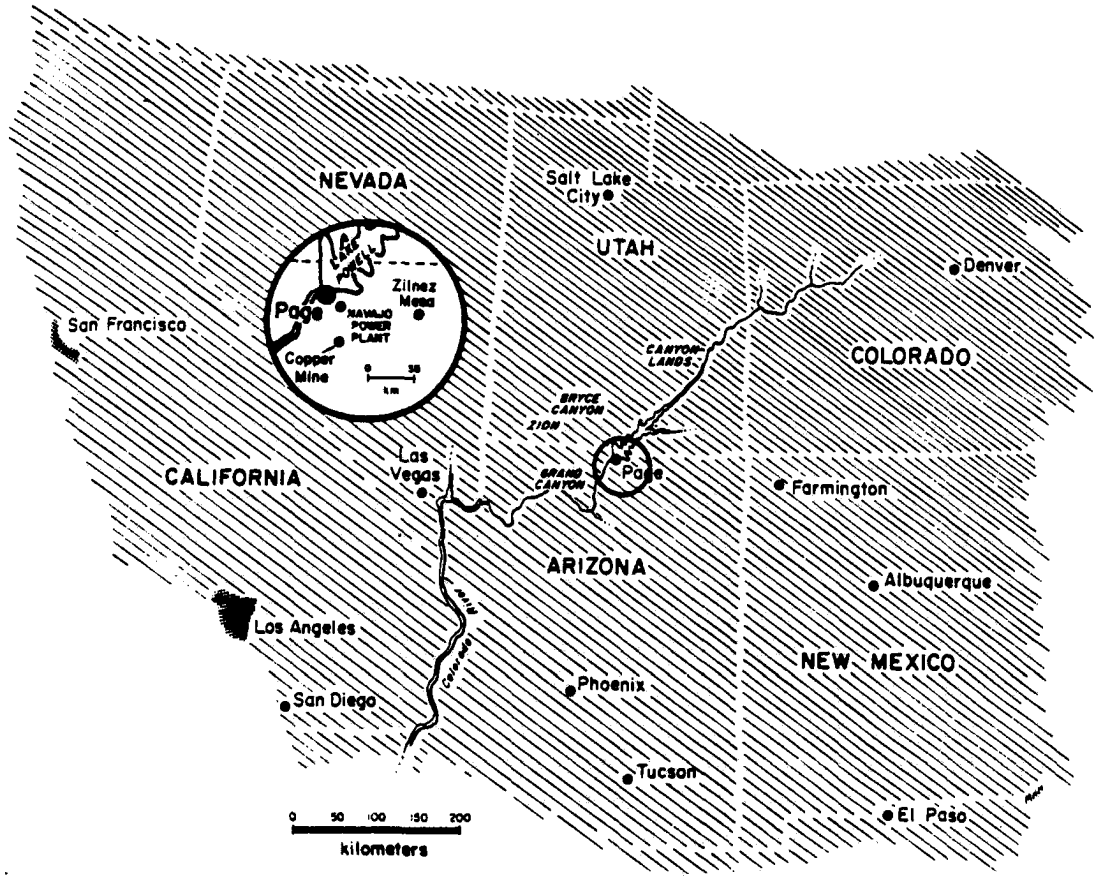

Figure 1.2: Study region for Los Angeles pollutant flow to the Grand Canyon. X's indicate large potential pollutant contributors to Grand Canyon visibility problems. X_1 – the Los Angeles Basin, X_2 – the Navajo Generating Station, and X_3 – the copper smelter region of southern Arizona (an average location for many sites). Adapted from Blumenthal et. al., 1981.

the Grand Canyon and surrounding areas. The three major pollutant source regions are encompassed within the study area: 1) the Los Angeles/southern California Basin; 2) the southern Arizona Copper smelters; and 3) the Navajo Generating Station. These regions are marked in a general sense by X's. Figure 1.3 depicts the RAMS model representation of the study region with topography (in 200 m contours) interpolated from a 10-minute gridded topography data set. Other details of modeling will be given in upcoming chapters.

For comparison, a total of three modeling runs are completed. The first encompasses the study region as depicted in Figure 1.3 and uses flat terrain. RAMS simulates 54 hours

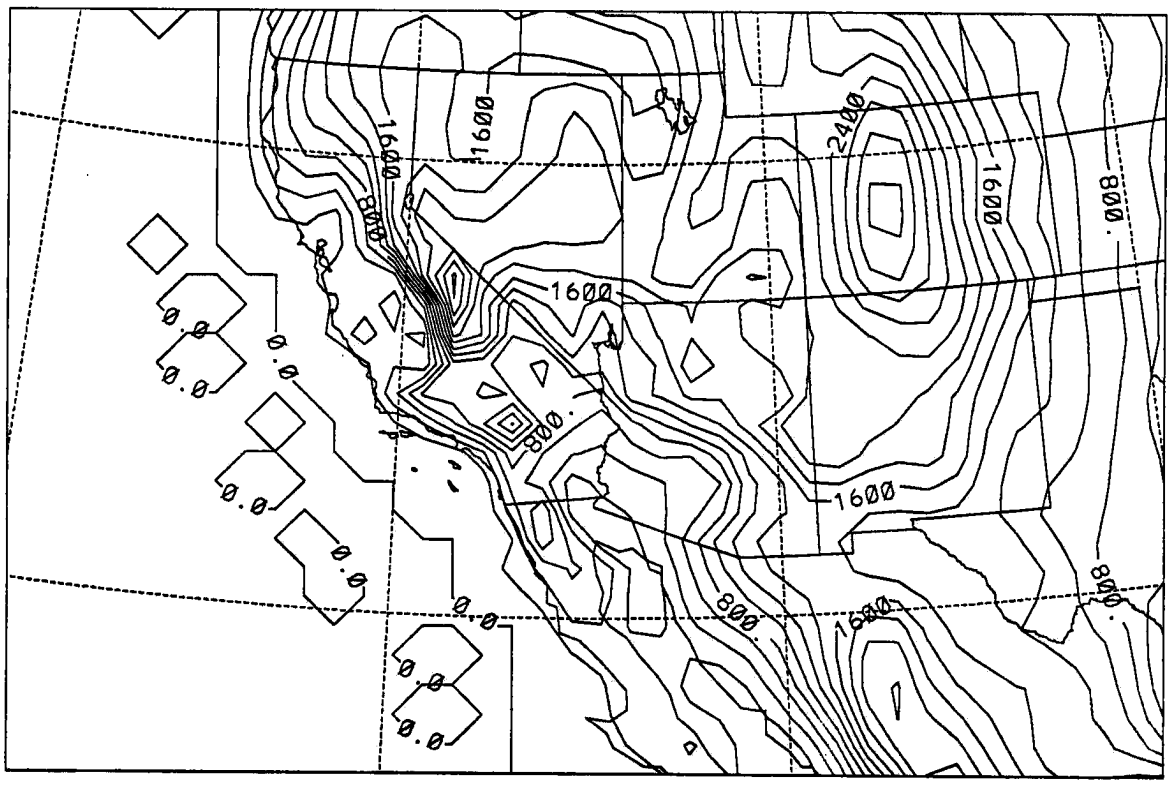

Figure 1.3: A contoured (200 m intervals) view of topography of the study region as used in RAMS simulations. The contouring is based on terrain heights at 72 km spaced grid points over the domain and is smoothed considerably.

of real-time atmospheric conditions with complex terrain. The second run has realistic terrain being otherwise the same as the first run. From the second model run insight will be gained into the importance of the actual terrain which exists between Los Angeles and the Grand Canyon to dispersion. RAMS model run three will also be very similar to run one, except that a finer grid nest is added around the Los Angeles Basin to better resolve mesoscale atmospheric flows and their importance to pollutant transport out of the Los Angeles Basin. A comparison between model runs two and three will be useful in determining the sensitivity of pollutant concentrations to better resolved mesoscale flows.

Chapter 2

BACKGROUND

2.1 The WHITEX Report

The Winter Haze Intensive Tracer EXperiment (WHITEX) was commissioned by SCENES participants to "address persistent questions about the nature and sources of winter haze conditions." By using various models, the extent to which Navajo Generating Station emissions could be linked to visibility impairment at the Grand Canyon, Canyonlands National Park, and Glen Canyon National Recreation Area was to be accessed. The four receptor modeling methods of attribution (described in Malm et al., 1990) are Tracer Mass Balance Regression, Chemical Mass Balance, Differential Mass Balance, and Deterministic Model Calculations.

The data for these different methods was gathered at various Four Corners area locations, including the Grand Canyon, during haze conditions in February, 1987. A unique tracer, heavy methane (CD_4), was released from within the NGS smokestack to attribute the power plant to a specific portion of Grand Canyon contaminants. CD_4 was released during an extremely poor air quality event, February 10-13, 1987. Using the above-mentioned techniques the Navajo Generating Station was strongly implicated as the major contributor during this episode. Four major reasons were cited by Malm et al. (1990) that cause the NGS to be a likely contributor, 1) the magnitude of emissions, 2) its proximity to the Grand Canyon, 3) the NGS and Grand Canyon lie in the same air basin and, 4) downslope drainage flows in this basin, if deep enough, would transfer NGS emissions directly into the Canyon. Specific estimates of NGS contribution to haze conditions at Hopi Point were generated by the various methods, ranging from 50% to 75%.

In response to the WHITEX conclusions, the Salt River Project (SRP), part owner of NGS, commissioned studies of the methodology used in the WHITEX report. These studies questioned a number of WHITEX assumptions, including the assumption that low-level drainage flows were responsible for bringing NGS tracer/emissions into the Grand Canyon. They cited the existence of southwesterly flow aloft as a potential transport mechanism for Los Angeles Basin pollutants. Once transported to the Grand Canyon region, pollutants of southwest origin could be mixed into the Grand Canyon atmosphere in high amounts, they hypothesized.

The natural response to these allegations is that low-level drainage winds cannot be ignored since anthropogenic sources, such as the NGS plume, are released in low-levels. Also, while Los Angeles has been implicated as a source to Grand Canyon haze in numerous summer studies, as will be shown in upcoming sections, very few winter studies exist with similar conclusions. So the question of wintertime Los Angeles Basin contribution to Grand Canyon haze conditions, particularly during the February 10-13, 1987 period, needs to be answered. This study endeavors to determine the extent of Los Angeles Basin pollution contribution to the Grand Canyon haze February 10-13, 1987 period.

This is done by the initialization of atmospheric conditions in the RAMS model with southwesterly flow toward the Grand Canyon. This condition, in the presence of flat terrain and no diurnal variations in the boundary layer structure, would be expected to result in the maximum impact of Los Angeles on GCNP. The actual conditions that existed during the February 10-13 period, however, had diurnal variations, mesoscale circulations, and synoptic flow spatial gradients which would enhance the dispersion of pollutants from Los Angeles prior to their arrival at the Canyon area. This study investigates the influence of the first two of these effects for February 10-13, 1987 WHITEX period.

2.2 Long-range Transport

Perhaps the most complete manner in which to describe previous work regarding the transport of pollutants from the Los Angeles Basin to Grand Canyon National Park is to

establish the concept of long-range transport. The straight line distance from Los Angeles to some of the most well-known views in the Grand Canyon in 600 km. Is there evidence that pollutants can be transported this far and still maintain significant concentrations? How strongly do meteorological conditions influence concentrations arriving at a distant location? The concept of pollutants traveling large distances in not a new one. In fact, the diffusivity of far-reaching plumes was noted by Richardson in 1922. Richardson (1922) states, "The smoke trails from cities have been observed by aviators to be hundreds of miles long. If aviators would also take note of the horizontal breadth of the trail at various distances from the source, and of the speed of the mean wind, it might be possible to extract a measure of the horizontal diffusivity." Despite these modestly early beginnings, the significance of the contributions of long-range sources has only been technically feasible to estimate in recent years. Given that pollutant transport occurs on all scales, global to micro-, how is long-range transport defined?

2.2.1 Definition

Answering this question requires posing another. What is long? In the literature, long-range transport is generally considered from meso-α to synoptic-scale, roughly 300 to 10,000 km. Under 300 km is medium-range and above 10,000 km is hemispheric or global transport. These boundaries are far from concrete however. Sisterson and Shannon (1979) investigate regional-scale transport from 100 km to several hundred kilometers. Meso- or medium-scale transport has been cited as the distance a plume travels in one day; distances beyond that, up to many thousands of kilometers, are considered long-range (Lyons et al., 1977). Long-range transport has also been defined to occur meteorologically when synoptic-scale winds dominate local circulations (Pielke et al., 1985). With a variety of definitions for long-range transport, consensus appears to exist between 300 and many thousands of kilometers. For the purposes of this study this definition is sufficient.

2.2.2 Global

The long-range transport of air pollutants is an environmental problem with global scope. Contamination from distant sources have been found in the Arctic from Western

Europe and Russia (Barrie et al., 1989; Trivett et al., 1988), in Europe from the Sahara Desert (D'Almeida, 1985), in Gibraltar from the Mt. St. Helens volcano eruption (Crabtree and Kitchen, 1984), in Europe from North America (Whelpdale et al., 1988), in Sweden from the U.S.S.R.'s Chernobyl nuclear power plant (Rodriguez, 1988; Persson et al., 1987), and along the Pacific Rim from coastal cities (Kotamarthi and Carmichael, 1990), among many other examples.

2.2.3 United States

In the U.S. long-range transport of air pollutants is also a problem. The Ohio River Valley is cited as a large contributor of sulfur to acid rain in Canada and the New England states (Mohnen, 1988). The long-range transport of SO_4^{2-} can have severe effects on alpine vegetation (Lovett and Kinsman, 1990). The U.S. Environmental Protection Agency (EPA) has investigated these problems in the National Acid Precipitation Assessment Program (NAPAP, 1985; Sisterson et al., 1990). The transport of herbicides from aerial application to wheat fields tens of miles away has been found in south-central grape growing regions of Washington state (Reisinger and Robinson, 1976). Plumes of pollutants from the central mid-west have been observed in the Great Plains, and, in a unique case meteorologically where a strong cyclone over the midwestern U.S. circulated pollutants westward, at the Pacific Coast of the U.S. (Bresch and Reiter, 1987; and Hall et al., 1973).

2.2.4 Southwest United States

Most important to this study is evidence of long-range transport of pollutants from southern California to northern Arizona. As discussed earlier, visibility reduction over time in the Grand Canyon has led to numerous studies in the California–Arizona corridor. As will be shown in the upcoming discussion these studies' conclusions, in most cases, have generally found southern California or the Los Angeles Basin to be responsible for some of the decrease in visibility at the Grand Canyon. These studies were neither long term, nor did they cover a wide range of meteorological conditions and seasons. For this reason, the only valid conclusion must be case study oriented. As detailed in the following

several paragraphs, with respect to the reduced visibility, the source responsible for the degradation differs with varying synoptic and mesoscale flows.

This conclusion is readily supported by a number of studies worldwide (Scholdager et al., 1978) and in the United States. Henmi and Bresch (1985) found, by trajectory and statistical analysis, that southerly flow encourages the transport of copper smelter sulfur compounds to the Grand Canyon. This was supported by backward trajectories of the ARL-ATAD model. This conclusion is reinforced by sulfate level changes during the 1980 copper smelter strike. During this period, the summer of 1980, sulfate levels at sites 100 to 600 km from the smelter region dropped to half their typical levels (Eldred et al., 1983). Summer average resultant vector winds were southerly. Some measure of the seasonal variation of the copper smelter contribution to visibility degradation in the Grand Canyon is reported by Nochumson and Williams (1984). It was found that with production curtailment on the smelters during adverse meteorological conditions for dispersion the percent extra extinction is 71.1% in Autumn compared with 14.2% in the Spring at the Grand Canyon. Perhaps climatological differences in wind direction by season play a crucial role in the seasonally varying contribution.

Evidence that the copper smelter influence may be directly linked to flow conditions is found in Blumenthal et al. (1981) based on data taken during the summer of 1979. Their research was associated with the EPA project Visibility Impairment due to Sulfur Transport and Transformation in the Atmosphere (VISTTA) and is quite thorough. They state, "During the study, no strong evidence was seen of the copper smelters in southern Arizona. The sampling periods occurred, however, during times when prevailing flow was more westerly than southerly.... The greatest causes of visibility impairment ...were...due... to: (1) Long-range transport from the southern California area, 800 km away, (2) Wildfires."

Project VISTTA is just one of several large-scale pollutant/visibility studies completed in the southwest. Several of these studies confirm southern California as a major contributor to reducing visual range in the Four Corners region. Using the CAPITA Monte Carlo model, which transports emissions in quantized units, advected horizontally within

one well-mixed layer, Macias et al. (1981) concluded that a significant impact on southwestern visibility came from southern California. Pollutant guiding winds were supplied by surface wind observations (multiplied by a factor of 2.5 and veered by 20°). With these somewhat unrealistic model constraints, however, the importance of the Navajo Generation Station (NGS) as a source was downplayed.

The use of enrichment factors of background air elemental compositions can also be used to identify sources. Hering et al. (1981) analyze VISTTA species data to determine that during poor visibility the southwest's air is enriched by compounds most likely generated in the Los Angeles Basin. Their conclusions are supported by independent trajectory calculations during the summer of 1979.

The Western Fine Particle Network (WFPN) supplied particle data from August 1979 through September 1981 in the southwest. Ashbaugh (1983) organized a number of trajectories based on this data using a mixed layer trajectory model. He concluded that high sulfur loading episodes in the Grand Canyon are associated with *slow* transport from southern California. Interestingly, *strong* southwesterly flow from southern California was associated with low sulfur concentrations.

Another large southwestern U.S.-oriented study was SCENES (Sub-regional Cooperative Electric Utility, Department of Defense, National Park Service, and Environmental Protection Agency Study on Visibility). Yamada et al. (1989) used early October wind measurements of SCENES to 'nudge' model winds toward actual winds by a 4DDA (Four-dimensional data assimilation) technique. Under stagnant high-pressure conditions, pollutants released from downtown Los Angeles into the 'nudged' wind field did not reach the Grand Canyon in 48 hours (although the plume was approaching). Under the influence of a weak cold front and geostrophic flow from the west, pollutants were able to reach the Grand Canyon in less than 24 hours. Yamada et al. (1989) were able to show the importance of resolving mesoscale flows versus the inadequacy of simply resolving synoptic flows. The authors suggest that, for further resolution, a nested-grid model be used to study this problem. RAMS is such a model.

Many remote areas in the western U.S. are located in the area surrounding the Four Corners region. The Four Corners is the point of state border intersection of Utah, Colorado, New Mexico, and Arizona. Malm et al. (1990) found that major sources contributing to fine sulfur throughout the year were southern California, northeastern Mexico, and coal-fired power plants, such as the Navajo Generating Station. They used two methods in their determination: 1) area of influence analysis (using persistence of endpoints of back trajectories); and 2) principal component analysis (examining spatial eigenvector gradients of fine sulfur concentration). That sources well outside the Four Corners area contribute significantly to degrade local air quality throughout the year is supported by Nochumson (1983) in his discussion of the Four Corners study. Without quantifying his statement, Nochumson concludes, "Extra-regional aerosols were estimated to contribute substantially to the aerosol concentration and light scattering in the study region." ('study region' refers to the Four Corners study region). Both urban centers and southern Arizona copper smelters were considered extra-regional.

Long-range transport of air pollutants is important with respect to air quality around the globe. Depending on meteorology, often simply from which direction the wind blows, the major contributor(s) to a location's air quality may change. Our review above shows the Grand Canyon to be a prime example of such a case. In this section the WHITEX study is that the Navajo Generating Station (NGS) is within 300 km of most major vistas in Grand Canyon National Park (GCNP) making it a medium- or short-range source, thus not appropriate for discussion here.

2.2.5 Meteorological Effects

Having reviewed the extent to which long-range transport occurs around the U.S. and the world and some of the different modeling approaches, it is logical to wonder how atmospheric flows affect this transport. One might expect that the large-scale synoptic flow fields existing in the same vertical layer as a particular pollutant would influence its long-range transport entirely; however, as is discussed below, mesoscale motions are significant and can dominate pollutant movement.

Synoptic Effects

Horizontal wind fields created by synoptic-scale pressure gradients are perhaps the most important factor determining the direction of pollutant flow. Synoptic vertical motions are generally week but are very important in determining at what level pollutants will travel. Indeed, some measure of this velocity is necessary in every existing long-range transport model. Among others described in the modeling subsection, Pudykiewicz et al. (1985) report the use of wind velocity output by a meteorological forecast model as input into a large-scale, long-range transport model. Their system is developed with a horizontal resolution of 100 km; a resolution too coarse to resolve large vertical motions.

Horizontal, large-scale winds are generated by synoptic conditions existing in the region of interest. Typically, the horizontal wind field can be determined by use of isobaric analysis and the gradient wind approximation based on synoptic weather maps. In some cases, such as described in Artz et al. (1985), pollutant trajectories can be calculated along isentropic (lines of constant potential temperature) surfaces on the synoptic scale. This methodology contains synoptic vertical motions inherently, allowing more accurate pollutant trajectories to be calculated in the vicinity of synoptic fronts where such motions are frequent. Poor air quality episodes are linked both to low and high pressure systems. Thermal lows, low pressure cyclonic circulations associated with very warm temperatures that reside in the lower layers of the troposphere (depending on their strength), have been cited as an integral synoptic contributor to air pollution periods in Japan, on the Iberia Peninsula, and in the southwestern U.S. (Kurita et al., 1985; Kurita et al., 1990; Kurita and Ueda, 1986; and Millán et al., 1991). Three main factors contribute to the thermal low's association with poor air quality: (i) above this shallow form of low pressure often resides a subsident high pressure which confines pollutants vertical transport; (ii) the conditions in which thermal lows develop are typically warm and with intense solar radiation, a scenario conducive to photochemical oxidant production; and (iii) because thermal lows are often persistent features unfavorable flows associated with them can continue for long periods.

Other synoptic features are noted for their significance to long-range transport. Poor air quality is often associated with high pressure stagnation (van Dop et al., 1987; Hall et al., 1973; and Malm et al., 1989). Bresch and Reiter (1987) examine the flow fields around an intense cyclone in the midwestern U.S. associated with unusually high sulfur concentrations at the Pacific Coast. Yamada et al. (1989) relate specific synoptics of a cold front in the southwestern U.S. to significant transport from southern California to northern Arizona. Pack et al. (1978) note that large transport computational errors can occur if warm and cold air advection processes are ignored. An appropriate model of long-range transport should then be able to resolve important synoptic frontal features such as advection.

The general nature of dispersion based on a location relative to a synoptic cold/warm frontal system typical of the mid-latitudes was developed by Pielke et al. (1984). Based on the synoptic classification scheme of Lindsey (1980), Pielke et al. (1984) characterized different synoptic types. Table 2.1 summarizes the air quality aspects by synoptic type.

Note that the WHITEX period was dominated by Category 4 conditions, including the February 10-13, 1987 period. As shown in the Table, transport would be expected to be local in nature, ventilation would be poor and, among other mesoscale flows, mountain-valley (i.e. drainage) flows would dominate. An example of mesoscale flows being significant under this condition is made evident in Yu and Pielke (1986). They found the trapping and recirculative flows in the Lake Powell Basin in polar high (Category 4) conditions are such that local sources are quite likely to create poor air quality.

That synoptic-scale flows can influence or be influenced by mesoscale flows depending on their relative strength as was pointed out in a modeling study by Ulrickson and Mass (1990). To what extent do mesoscale flows effect long-range pollutant transport?

Mesoscale Effects

While a pollutant plume is transported in a general sense by the synoptic wind, a number of smaller scale meteorological interactions may be encountered along any transport route. Examples of such interactions on the mesoscale are:

Table 2.1: Overview of air quality related aspects of five synoptic categories as applicable to the northern hemisphere (Pielke et al., 1984).

Category characteristics	Category 1	2	3	4	5
Category class	mT; in the warm sector of an extratropical cyclone	mT/cP, mT/cA, mP/cA; ahead of the warm front in the region of cyclonic curvature at the surface	cP, cA; behind the cold front in the region of cyclonic curvature to the surface isobars	cP, cA; under a polar high in a region of anticyclonic curvature to the surface	mT; in the vicinity and west of a subtropical ridge
Surface winds	Brisk SW surface winds	Light to moderate SE to ENE surface winds	Strong NE to W surface winds	Light and variable winds	Light SE to SW winds
Vertical motion	Weakening synoptic descent as the cold front approaches	Synoptic ascent due to warm advection and positive vorticity advection aloft	Synoptic ascent due to positive vorticity advection aloft (in this region this ascent more than compensates for the descent due to cold advection)	Synoptic descent (due to warm advection and/or negative vorticity advection aloft)	Synoptic subsidence (descending branch of the Hadley cell). Becomes strong as you approach the ridge axis
Inversion	Weak synoptic subsidence inversion caps planetary boundary layer	Boundary layer capped by frontal inversion	Deep planetary boundary layer	Synoptic subsidence inversion and/or warm advection aloft create an inversion which caps the planetary boundary layer	Synoptic subsidence inversion
Dominant mesoscale systems	Squall lines	Embedded lines of convection	Forced airflow over rough terrain systems; lake effect storms	Mountain–valley flows; land–sea breezes; urban circulations (thermally-forced systems)	Mountain–valley flows; land–sea breezes; urban circulations (thermally-forced systems)
Ventilation	Moderate to good ventilation	Poor ventilation of low level (i.e. below frontal inversion) emissions	Excellent ventilation	Night or snow-covered ground: poor ventilation; day: poor to moderate ventilation	Day: moderate to good ventilation; night: moderate to poor ventilation
Deposition	Dry deposition except wet deposition in showers	Dominated by wet deposition	Dry deposition except in showers	Dry deposition	Dry deposition except wet deposition in showers and thunderstorms
Transport	Long range	Long range above inversion	Long range	More local as you approach the center of the polar high	More local as you approach the center of the subtropical high

1. Variations in boundary layer height.

2. Land/sea or land/lake breeze.

3. Mountain-valley flows.

4. Interception by terrain features.

5. Local wind shear.

among others. When large-scale, quasi-horizontal flow encounters these smaller scale meteorological phenomena long-range transport can be significantly affected. As an example, along the pathway from the Los Angeles Basin to the Grand Canyon, a pollutant plume under the influence of west-southwesterly flow might be affected by the land/sea breeze circulation in Los Angeles, low boundary layer heights and katabatic wind flows near the Santa Anna mountains 25 km inland, terrain-forcing as the plume intercepts the mountain, strong vertical motions from mountainside solar heating, mountain waves as the plume travels over the mountains, a deep, turbulent boundary layer in the desert, rapidly changing surface vegetation as the desert turns into the forests, and further complex terrain and boundary layer interactions in the Grand Canyon region.

Obviously, a volume of pollutants affected by such phenomena will not be uniformly transported such as a strict horizontal Gaussian approximation might suggest. Blondin (1984) states, "Whatever the strategy of environmental protection may be, one must deal correctly with the atmospheric phase of pollutant cycles and so try to understand and take into account the meteorology involved...". This statement by Blondin emphasizes what researchers have been gradually finding to be true that multiple scales of meteorological phenomena are important to large-scale pollutant transport.

Many mesoscale circulations contain strong, local vertical motions. Martin et al. (1987) specifically investigated the importance of vertical motions to the pollutant transport problem. Their study suggests that the vertical wind component, albeit synoptic in their cases, should be used to determine realistic pollutant transport in the free troposphere. Their result is supported on smaller scales by a number of studies such as Smith

and Hunt (1978), Fisher (1984), van Dop et al. (1987), Blondin (1981) , Ulrickson and Mass (1990a,b), Stocker and Pielke et al. (1987), Sisterson (1979), Pielke et al. (1987), and Scholtz (1986). The vertical component of the vector wind, w, transports pollutants vertically. This obvious statement suggests that the notion of using only quasi-horizontal winds in long-range transport contains a basic flaw when not including stronger mesoscale vertical advection. In this case, vertical transport is often limited to parameterized vertical diffusion or small, synoptic scale . A particle in the no-vertical-wind environment would be incorrectly positioned in the vertical. This, in turn, would subject the particle to improper layer winds.

In many long-range transport models the planetary boundary layer (PBL, or atmospheric boundary layer, ABL) is a constant height. The height of the PBL is often called the mixing height. Ulrickson and Mass (1990a) and Fisher (1983) discuss this terminology. Through the diurnal cycle the boundary layer normally changes height with time. Typically, the mixing height is lowest overnight and grows during the daylight hours. Of course, the extent to which the boundary layer changes depends on atmospheric conditions. Often it is not accurate to model pollutant transport on large scales using the constant boundary layer height assumption. The evolution of the boundary layer and its significance to pollutant transport is discussed by van Dop and de Haan (1984), Reiff et al. (1987), and Pudykiewicz et al. (1985).

Within the planetary boundary layer numerous other mesoscale effects also exist. The fate of a particle in the atmosphere with respect to long-range transport can depend on recirculation. Land/sea breezes have been noted for their ability to capture pollution within the circulation over many days (Cass and Shair, 1980; Lyons et al., 1990c). After accumulating, these pollutants can be injected by strong upward vertical motions along strongly heated mountain sides into higher atmospheric layers. Once above the boundary layer the pollutants can participate in long-range transport. A coherent discussion of this mechanism can be found in Millán et al. (1990). The existence of land/lake breezes has also been found to effect pollutant transport (Lyons et al., 1990a,b). Circulations similar to land/sea/lake breezes have also been found over land where the landscape varies greatly

(i.e. vegetation–bare ground, irrigated–non-irrigated, snow-covered–not snow-covered). Such differences create a 'landscape variability' or physiographic breeze which can greatly effect the dispersive nature of pollutants (Pielke et al., 1991). In order to simulate long-range pollutant transport from Los Angeles to the Grand Canyon, not only is a model capable of such simulations necessary, but also knowledge of the source region.

2.3 Southern California/Los Angeles Basin Pollution

In the previous section the topic of long-range transport was reviewed because this mechanism would be responsible for the transport of Los Angeles pollution to the Grand Canyon. The investigation of this transport problem also requires an understanding of the sources and meteorological processes active in the Los Angeles Basin. Because of the publicity and severity of the pollution problems in Los Angeles numerous studies have been completed in the region. To list some of the major studies:

1. Hidy et al. (1975 – The Aerosol Characterization Experiment – ACHEX).
2. Feigley and Jeffries (1979 – The Los Angeles Reactive Pollutant Program – LARPP).
3. Wakimoto and Wurtele (1984 – Basic studies on Airflow, Smog, and the Inversion – BASIN).
4. Rogers and Bastable (1989 – The Greater Los Angeles Distant Impact Study – GLADIS).
5. Sonoma (1986 – The Southern California Air Quality Study – SCAQS).

This immense amount of studies combined with the literally hundreds of other authored studies (Sonoma, 1986) makes the Los Angeles Basin/southern California region the most studied pollution problem in the world. Given this vast data source only information particularly relevant to this study will be overviewed.

2.3.1 Pollutant Sources

Within the Los Angeles Basin numerous source types emit sulfur oxides. In Figure 2.1 Cass and and Shair (1980) pinpoint the most significant point sources. Of course, other large sources of nitrogen oxides, carbon monoxide, O_3, and less voluminous pollutants exist as well. While industrial sources may individually contribute the largest amounts,

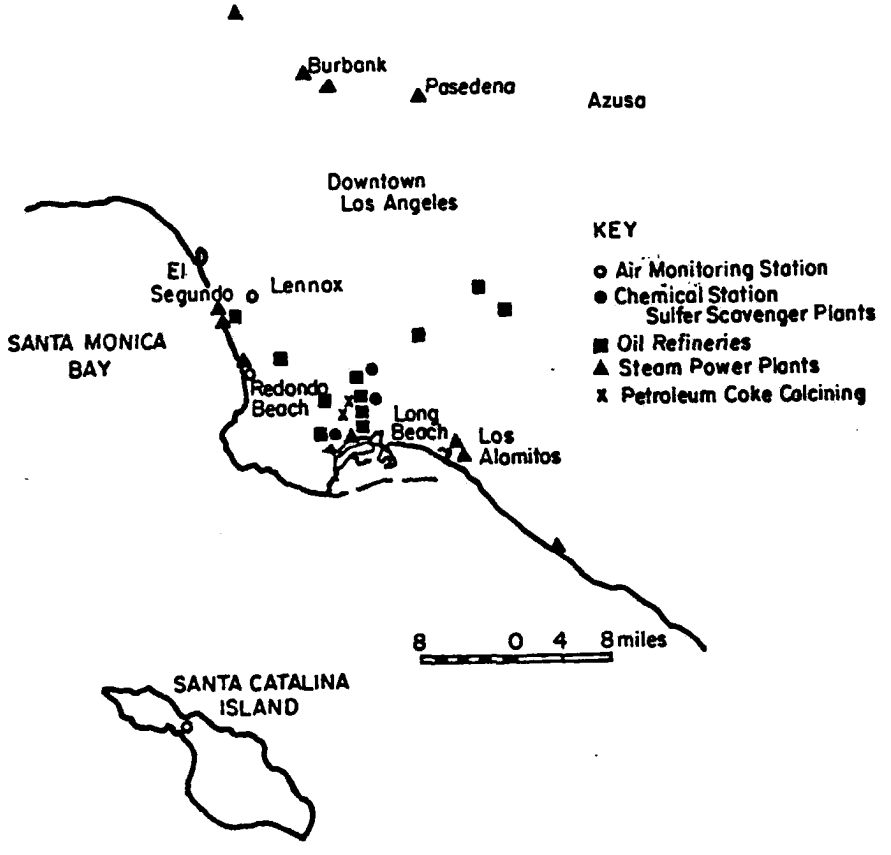

Figure 2.1: Major point sources of sulfur oxides in the Los Angeles Basin (Cass and Shair, 1980).

the sum of many small point sources, cars and other transportation, also is a large factor in pollutant totals (see Figure 2.2). Taken as a whole, these sources combine into a large volume source bounded (taken loosely) by the Pacific Coast and mountain ranges within the Los Padres, Los Angeles, and San Bernardino National Forests. This volume of pollutants is subject to the meteorological processes affecting long-range transport.

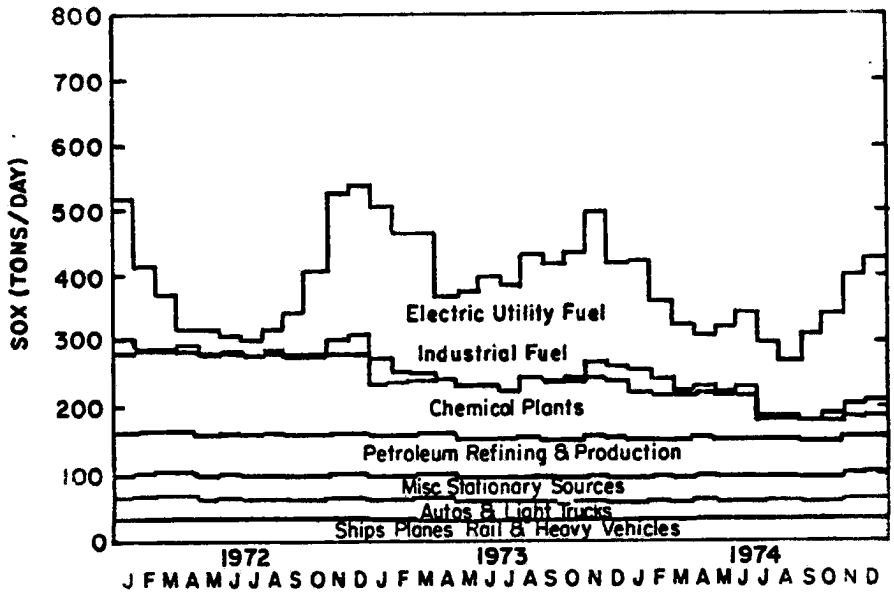

Figure 2.2: Time-wise breakdown by source type of sulfur oxide emissions in the Los Angeles Basin for 1972–1974 (Cass, 1978).

The SCAQS Program plan (Sonoma, 1986) reviews the major pollutant constituents of the Los Angeles Basin atmosphere based on a 1979 emissions inventory. Their figures are a decade out of date in magnitude but one expects the percentages they represent to be roughly accurate today. Table 2.2 presents data adapted from the Sonoma (1986) report. Although in 1979 the region represented by these figures was only 4% of California's land area, it emitted between 25% and 35% of all but primary particle pollutants. Note that on-road vehicles contribute significantly in all categories, and in a large part to reactive organic gases, carbon monoxide, and nitrogen oxides. Fuel combustion dominates sources of sulfur oxides. Also evident from Table 2.2 is the largely invariant nature of Los Angeles Basin pollutant levels from summer to winter.

2.3.2 Pollutant Flows in the Los Angeles Basin

The pollutant sources summarized in the previous section are subject to complex meteorological interactions when residing in the Los Angeles Basin and surrounding areas. Given the size of the basin such interactions are considered mesoscale. Although the RAMS model was not used to simulate all the flows that are described here, because it

Table 2.2: Emission rates in the South Coast Air Basin compared to those of California. Emission rates in tons/day based on one year of emissions. Data from ARB (1982) and Grisinger et al. (1982). TOG and ROG in equivalent weights of CH_4, NO, in equivalent weights of NO_2, SO_X in equivalent weights of SO_2, and TEP containing all particles less than ≈ 50 μm.

Emissions Source Categories	Location	Total Organic Gases (TOG)	Reactive Organic Gases (ROG)	Carbon Monoxide (CO)	Nitrogen Oxides (NO_X)	Sulfur Oxides (SO_X) (TEP)	Total Emitted Particles
Fuel Combustion	SOCAB	55.3	26.2	110.2	371.6	114.1	32.7
	California	149.8	74.5	370.0	1168.5	559.1	121.1
Waste Burning	SOCAB	0.3	0.1	1.5	0.3	3.4	0.4
	California	99.1	45.7	931.4	5.6	7.3	100.5
Solvent Use	SOCAB	371.8	340.0	0.3	0.5	0.0	2.7
	California	863.7	787.3	0.3	0.5	0.0	2.8
Petroleum Processing, Transfer & Storage	SOCAB	466.3	179.8	15.5	13.2	57.0	3.1
	California	1432.6	863.8	109.0	28.0	117.0	14.4
Industrial Processes	SOCAB	26.6	22.3	171.1	9.9	16.0	32.6
	California	122.1	86.5	506.8	28.9	124.0	188.6
Misc. Processes	SOCAB	1888.3	122.3	289.3	10.3	0.5	445.5
	California	3052.2	447.9	555.8	61.7	4.7	4855.8
On-Road Vehicles	SOCAB	806.5	753.7	5747.0	723.2	47.7	82.5
	California	1911.2	1786.5	13034.9	1824.9	110.7	201.0
Other Mobile Sources	SOCAB	74.7	71.1	431.8	109.0	25.8	7.1
	California	311.4	299.5	1632.3	2252.4	189.6	249.6
All Sources (annual)	SOCAB	3689.8	1515.6	6766.6	1238.1	254.5	606.6
	California	7942.1	4391.6	17140.3	3545.7	1001.7	5532.8
All Sources (summer weekday)	SOCAB		1697.0	6430.0	1335.0	274.2	660.0
All Sources (winter weekday)	SOCAB		1560.0	6839.0	1359.0	314.0	559.0
Uncertainty	SOCAB		±10%	±16%	±11%	±9%	±19

was applied to a specific winter period, it is prudent to be aware of the various possible effects on pollutant flow from the Los Angeles Basin.

In a general sense, the Los Angeles Basin, with its coastal location and nearby mountainous terrain, contains all the 'ingredients' for complex pollutant flows. Perhaps the most obvious is the land/sea breeze cycle generated by diurnal thermal contrasts. The sea temperature off the coast of California near Los Angeles varies much less than the land surface temperature during the year. In summer, the land temperatures are generally much higher than the sea temperatures during mid-day creating a strong sea breeze (Cass and Shair, 1980). At night the land temperature does not become much less than the ocean temperature causing a weak to non-existent land breeze (from the land to the sea) allowing katabatic flows to become significant. In winter, when daytime land temperatures are much lower, the sea breeze is correspondingly weaker, whereas land breeze effects at night ventilate more strongly (Sonoma, 1986). Ulrickson and Mass (1990a) present results showing the ability of the Colorado State University Mesoscale Model (a less advanced, precursor of RAMS) to simulate such diurnal variations. They found that while some model shortcomings existed, for the most part, it performed well. The land/sea breeze circulation has been cited for its contribution to the accumulation of sulfates over numerous days. Cass and Shair (1980) call this effect sloshing and note the inappropriateness of Gaussian calculations under such conditions.

The variation and magnitude of the stability of the Los Angeles Basin atmosphere can also drastically affect pollutant conditions. The diurnal variation of the mixing depth was discussed in the section on mesoscale effects on long-range transport. The mixing depth is intimately related to atmospheric stability. Indeed, as the typical morning stable layer erodes or is lifted by processes associated with solar isolation, the mixed layer forms beneath it. The depth to which this layer evolves, for the most part, determines the volume within which city-wide pollutants will be trapped. Further variations in mixing depth are forced by the transition from marine to land surface or somewhat flat to irregular, mountainous terrain. Rogers and Bastable (1989) note stability changes as significant to pollutant transport. They found that pollutants from the Los Angeles Basin could be

injected into elevated stable layers when transported to the California-Nevada-Arizona border. Regarding the diurnal atmospheric stability cycle Bastable et al. (1990) state (for summer conditions), "A diurnal cycle is observed with unstable air ($R_i < 0.25$) during the morning and early afternoon, followed by long stable ($R_i > 0.25$) periods at night." R_i refers to the bulk Richardson number. Bastable et al. (1990) note that the residence time for an air parcel in the Los Angeles Basin was about 6 hours during the daytime, unstable period and as much as 14 hours if overnight. By what routes and processes might a pollutant contaminated parcel exit the Los Angeles Basin?

The main barriers to outflow from the Los Angeles Basin are mountains and the capping inversion. Given the height of the surrounding mountains (often greater than 3 kilometers) it is unlikely that the boundary layer/mixing height will exceed the barrier height on any day, especially in low isolation periods (i.e. winter). Pollutants are then subject to escape from the Los Angeles Basin by effects that either force air over the mountains or channel air through lower portions of the terrain such as passes or valleys. Also, unblocked westward routes to the ocean from the Los Angeles Basin exist. These rate are significant during the development of a land-breeze, but since this investigation concentrates on eastward pollutant pathways and movement, the westward routes are only significant when pollutants that have moved westward later move eastward. This west/east circulation is possible within the land/sea breeze cycle.

Smith et al. (1984) plot the dominant convergence zones in the Southern California Air Basin. At a convergence zone near or at the surface, winds are forced together causing upward motion. This vertical motion transports air parcels upward potentially above the planetary boundary layer. Once aloft, pollutants are subject to large-scale, often stronger, winds in which they can be more easily transported from the Los Angeles Basin. Such convergence zones were modeled by Ulrickson and Mass (1990a).

A process somewhat similar to convergence zone evacuation can occur as air impinges on mountain barriers. A west wind containing polluted air is forced upward or channelled by the mountains. McElroy (1987) with airborne lidar, Bastable et al. (1990) with surface and upper air meteorological measurements, Ulrickson and Mass (1990a,b) in a modeling

study, and Grant (1981) an airborne laser absorption spectrometer all confirm that such flows are significant to transporting pollutants from the Los Angeles Basin. Figure 2.3 (McElroy, 1987) displays the relative 'flushing or removal' efficiencies of the eastern Los Angeles Basin barriers. It is obvious from the low efficiencies associated with the mountain

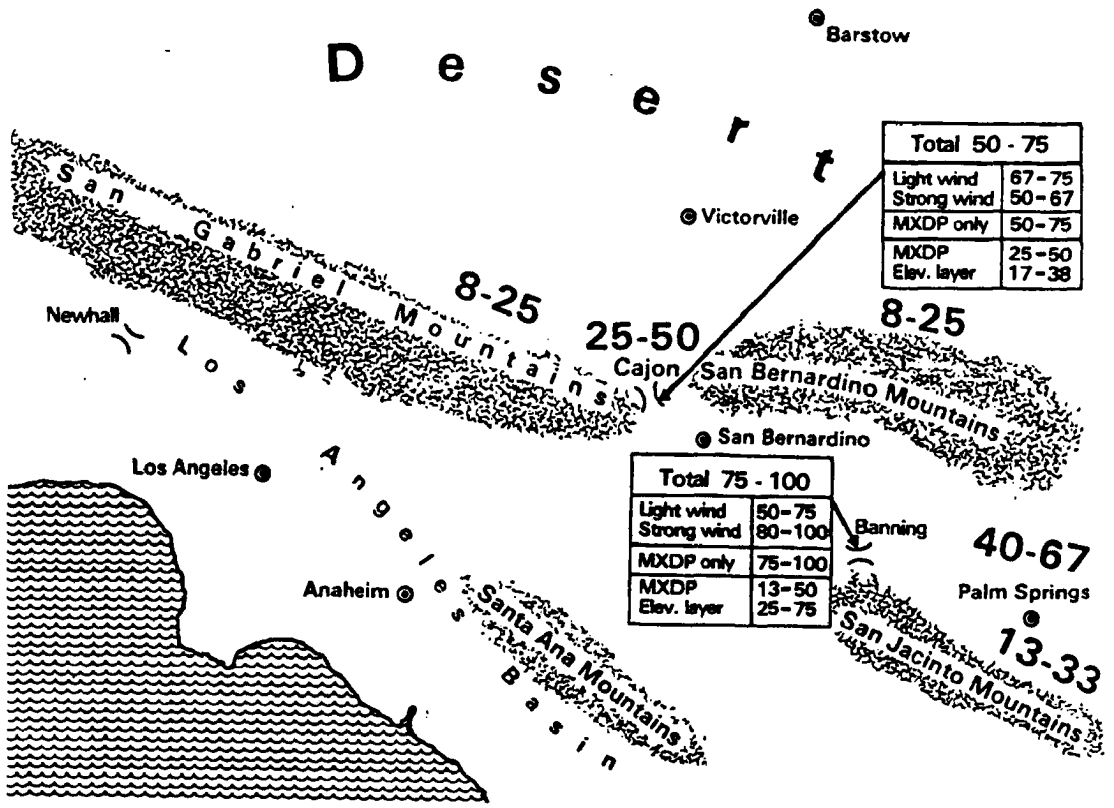

Figure 2.3: Estimates of air pollutant transport efficiency over the slopes of the San Gabriel, San Bernardino, and San Jacinto Mountains and through Cajon and Banning Passes (McElroy, 1987). Values enclosed by boxes represent passes, bold numbers represent 'efficiencies' to the lee side of the particular barrier.

areas that preferred transport routes are Cajon and Banning passes. These values were calculated based on the ratio of the integrated lidar backscatter upwind of a barrier or pass to the backscatter within or to the lee side of the barrier or pass. McElroy considers these percentages indicative of the relative amount of pollutant mass able to be transported via individual potential transport routes.

The flushing of pollutants along mountain sides can quite often be either supplemented by or completely driven by thermal flows. Because of the orientation of incoming sunlight, to the south-facing slopes of mountains receive greater insolation during the day in comparison to flat terrain. Subsequently, the mountains tend to warm more quickly than flat regions. The sensible heating of the lowest layer of air creates a warmer parcel beneath cooler air just above. The occurrence of this sensible heating process along the whole mountainside combines to generate thermally-driven upslope flow. Pollutants are transported from the lowest layers near the base of the mountain to upper levels. Such strong upslope winds can inject pollutants high enough to be transported over the mountains or at least through the passes. Smith et al. (1984) noted that such flows were among the most important flushing mechanisms from the Los Angeles Basin. Segal et al. (1985) reiterate this result in a modeling study centered on south-central California. They state, "Estimates of vertical motion associated with these features (referring to sea/land breeze and mountain-valley convergence zones) must be obtained so that the potential for venting of pollution can be evaluated." That Segal et al. (1985) could use a less-complicated precursor to RAMS to accurately, numerically model the Los Angeles region's complex flow field is encouraging.

Chapter 3

RAMS MODEL DESCRIPTION

3.1 General Description

RAMS is the model chosen for this study. Its' code has been developed to be very flexible, generating atmospheric variables from cloud to base state variable scales from hundreds of meters to thousands of kilometers. RAMS has been used for applications from turbulent eddy flows around building structures to synoptic flow fields, and from subtropical thunderstorms to mid-western U.S. tornadoes.

The most current version of RAMS was conceived by the unification of a non-hydrostatic cloud model and two hydrostatic, mesoscale models at Colorado State University (Cotton et al., 1982; Tripoli and Cotton, 1980, 1982, 1989; Pielke, 1974; Mahrer and Pielke, 1977; McNider and Pielke, 1981; McCumber and Pielke, 1981; and Tremback et al., 1985). More complete overviews of RAMS can be found in Tremback et al. (1986), Cotton et al. (1988), and Tremback and Walko (1991). Subsequent improvements to the RAMS formulation have made a breakdown of the existing RAMS versions necessary. The version used in this study, the most up-to-date RAMS available in complete form, is RAMS 2C.

A number of features make RAMS a desirable model formulation. Written in standard Fortran, RAMS can be transferred to almost any computer of sufficient size. It is composed of 19 basic modules and 15 library modules. Depending on the type of model run one desires (hydrostatic vs. non-hydrostatic, horizontally homogeneous vs. variable initialization, etc.) different sets of modules are necessary. In addition to the meteorological model that is the core of RAMS, there exist three other standard Fortran packages to assist the user. These are:

1. **Isentropic Analysis** – Developed to set-up variable initialization, this package organizes and formats meteorological surface and upper air data for assimilation into the model as it progresses in simulated time. The data is interpolated to isentropic surfaces. This package is not used in this study.

2. **Visualization and Analysis** – This package manipulates RAMS output such that it can be plotted. In this way the user is able to visualize the changes occurring in time to his/her model atmosphere. Plots can be made in X-Z, Y-Z, and X-Y cross-sections, of atmospheric variables such as u, v, and w wind, mixing ratio, cloud water, cloud ice, temperature, potential temperature, and others. Many plots from this package are included as figures in this study.

3. **Lagrangian Particle Dispersion Model (LPDM)** – The use of the LPDM with RAMS is described by McNider et al. (1988) and Pielke (1984) and is an independent extension of the Visualization and Analysis Package. In addition to meteorological fields, the LPDM allows the user to visualize the trajectories of particles in time. Based on information contained in files produced by the RAMS meteorological code, particles released as point, line, or volume sources from locations within the domain, are moved in time by model produced flows. If selected, parameterized subgrid-scale turbulent velocity components can be calculated at specified time periods for each particle as well. The LPDM is used extensively in this study to simulate pollutant flows from Los Angeles under given southwest flow conditions. Plots are available in X-Z, Y-Z, and X-Y cross-sections of particle position and meteorological field.

3.2 RAMS Formulation and Options

Whereas the above three packages either prepare data for the meteorological model or manipulate its output data, the meteorological model itself, RAMS, is considerably more complex.

3.2.1 Variables

The basic goal of RAMS is to predict the future state of the given domain's atmosphere based on initial conditions. The model's prognosis, as with most numerical models, is based on the iteration of time-dependent conservation equations. To adequately simulate atmospheric phenomena, equations describing the conservation of mass, momentum, and thermodynamic properties are necessary. In RAMS, these conservation equations are composed of four basic atmospheric variables; the ice-liquid water potential temperature (θ_{il}), the mixing ratio (r), the Exner function ($\pi = \left(\left(\frac{p}{p_o}\right)^{\frac{R}{C_p}}\right)$, and the u, v, and w wind components. The ice-liquid water potential temperature of a parcel is conserved even when phase changes of water occur within the parcel (Tripoli and Cotton, 1981). From the Exner function prognosis, density changes are diagnosed. Potential temperature (θ), temperature, pressure, cloud droplet mixing ratio, and water vapor mixing ratio are also diagnosed from the prognoses of the four basic atmospheric variables and, when the cloud model is employed, mixing ratios of rain droplets, pristine ice crystals, and graupel particles are also included (Tripoli, 1986). Because these equations are iterated within a grid structure stable, numerical, time-differencing schemes are used to evaluate the equations in time.

3.2.2 Gridding System

RAMS utilizes the standard C grid as described by Arakawa and Lamb (1981). The user may choose the grid increments desired based on the limitations of resolved features and numerical stability (or computer limits). These increments are chosen in the x, y, and z directions. To resolve further atmospheric detail one may also 'nest down' (add a finer sized grid within the coarse grid) in a specific location of interest. For example, in this study a coarse grid increment of 32 km is chosen over a domain covering much of the southwest U.S. (see Figure 1.2). In the third simulation, a fine nest is added within the coarse grid with grid increment one-fourth that of the coarse grid. Thus, the fine grid has an increment of 8 km and specifically covers the Los Angeles Basin to better resolve mesoscale atmospheric features in that region.

Grid increments in the horizontal are placed via a polar stereographic system. This eliminates the problem of the distance between longitude lines changing with latitude which was inherent in the latitude-longitude coordinates which existed in earlier versions (i.e. 2A) of RAMS. Within memory limitations, as many grid points as one desires may be chosen in the x- and y-directions. The increments do not have to be the same in x and y, and increments have varied from as small as a few meters to hundreds of kilometers. In the vertical, the terrain following σ_z system and associated coordinate transformation of Gal-Chen and Somerville (1975a,b) is used. The vertical position in this system, z^*, is related to the general vertical coordinate, z, by $z^* = H\left(\frac{z-z_s}{H-z_s}\right)$, where H is domain depth and z_s is topography height. The user can select vertical grid levels as desired such that high resolution is achievable for any layer of the atmosphere.

3.2.3 Atmospheric Moisture

Four different levels of moisture complexity can be chosen for a specific RAMS model simulation. The first level makes a simulation completely dry such that moisture effects on atmospheric variables are ignored. The second option also limits the effect of water substance by using vapor as a passive tracer. The third option condenses vapor to droplets at water saturation. The fourth choice available is complete microphysics. This needs to be chosen when cloud simulations are completed (i.e. thunderstorms, weather fronts) or when atmospheric water physics is deemed an important influence on simulated conditions. Within the microphysics module (Flatau et al., 1989) processes such as nucleation growth, collection, and precipitation are modeled for atmospheric hydrometeors such as rain, graupel, aggregates, snow, and pristine ice. Microphysical effects are not studied here, so the second level of moisture complexity (vapor passive tracer) is chosen.

3.2.4 Radiation

One has the option of using short and longwave radiation effects. Chen and Cotton (1983a,b) describe the radiation scheme used in this study. In addition to diurnal incoming and outgoing radiation effects, this scheme includes the influence of water vapor and condensate, ozone, and carbon dioxide. Because radiation effects have a very

important influence on the evolution of atmospheric structure, radiative flux divergence was represented in this study.

3.2.5 Model Boundaries

As stated earlier the vertical coordinate in RAMS is σ_z. σ_z, combined with the rigid surface condition, creates simple reflective lower boundary conditions. The model surface attempts to simulate real earth ground conditions by using the surface layer scheme of Businger et al. (1971) and the soil model of Tremback and Kessler (1985). Given soil type, land percentage, and surface layer gradients, the soil model prognoses the evolution of soil moisture and heat contributions to the atmosphere.

For non-hydrostatic, complex terrain model runs such as those in this study, the top boundary condition available for long simulations is the 'wall-on-top' option. However, the computational instability produced by a reflective upper boundary necessities the use of Rayleigh friction layers in the upper levels of the model atmosphere. For the model runs, five 950 m thick upper levels were used. Over a period 150 seconds, waves travelling within the 5 layer region were dissipated to avoid spurious interaction with lower level atmospheric conditions.

Lateral boundary conditions were chosen such that computational instability was minimized. This enabled the simulations to provide realistic meteorological fields for 25 hours of simulated time. The chosen scheme for the lateral boundaries was that described by Klemp and Wilhelmson (1978), which allows "...dominant gravity wave modes to propagate out through the lateral boundaries without significant reflection" in response to internal forcing.

3.2.6 Model Initialization

To initialize RAMS with wind, temperature, moisture, and pressure fields there are two available methods. The first, called variable initialization, is organized through the isentropic analysis package described earlier. This allows the user to begin the RAMS simulation with data assimilated from multiple upper air soundings within the domain. The second option is horizontally homogeneous initialization. As implied by the name,

the initial model fields are the same at the same vertical height throughout the domain. For example, as shown in Figure 3.1, the initial v wind at any height above sea level is the same horizontally. This seemingly unrealistic initial condition is eliminated quickly by iterating the model equations for a few minutes.

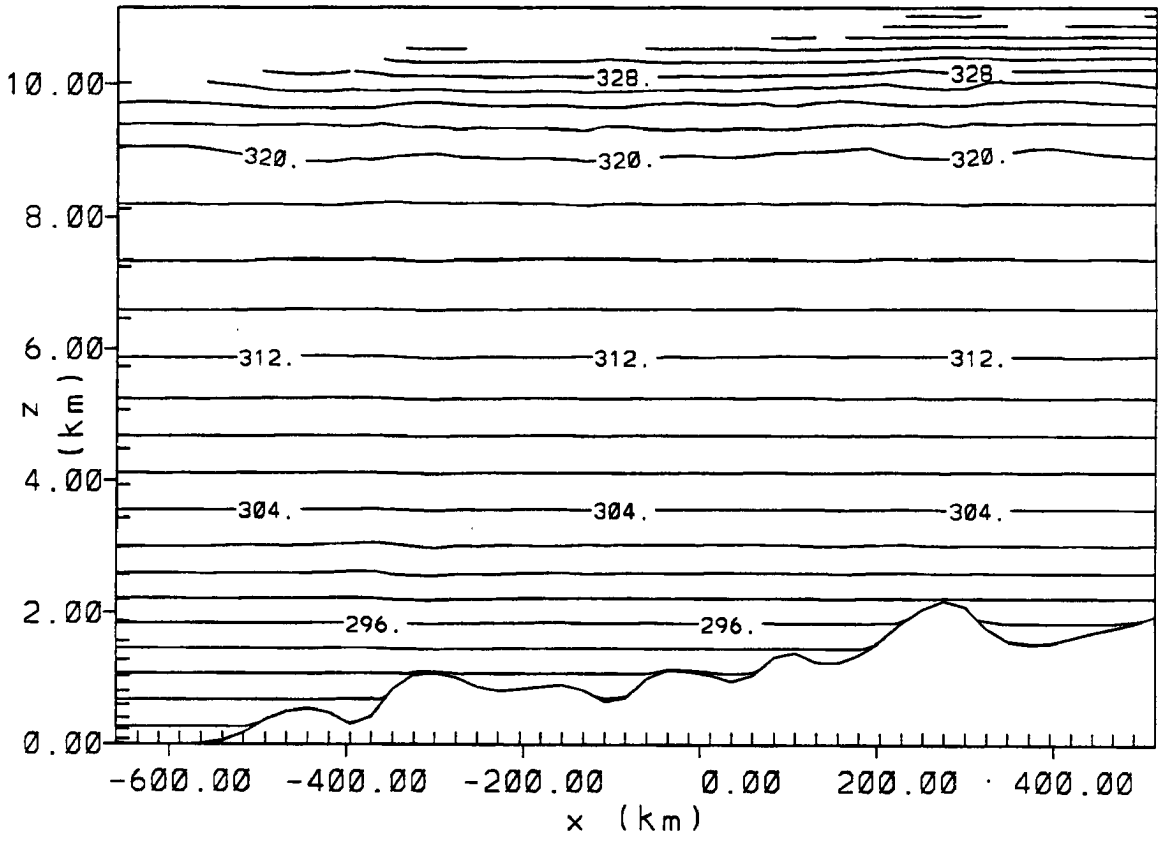

Figure 3.1: An example of horizontally homogeneous initialization as actually used in the second 3-D, complex simulation for this thesis. Contour intervals are 2 K for this plot of the potential temperature. The unusual appearance at the top of the plot is caused by the terrain-following coordinate system of RAMS.

In addition to initializing atmospheric condition, the domain surface also needs to be appropriately specified. RAMS is capable of simulating essentially any terrain feature. One may use flat terrain, an idealized shape (i.e. a Gaussian or sine wave shaped mountain), a user specific terrain height data set or heights from a specific latitude-longitude data set. The latter choice was used in these simulations. On the 32 km grid increment

domain terrain heights were read and interpolated from a file of 10-minute spacing between data points (approximately 15 km) and from a data set of 30 second spacing (approximately 750 m) for the 8 km grid increment fine nest. The 10-minute terrain-height data set interpolated to the 32 km grid increment domain is depicted in Figure 1.3.

Chapter 4

SIMULATIONS AND RESULTS

4.1 RAMS Model Simulations Overview

The three simulations used in this study were very similar except for select changes in gridding and terrain. All were three-dimensional, non-hydrostatic with a horizontal coarse grid (Grid 1) increment of 72 km, an innermost (Grid 2) of 24 km grid increment encompassing the Los Angeles–Grand Canyon Corridor, and a timestep of 150 seconds. All were begun at 1200 GMT and run for 54 hours of simulated time over the same domain size (as depicted in Figure 1.3). The first simulation, SW-1, used flat terrain for its surface although the region is actually of complex terrain. The purpose of SW-1 was to investigate the importance to pollutant transport of the terrain that actually exists in the Los Angeles to Grand Canyon pathway. To be complete in this regard a second simulation, SW-2, was completed with smoothed, real terrain included. Terrain was read from latitude-longitude height files with 10-minute resolution and interpolated to the 72 km and 24 km grid increments of Grids 1 and 2, respectively. The terrain appears in Grid 1 as shown in Figure 1.3. SW-2 allowed an investigation of the significance of topographical barriers to pollutant flow from Los Angeles in a coarse (96 km) resolution environment. The third simulation, SW-3, differed from SW-2 by the inclusion of a fine nest (Grid 3) of 8 km grid increment within the 24 km increment coarse grid (Grid 2, see Figure 4.1). Grid 3 better resolves mesoscale atmospheric features associated with the complex terrain. Because the 10-minute latitude-longitude terrain height data set contains data in approximately 15 km intervals and the smoother filters out terrain features less than 16 km ($2\Delta x$), the 10-minute data set was also used to initialize terrain on the fine grid.

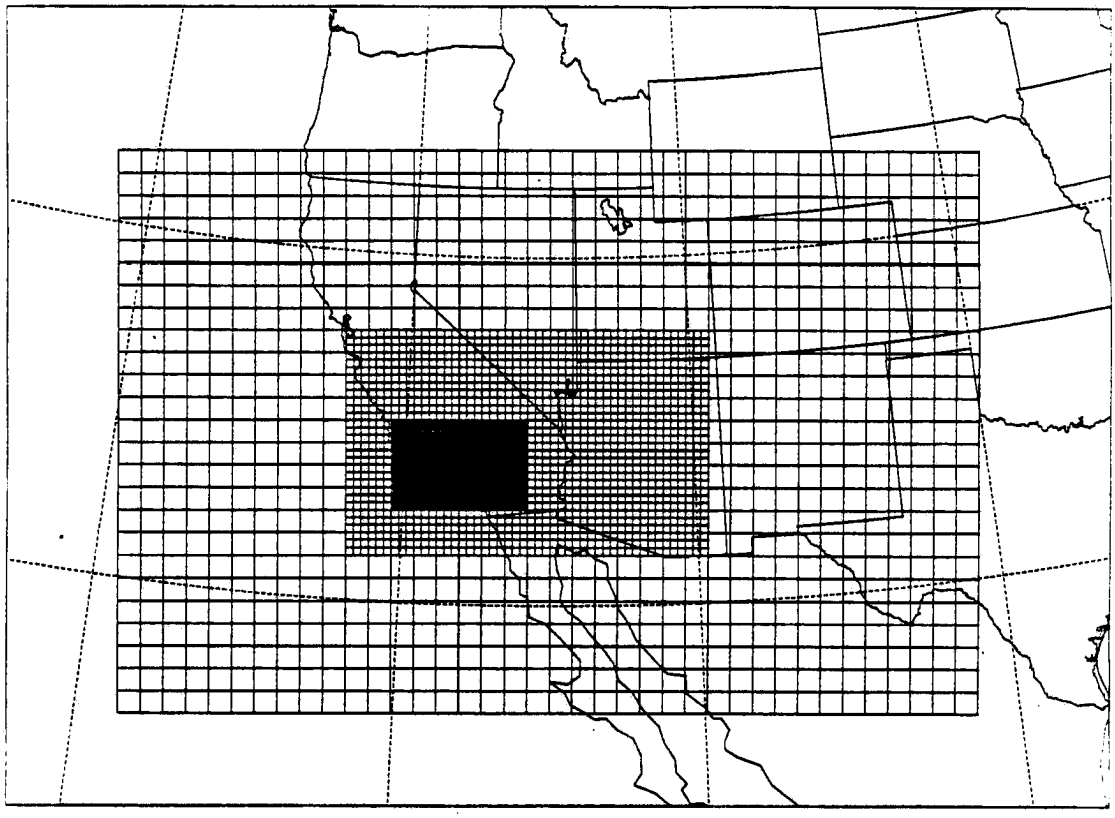

Figure 4.1: A plan view of the gridding for SW-3. Grids 1, 2, and 3 have grid increments of 72 km, 24 km, and 8 km, respectively. All extend vertically up through 35 levels to 21 km and down through 11 soil levels, respectively.

The sounding used to initialize the horizontally homogeneous conditions of the three simulations was a composite average of soundings taken within the domain. To represent the Los Angeles to Grand Canyon corridor atmosphere in the early morning hours, the soundings from San Diego, California, Las Vegas, Nevada, and Winslow, Arizona were combined. The time period of interest is February 10-13, 1987 during the WHITEX study, where upper air flow was generally consistent from the southwest, except at lower atmospheric levels and occasionally aloft, and on February 14th when a front passed through the region. Simple averages taken along the pressure surface at each station for each day of the period revealed winds blowing from 210°–270° throughout the period. The Grand Canyon would be directly impacted by pollutants flowing along a line of 251° through Los Angeles. It was decided that an average wind direction of 251° would be initialized vertically throughout the domain. This enabled an approximate worst-case analysis to be used to investigate Los Angeles' contribution to the February 10-13 period. Windspeeds, temperatures, and moisture-level data initial sounding are also composite averages over the period. All model runs were initialized with the same sounding, representing the 4-day period, February 10-13, 1987, as depicted in Table 4.1. Given the form of this initialization, integrating RAMS for 24 hours represents the model evolution of any one day in the period, each being approximately the same. The reader should recognize that in many cases land breeze, terrain-forcing, or surface inhomogeneities drastically alter low-level winds. These winds were ignored or averaged out in the initialization, but are at least partly regenerated by the RAMS formulation. Recall that the WHITEX study showed such winds, specifically katabatic easterly drainage flows from the Navajo Generating Station to the Grand Canyon, to often be partly responsible for pollutant entrainment into the canyon atmosphere. In these simulations, an attempt is made to determine if, even under near worst case conditions, Los Angeles' contribution could have been significant to WHITEX haze.

4.2 Lagrangian Particle Dispersion Model Simulations Overview

The LPDM was initially described in Section 3.1. The user must select a number of variables from the LPDM namelist to initialize a simulation. Namelist is a word used to

Table 4.1: The sounding used to homogeneously initialize with all height in RAMS simulations used in this study. It is a subjective composite of the San Diego, CA, Las Vegas, NV, and Winslow, AZ morning soundings for the 4-day period February 10-13, 1987.

Pressure (Pa)	Height (m)	Potential Temperature (K)	u-component Wind (m s^{-1})	v-component Wind (m s^{-1})	Dewpoint Depression (°C)
100000.0	0.0	286.66	2.10	0.80	1.0
85000.0	1354.2	293.38	4.00	1.40	7.4
70000.0	2928.0	301.70	9.20	3.30	12.9
50000.0	5529.5	311.07	13.70	5.00	14.6
40000.0	7157.1	315.58	17.40	6.30	14.6
30000.0	9136.3	320.20	24.40	8.90	40.0
25000.0	10331.1	327.82	27.00	9.80	40.0
20000.0	11772.8	349.57	32.50	11.80	40.0
15000.0	13612.0	371.44	31.50	11.50	40.0
10000.0	16118.2	398.16	18.90	6.90	40.0
5000.0	20301.1	484.94	11.00	4.00	40.0
3000.0	23381.5	560.91	5.40	2.00	40.0
2000.0	25850.3	642.39	4.20	1.50	40.0

describe the file wherein the user inputs the specific data necessary to run the model. The LPDM was run with the same particle sources for SW-1 through SW-3. The only major difference, indeed the most important and necessary difference, is that the meteorological input and surface conditions for each of the three LPDM runs came from the meteorological output produced by SW-1 through SW-3, respectively. The LPDM runs for SW-1 through SW-3 are SWP-1, SWP-2, and SWP-3, respectively.

Each of the five LPDM simulations per RAMS run were spawned by a continuous volume source in the LA Basin at 20 minutes of varying depths vertically and 28.8 km in the x- and y-directions centered on Los Angeles. One particle is released every 250 seconds from a randomly selected location within the volume. The turbulence parameterization within the LPDM (McNider et al., 1988) is turned on such that a turbulent, 3-D, wind fluctuation is applied to travelling particles. Although no terrain is in SWP-1, both SWP-2 and SWP-3 use the same terrain as exists in the model domain. For SWP-1 through SWP-3, LPDM wind fields were interpolated between meteorological fields created at regular intervals during the 54-hour period.

4.3 SW-1: Simulation Analysis

4.3.1 Meteorological Results: SW-1

The meteorological fields that evolve over the 54-hour period from 1200Z to 1800Z (2 days later) generically represent atmospheric conditions in any two days of the composited period. These fields are depicted in Figures 4.2 through 4.4. Figure 4.2 contains $x-z$ cross sections through the domain center point of vector wind in four hour intervals beginning 20 hours after run start through 44 hours. Figures 4.3 and 4.4 are the same cross section but depict the evolution of potential temperature, θ, and vertical velocity, w, respectively. Note that winds are very consistent in time and the vertical wind, while developed, is weak. The potential temperature profile exhibits little change in the upper layers while lower layers form a 1 km deep unstable boundary layer. This boundary layer begins to develop significantly between 1200Z and 1800Z and returns to nighttime levels by ~0000Z. The small depth of the model boundary layer is consistent with mid-winter conditions. The flat terrain of this simulation creates an environment with little forcing; thus winds are not subject to large change in time. In fact, the only surface inhomogeneity throughout the domain is the land/sea line along the California coast. Figures 4.5 and 4.6 show the evolution of horizontal vector winds on an $x-y$ cross section through 73.2 m and 1033.7 m, respectively. As made obvious in the Figures, these winds are quite consistent throughout the domain in both speed and direction over space and time although evidence of an inertial oscillation of $\sim$ 20 hours is present. The inertial oscillation period at these latitudes is, in fact, $\sim$ 20 hours which is consistent with the period of the horizontal vectors' oscillation. Particles released into such an environment would be expected to travel in a rather simple manner nearly parallel to the quasi-uniform wind vectors.

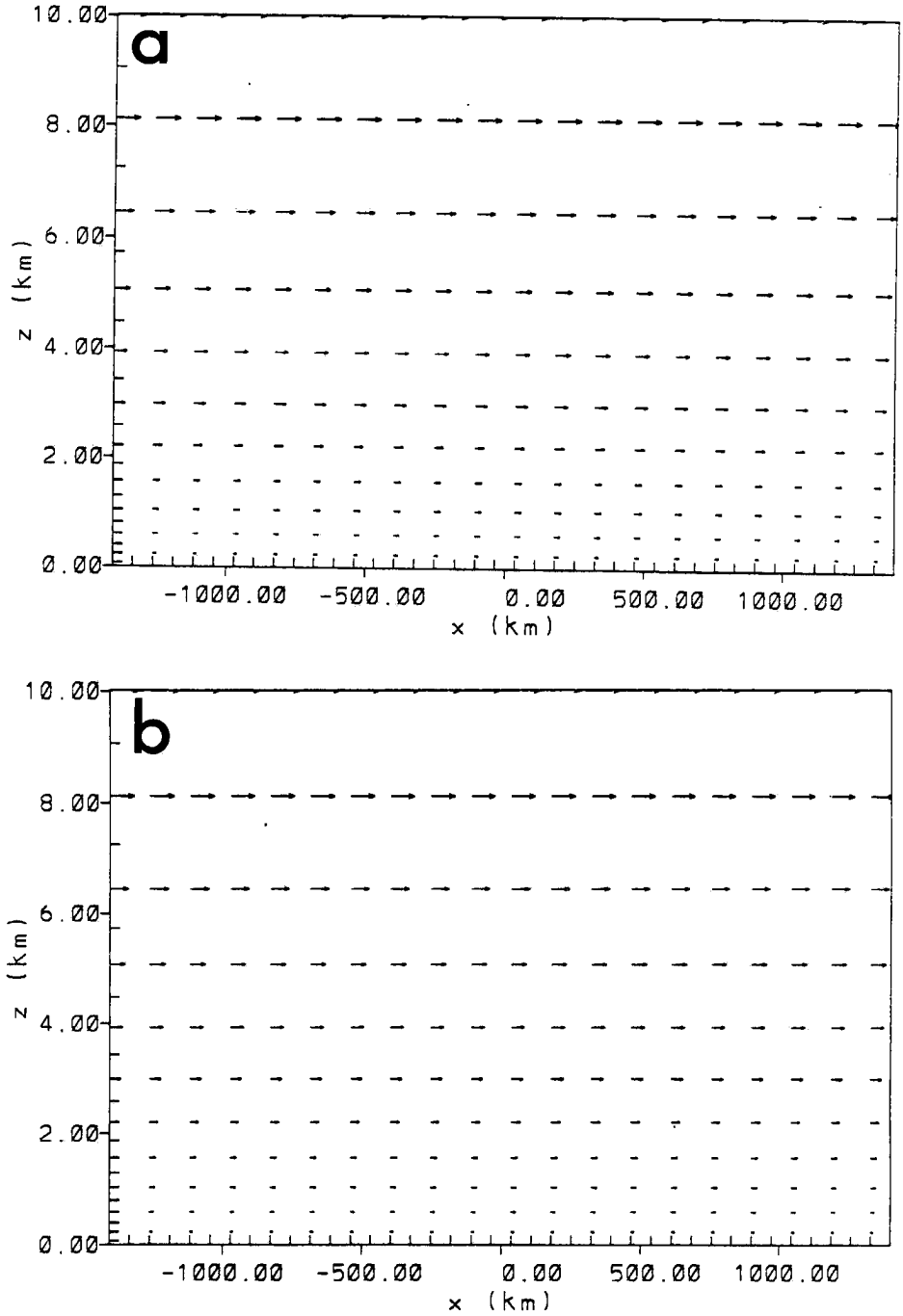

Figure 4.2: Vertical cross section of vector wind across Grid 1 of SW-1 at (a) 0800Z, hour 20; and (b) 1200Z, hour 24. The plates are in four-hour intervals beginning 20 hours after run initiation until 44 hours (2 a.m. – 2 a.m. next day). The longest vector represents $\sim$27 m s^{-1}.

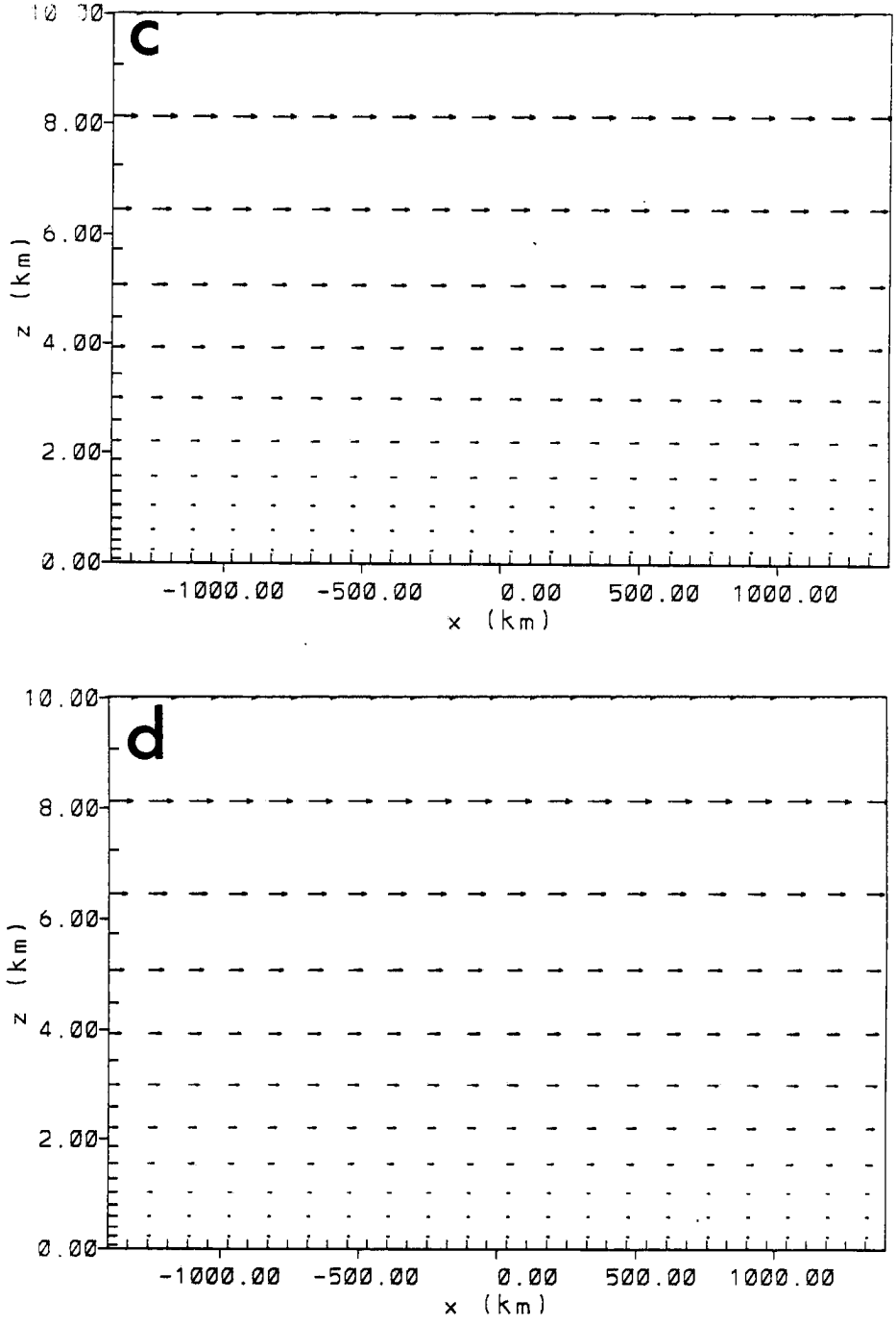

Figure 4.2: (c) 1600Z, hour 28; and (d) 2000Z, hour 32.

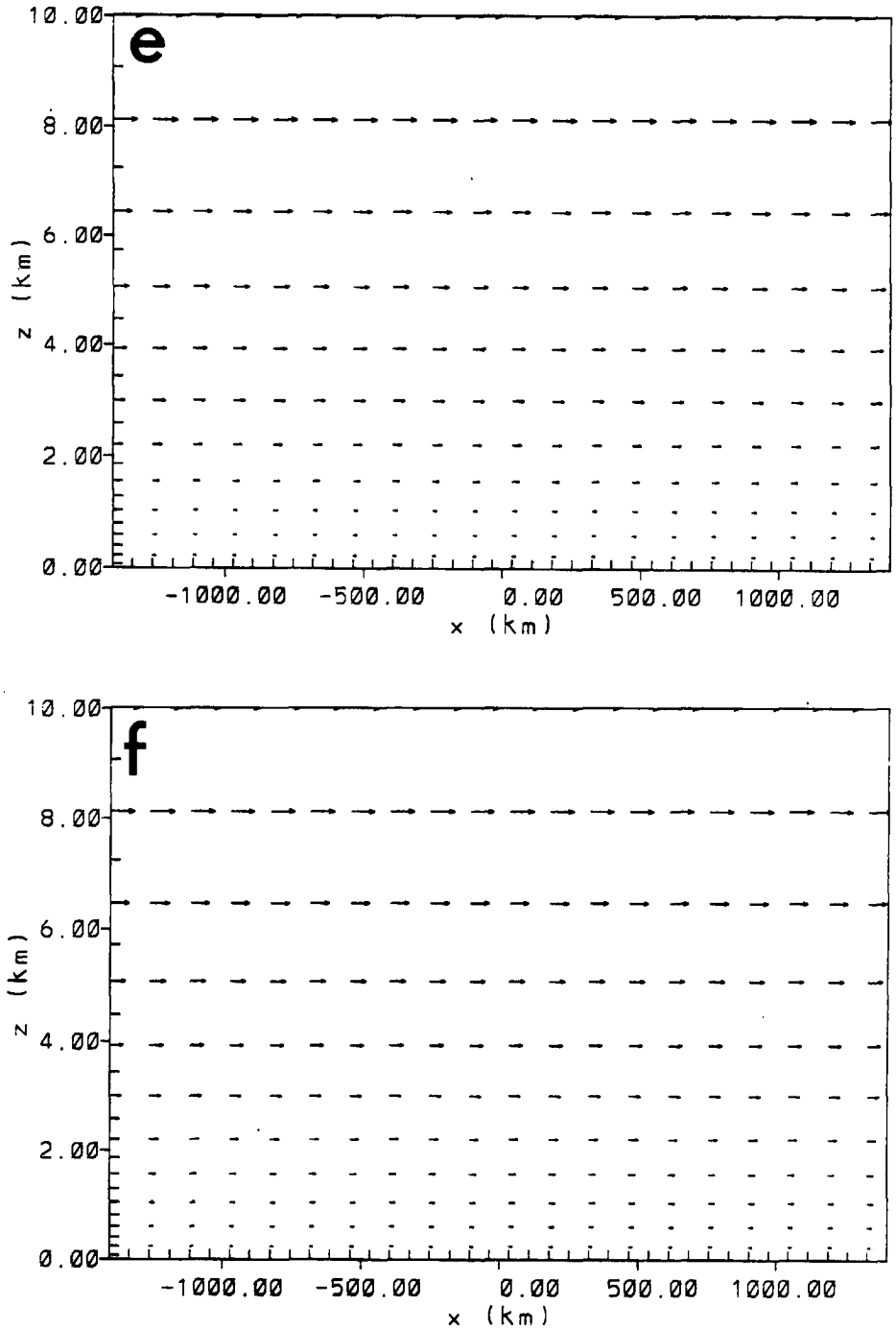

Figure 4.2: (e) 0000Z, hour 36; and (f) 0040Z, hour 40.

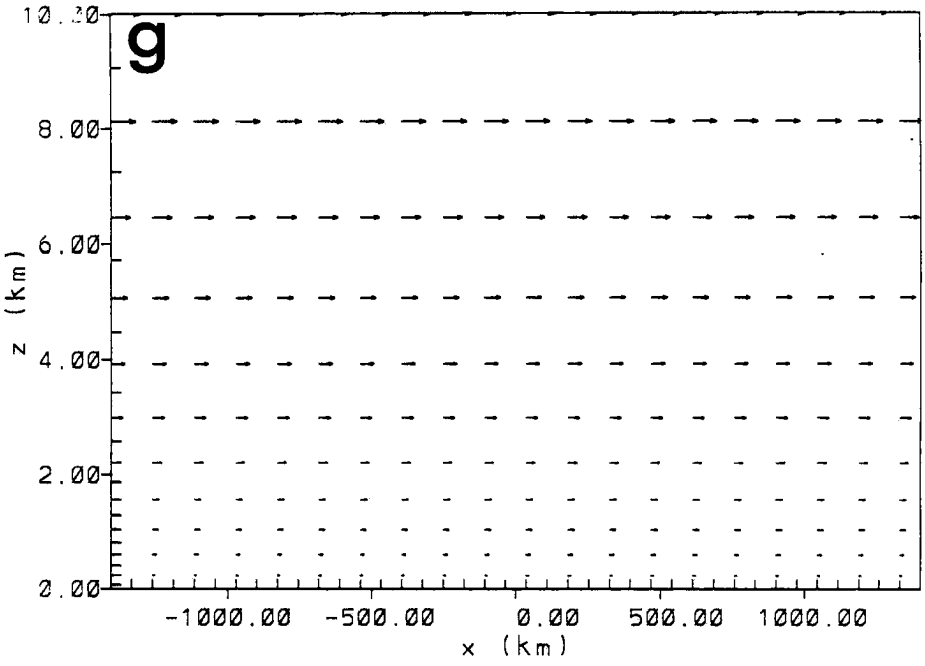

Figure 4.2: (g) 0800Z, hour 44.

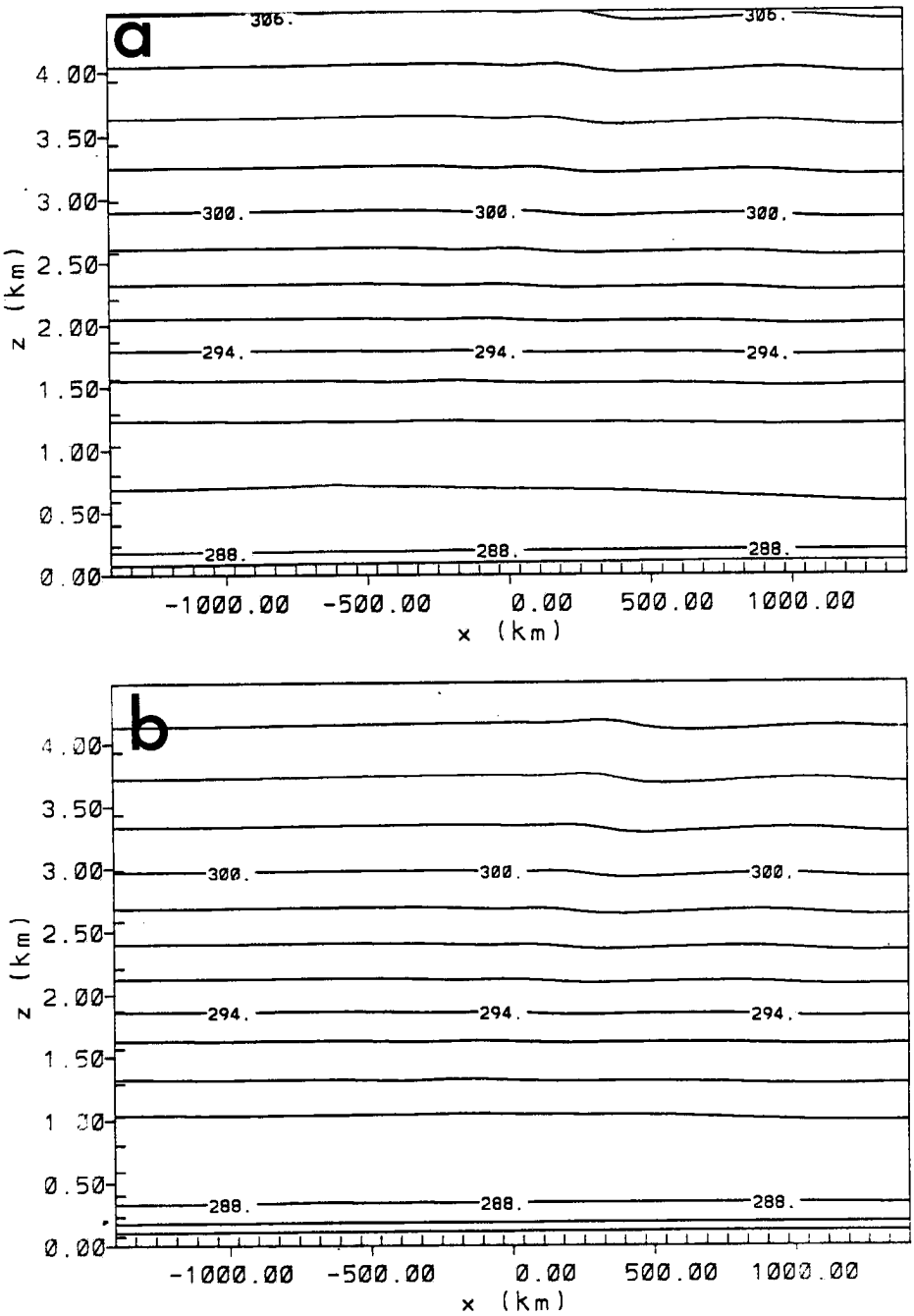

Figure 4.3: Same as Figure 4.2 except for potential temperature, θ at (a) 0800Z, hour 20; and (b) 1200Z, hour 24. The lowest 4 km of the 21 km vertical extent of the domain is shown to emphasize boundary layer development. Contour intervals are 1.0°C.

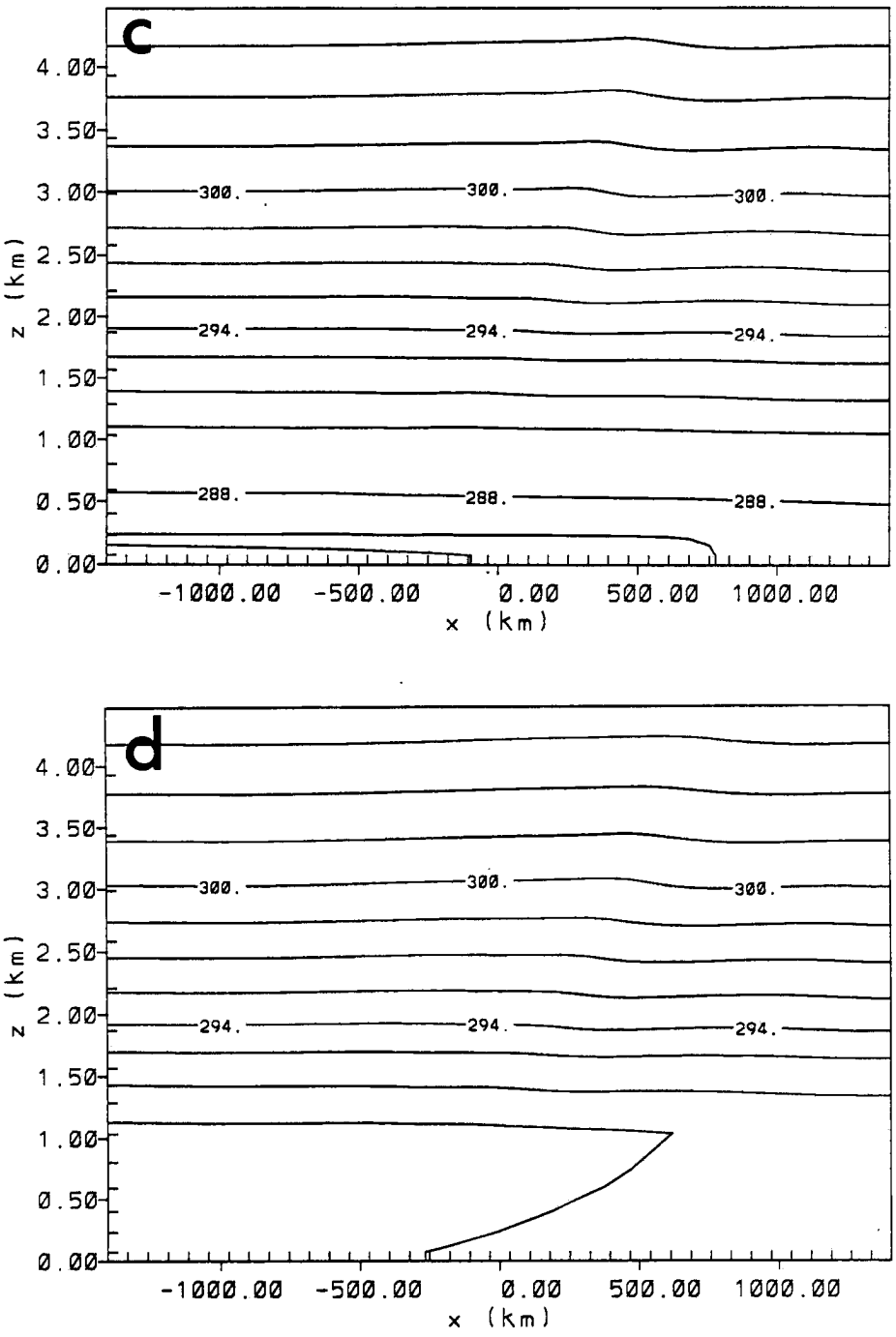

Figure 4.3: (c) 1600Z, hour 28; and (d) 2000Z, hour 32.

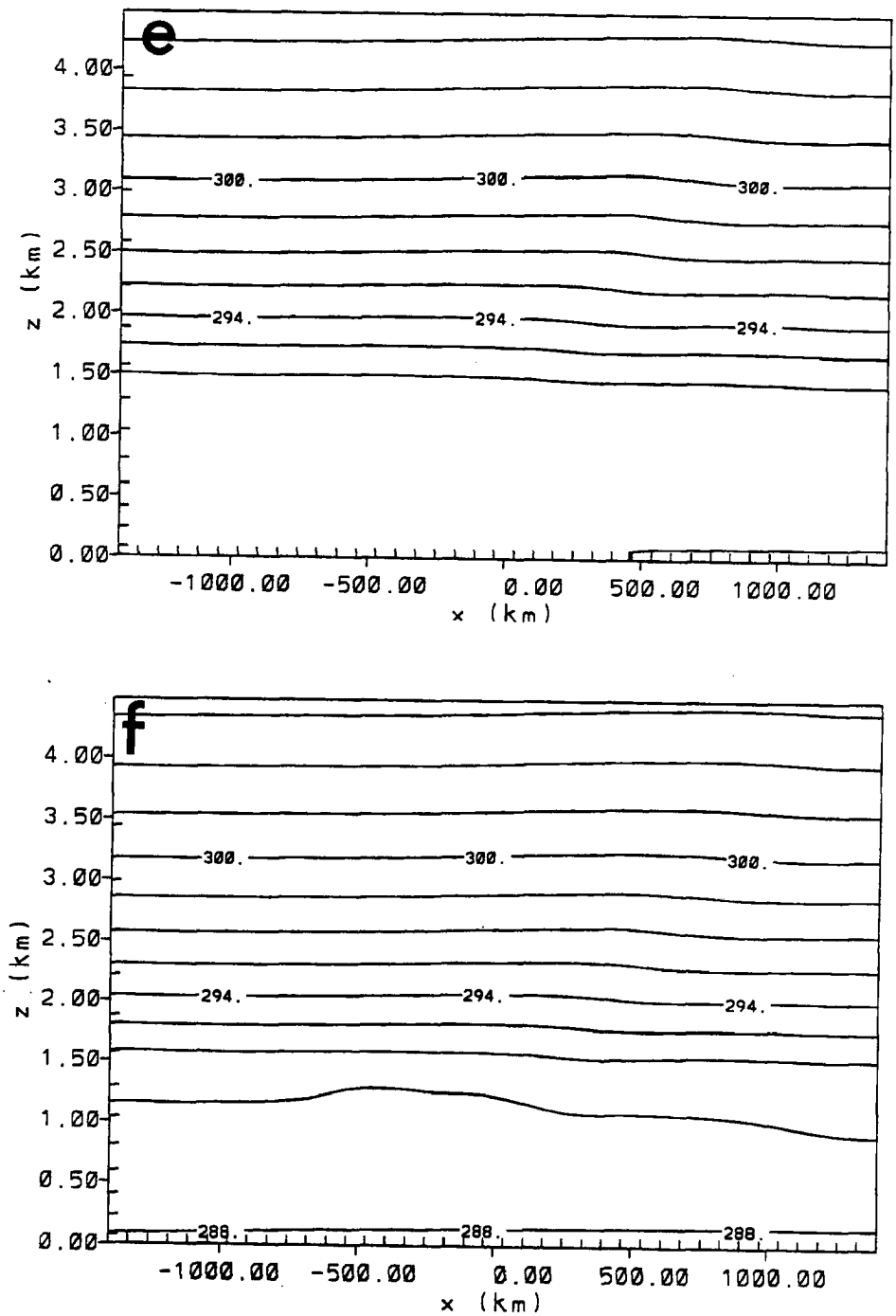

Figure 4.3: (e) 0000Z, hour 36; and (f) 0040Z, hour 40.

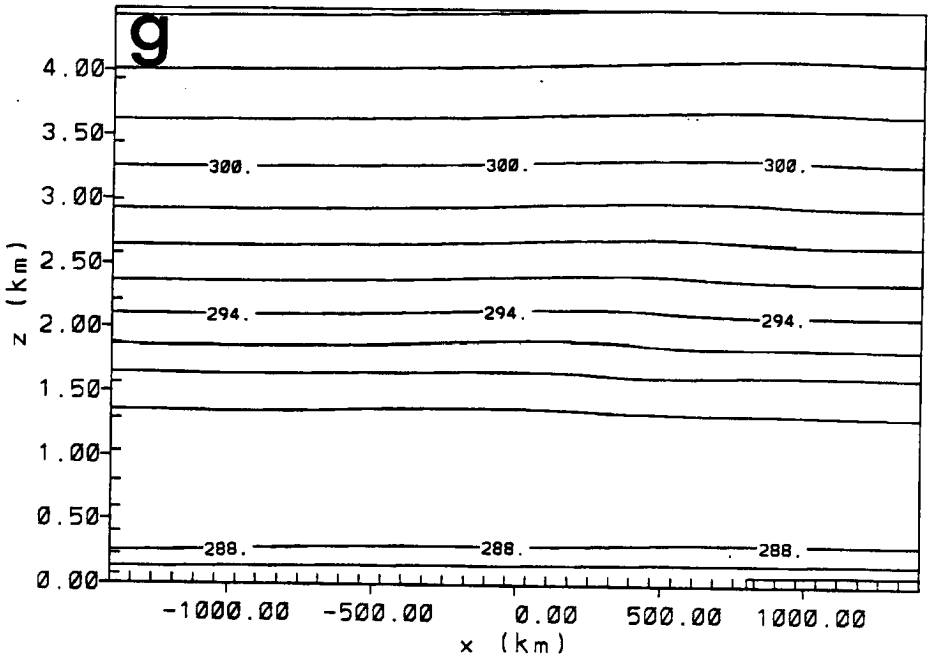

Figure 4.3: (g) 0800Z, hour 44.

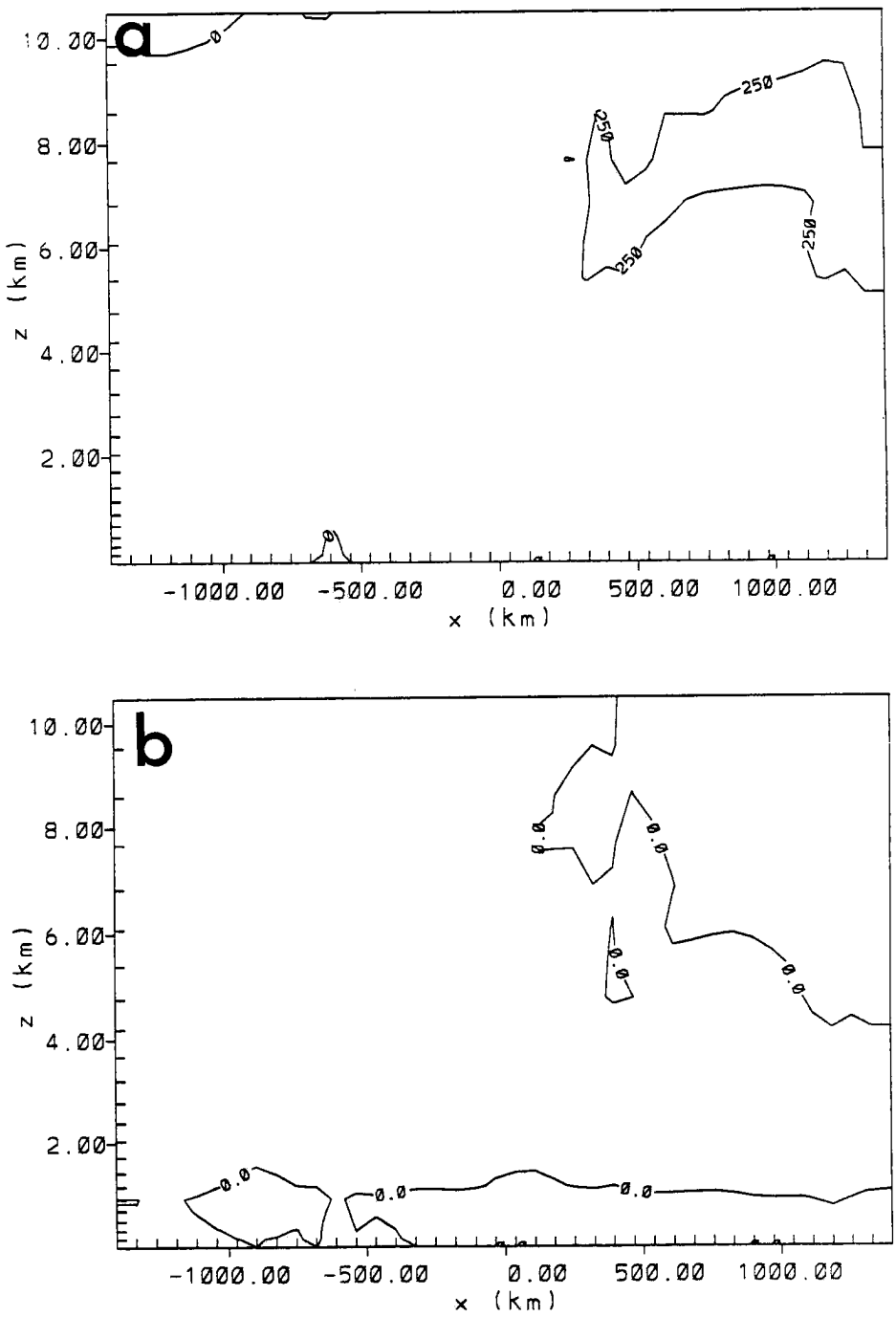

Figure 4.4: Same as Figure 4.2 except the evolution of vertical velocity, w at (a) 0800Z, hour 20; and (b) 1200Z, hour 24. Contour intervals are 0.25 cm s^{-1}.

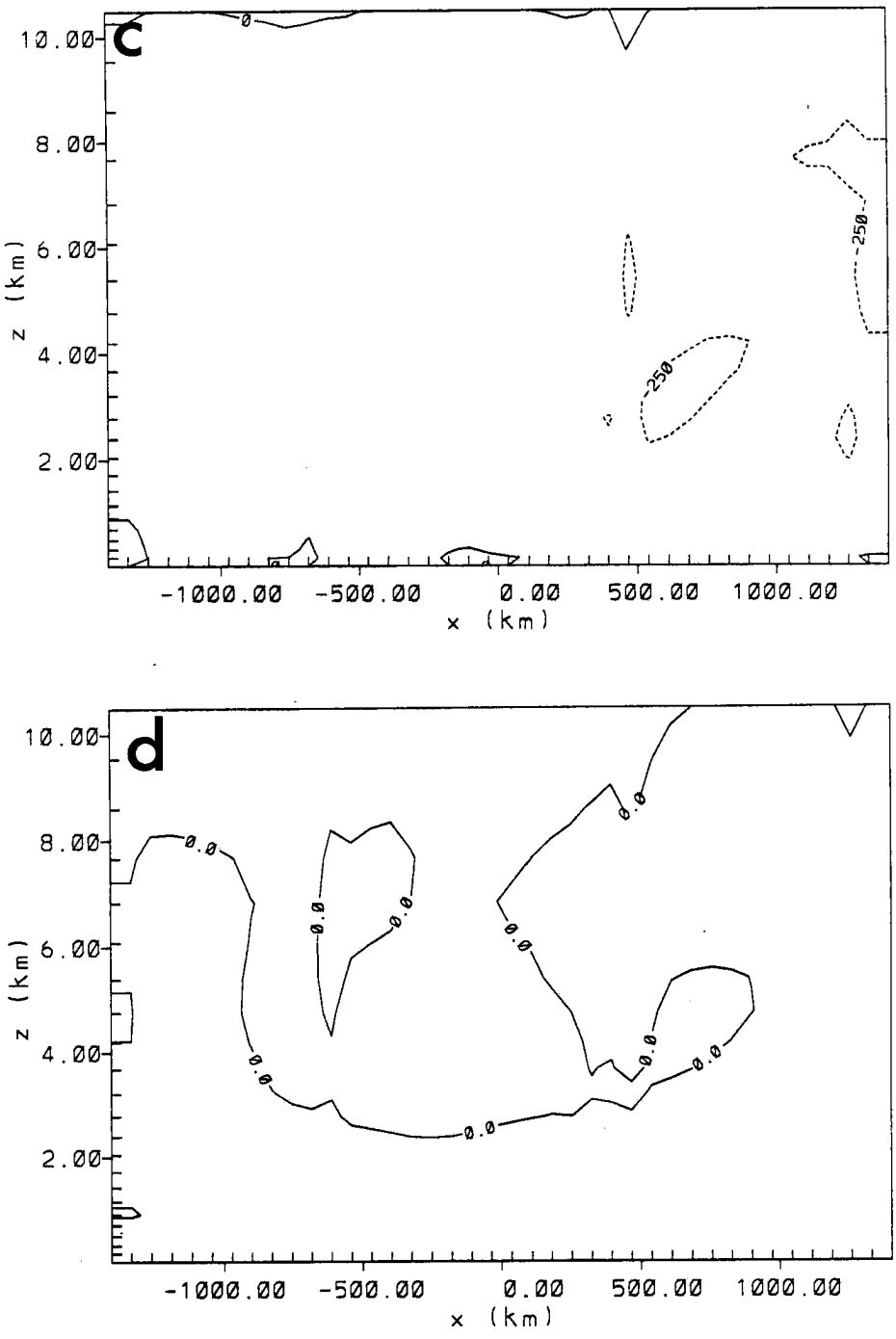

Figure 4.4: (c) 1600Z, hour 28; and (d) 2000Z, hour 32.

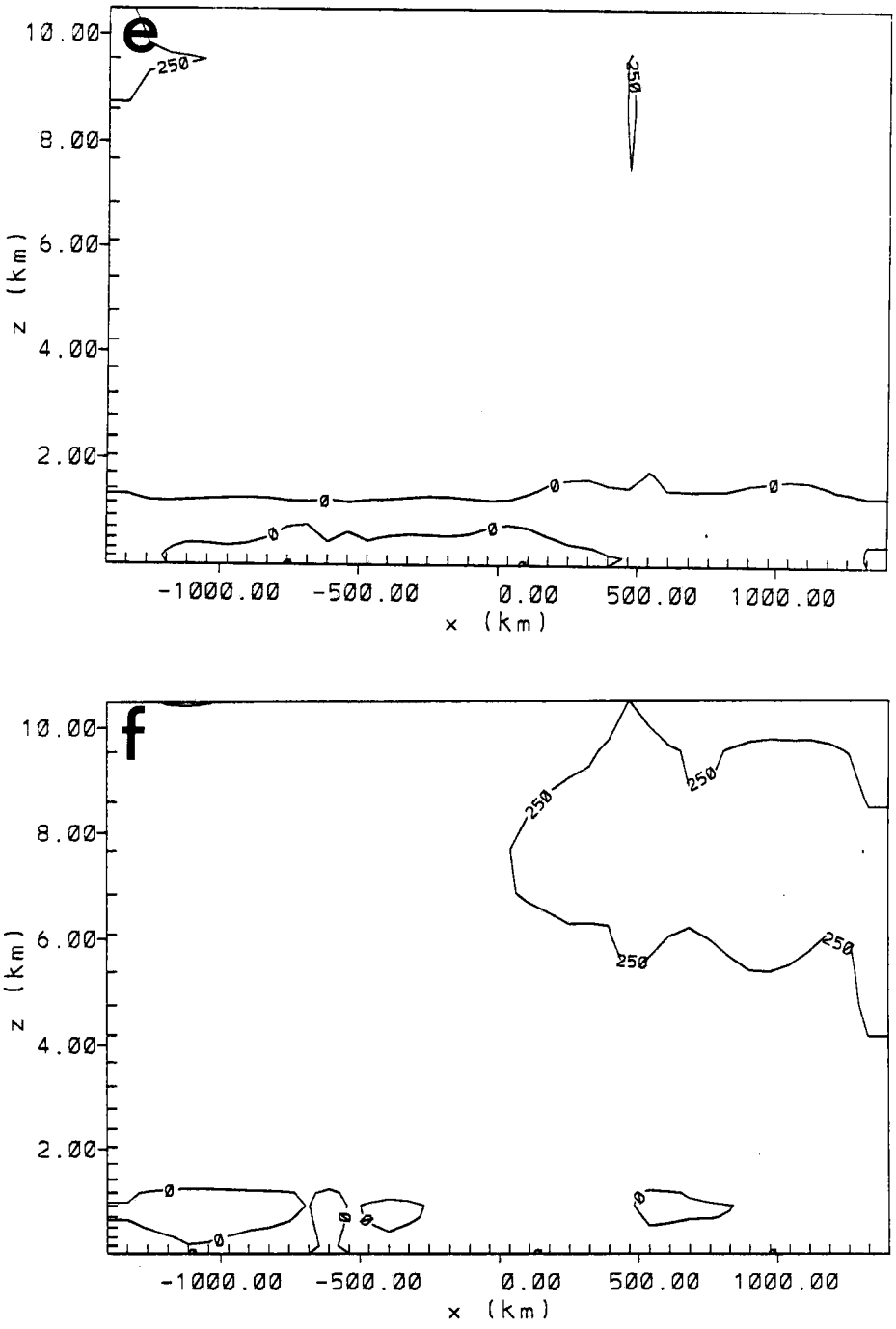

Figure 4.4: (e) 0000Z, hour 36; and (f) 0040Z, hour 40.

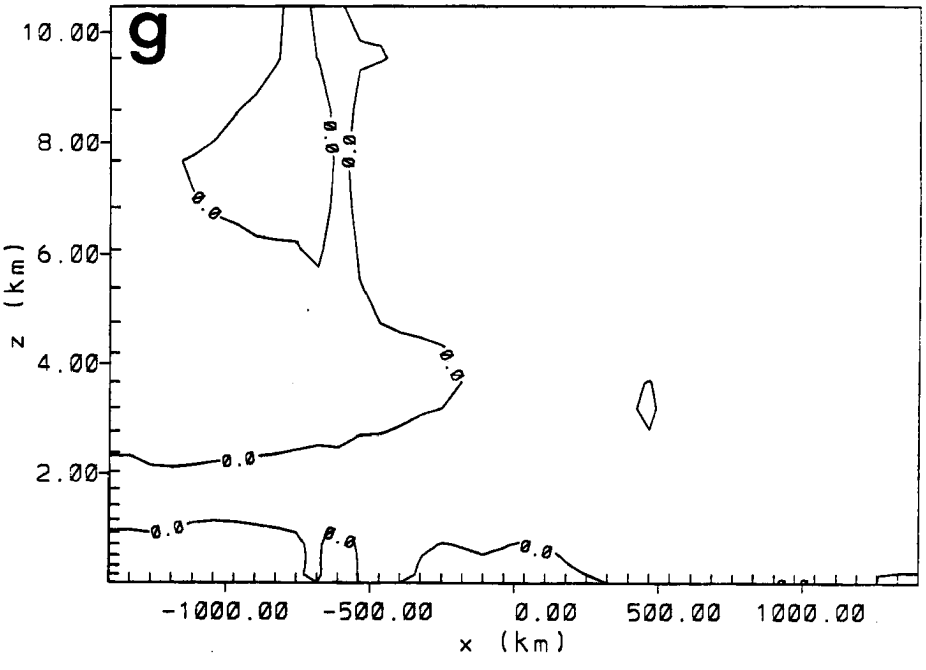

Figure 4.4: (g) 0800Z, hour 44.

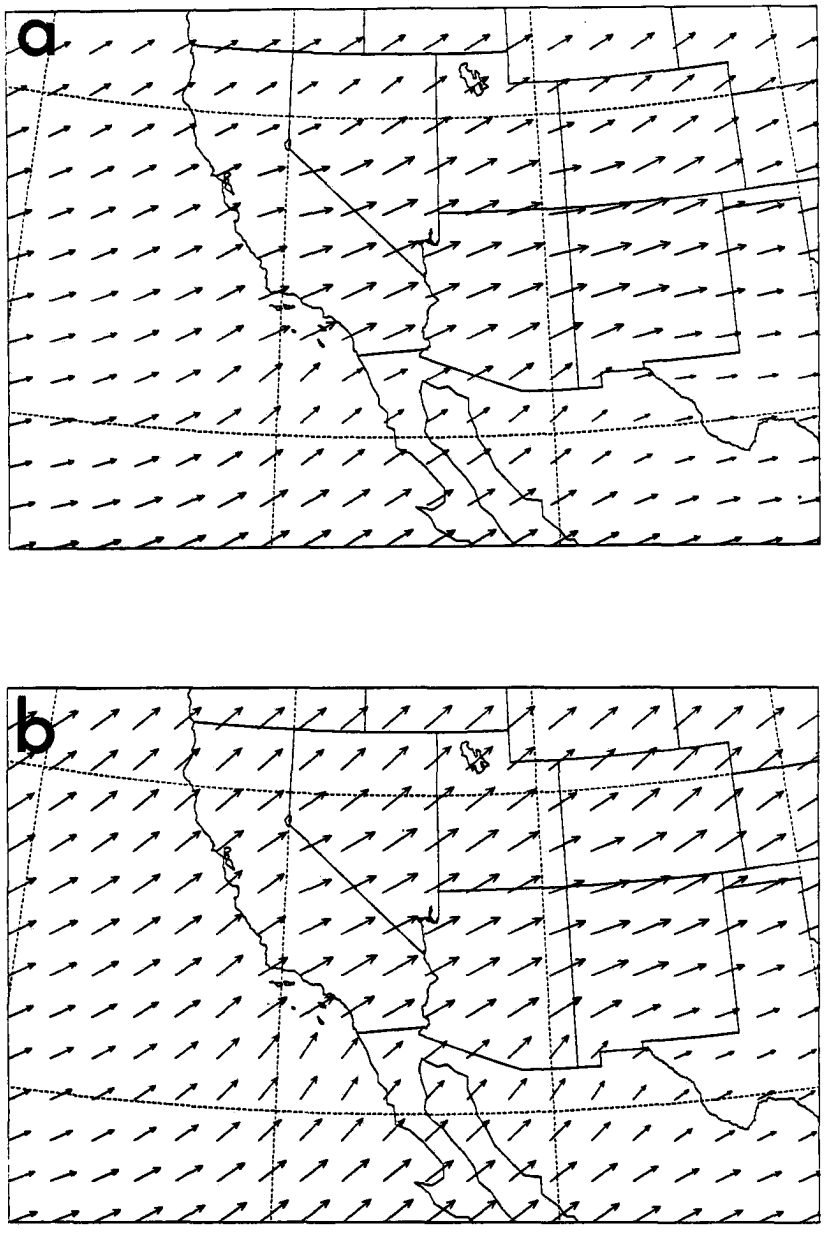

Figure 4.5: The evolution of horizontal vector winds over the 24-hour period 20 hours – 44 hours into the simulation in 4 hour intervals at (a) 0800Z, hour 20; and (b) 1200Z, hour 24. This is a plan view on Grid 1 at the first model level 73.2 m above ground level. An inertial oscillation period of ~20 hours is evident. The longest vector represents ~2.8 m s^{-1}.

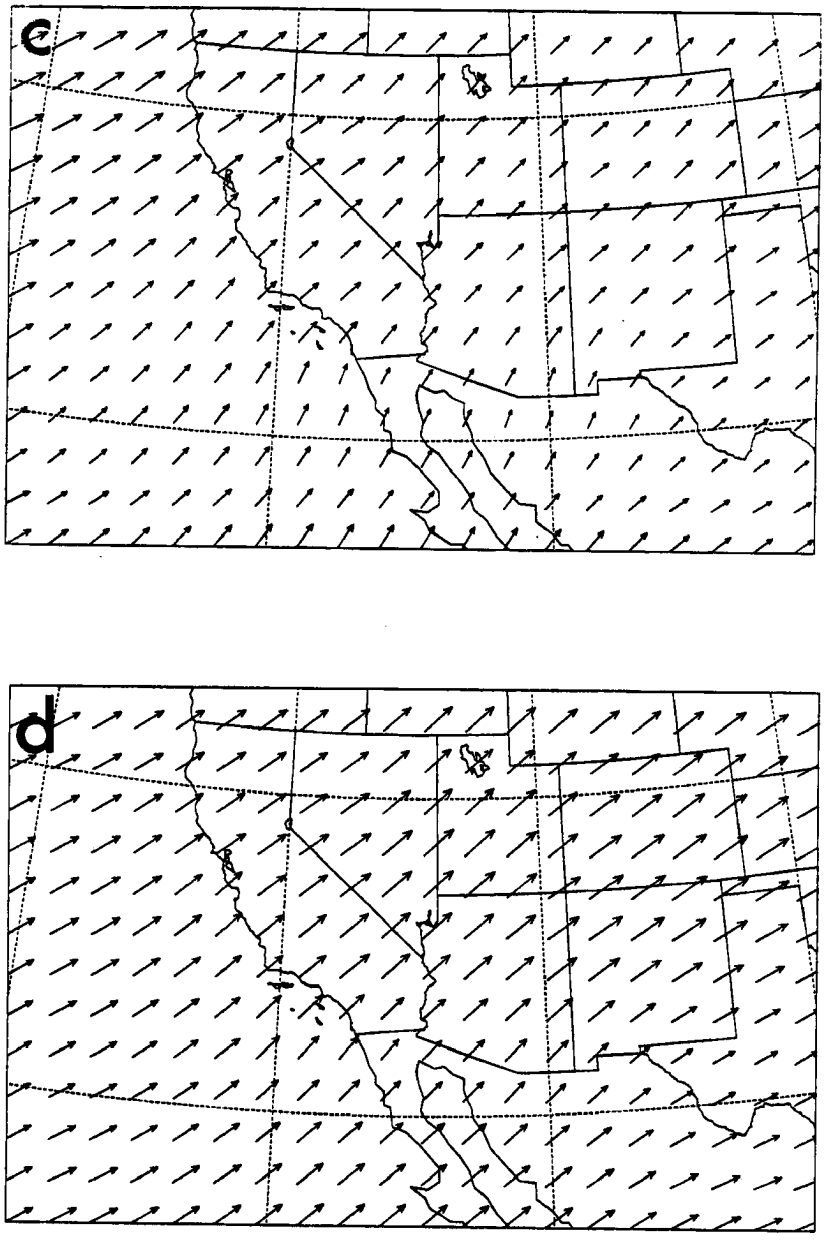

Figure 4.5: (c) 1600Z, hour 28; and (d) 2000Z, hour 32.

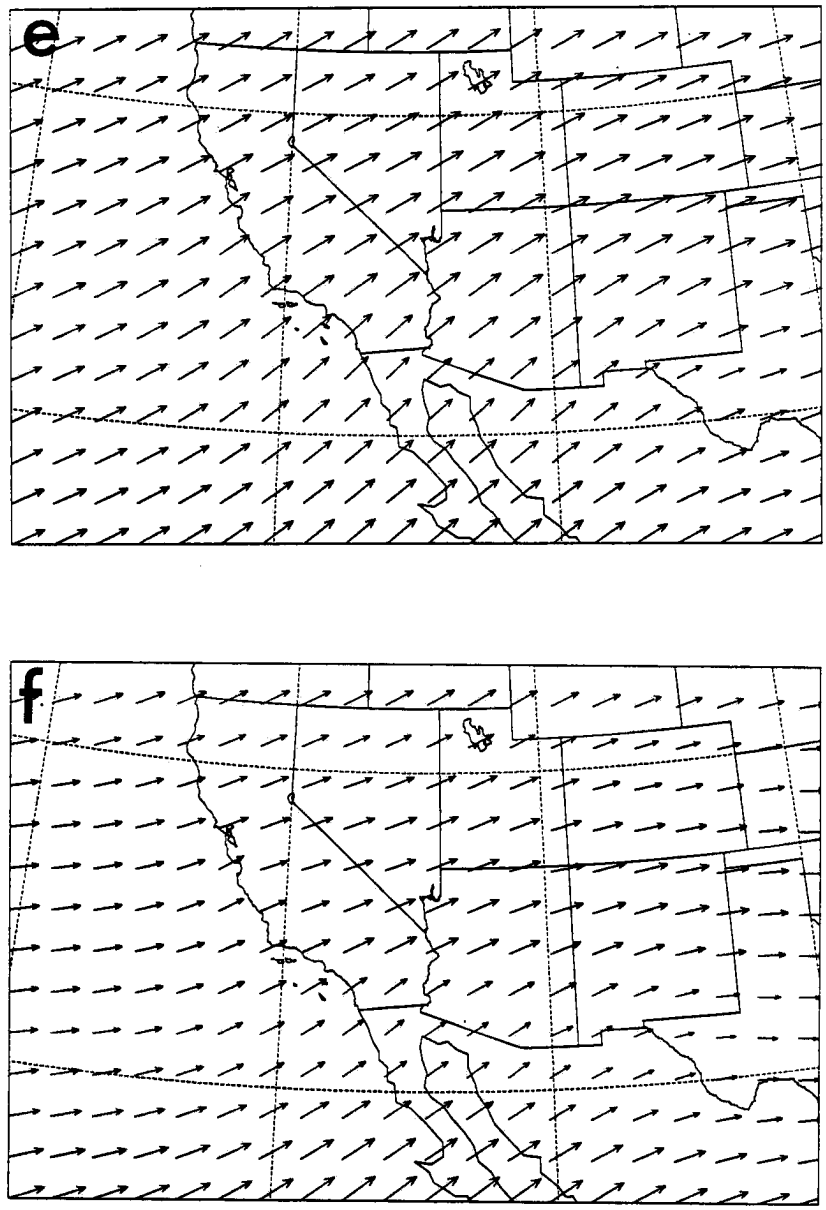

Figure 4.5: (e) 0000Z, hour 36; and (f) 0040Z, hour 40.

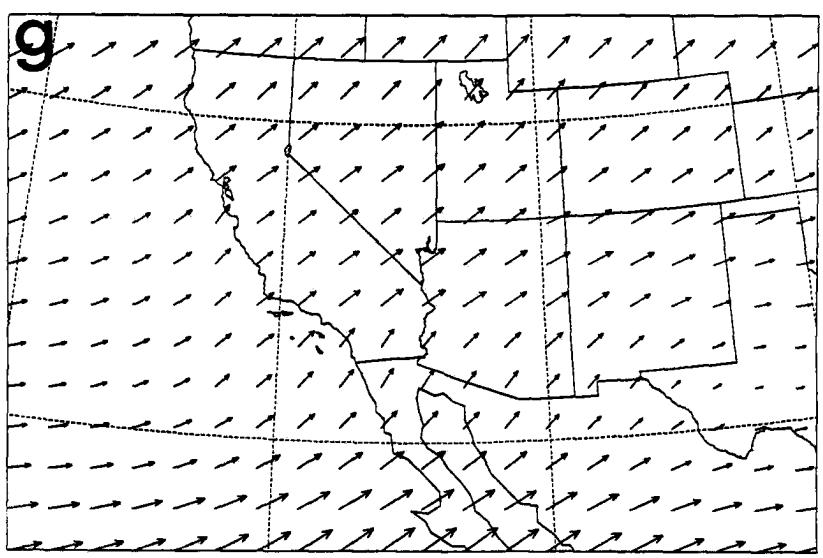

Figure 4.5: (g) 0800Z, hour 44.

4.3.2 LPDM Results: SWP-1

As described in 4.2 the Lagrangian Particle Dispersion Model was used to advect particles representing Los Angeles pollution within the RAMS domain. The 54-hour period of particle transport was animated on a Stardent console in 210, fifteen-minute increments. Five distinct particle releases were completed, all centered over Los Angeles. The five particle simulations are designated SWP-1a through SWP-1e. Their distinguishing characteristics are:

SWP-1a – A 20 m thick, pancake-like release from the surface (0 m) to 20 m.

SWP-1b – Also a 20 m thick release, but centered around 100 m.

SWP-1c – A 20 m thick release centered on 500 m.

SWP-1d – A 20 m thick release centered on 250 m.

SWP-1e – A 500 m deep volume from the surface to 500 m.

In each simulation one particle was released from within the designated release volume at the rate of one particle per 250 seconds. By using distinct levels of release, the particular significance of pollutants at a certain level to the general transport out of the LA Basin volume was shown. SWP-1e represents the volume of pollutants after accumulating to a depth of 500 m as generally might exist during stagnant periods such as WHITEX.

As one might expect, a flat terrain simulation of generically initialized wind conditions does not reveal much relevant data regarding true dispersion out of the LA Basin. These simulations are intended to be compared to terrain-inclusive RAMS runs (SW-2 and SW-3) to evaluate the importance of that terrain.

0–20 m Release: SWP-1a

The simulation and subsequent animation of LPDM results for the surface release reveals considerable vertical mixing but limited horizontal transport (relative to the plume axis, see Figure 4.7). Because windfields predicted by the model over the homogeneous, flat terrain change little throughout the 54-hour period, the LA Basin plume moves in

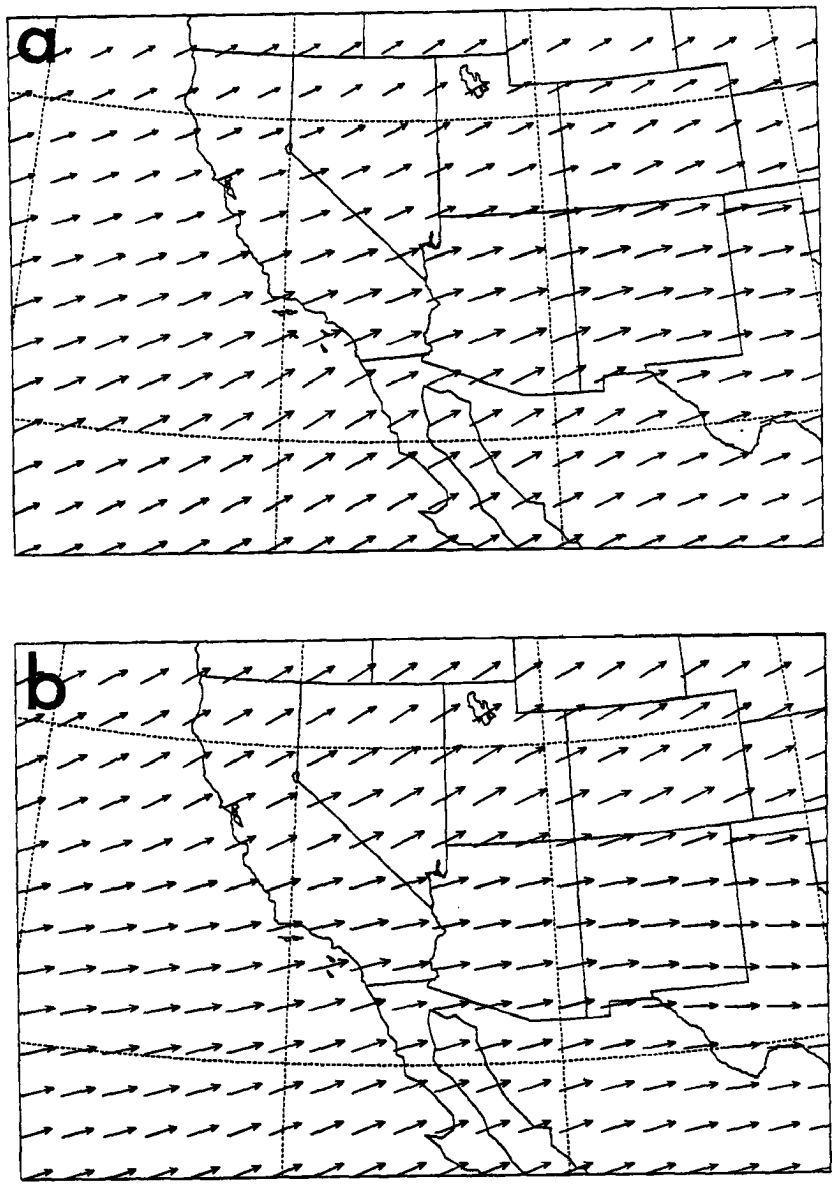

Figure 4.6: Same as Figure 4.5 except for 1033.7 m above ground level at (a) 0800Z, hour 20; and (b) 1200Z, hour 24. The longest vector represents ~5.0 m s^{-1}.

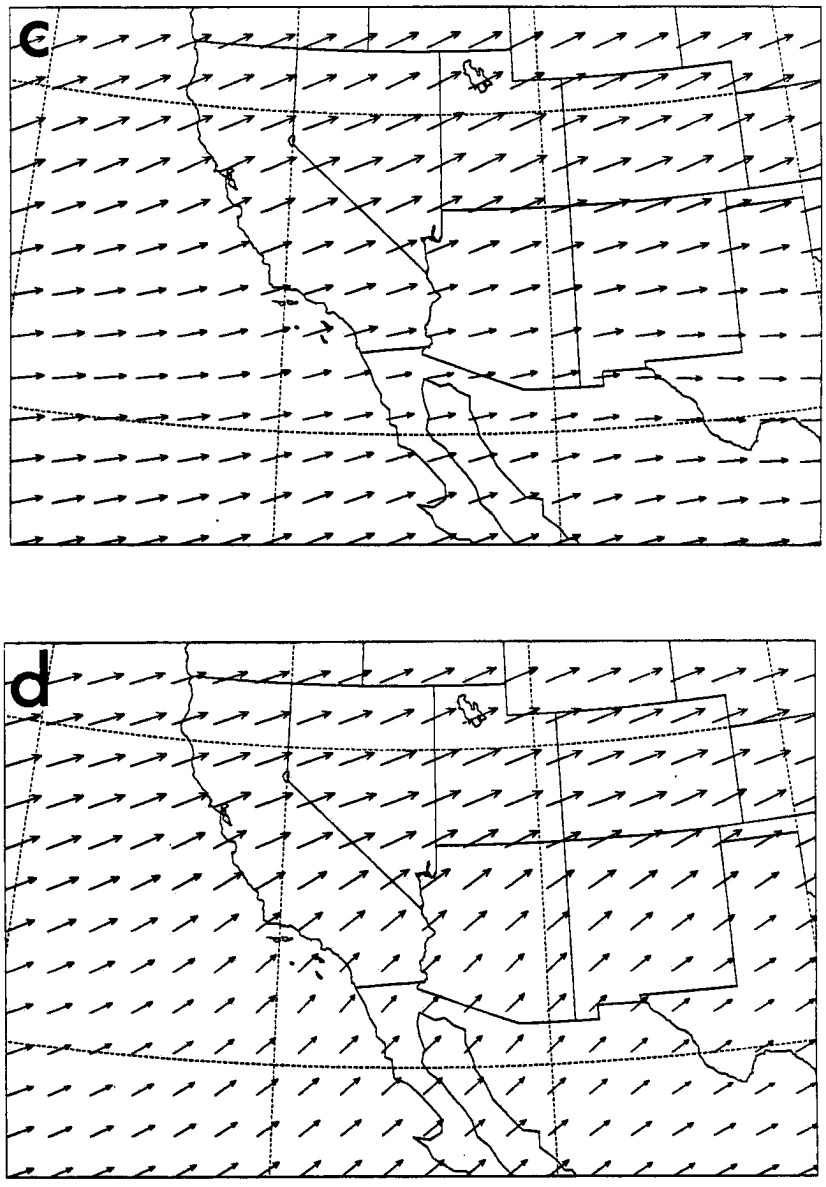

Figure 4.6: (c) 1600Z, hour 28; and (d) 2000Z, hour 32.

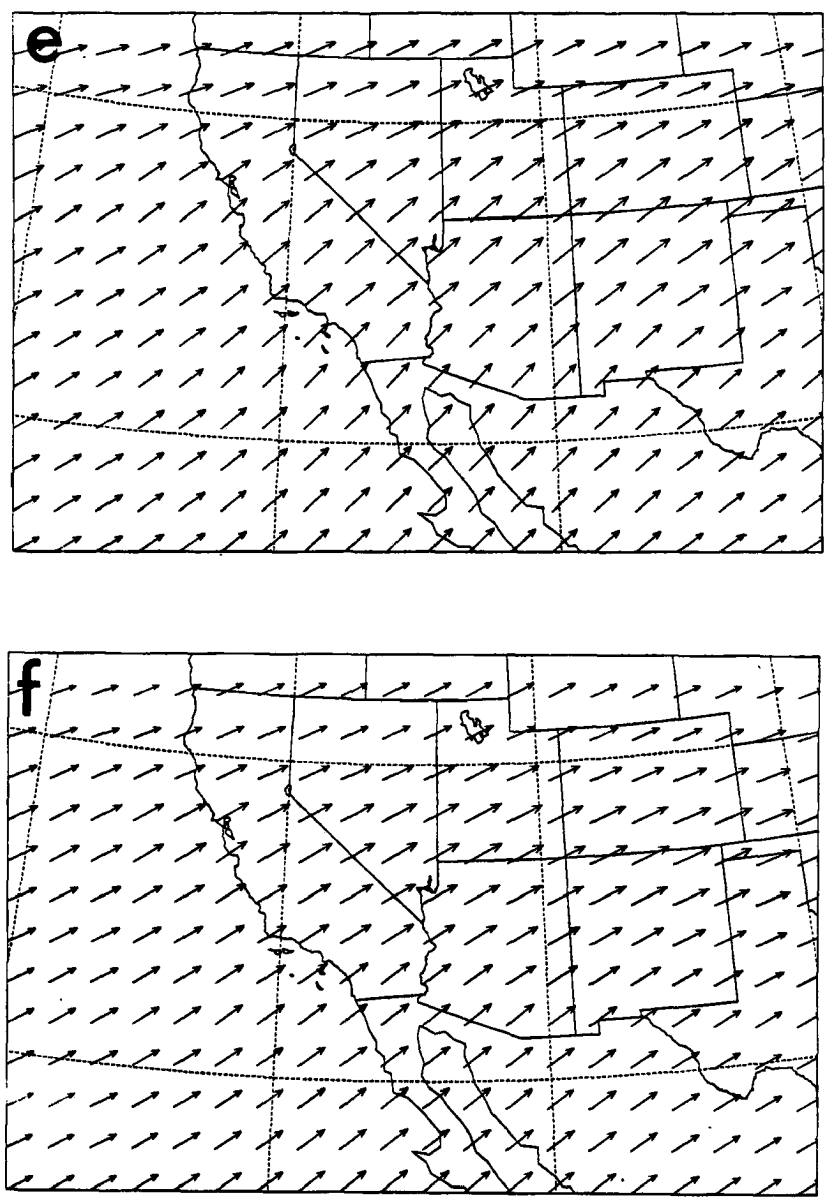

Figure 4.6: (e) 0000Z, hour 36; and (f) 0040Z, hour 40.

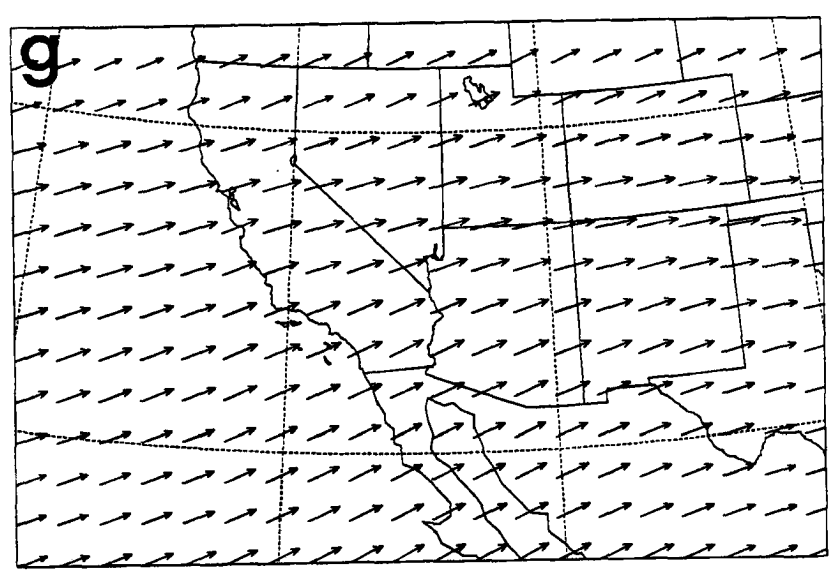

Figure 4.6: (g) 0800Z, hour 44.

the west-southwesterly wind directly toward the Grand Canyon. Figure 4.7, shows the progression of the plume toward the Grand Canyon at 1, 9, 18, 27, 36, 45 and 54 hours (13Z day 1 through 18Z two days later). Slight changes in direction from the 251° wind (initial) due to inertial oscillation are seen in the slight meander along the plume in time. Also some shear with height develops in response to surface friction causing the upper 300-500 m of plume to move with a more easterly component with respect to the lower portion of plume. From the initial release width of approximately 45 km the plume spreads horizontally to a maximum width of 100 km at simulation end.

Although horizontal dispersion is limited in this stable, wintertime environment, vertical dispersion is limited only by the extent of boundary layer growth. In this simulation the boundary layer grows to approximately 1 km. Correspondingly, particles initially in the 0-20 m layer during pre-boundary layer times (overnight) are quickly mixed to 1 km when to boundary layer does form. The animation further reveals that when the boundary layer depth again drops as evening approaches only a small number of particles are brought down with it. Particles predominantly remain elevated at the level they achieved prior to sunset and boundary layer decay. Particles released into the stable overnight atmosphere do not exhibit significant vertical dispersion, while horizontal dispersion continues although at a slower rate than during the day. Particles at lower levels move at a slower rate to the northeast than those aloft.

Under these conditions particles can be counted at different locations to roughly estimate dilution factors given plume dimensions in the region of interest. Using the volume containing the first 100 particles for reference, it is found that 100 particles reside within a volume approximately 5.0×10^4 m $\times$ 5.0×10^4 m $\times$ 20.0 m. Each particle, then, represents one-hundredth of the pollutant mass in the LA plume from the surface to 20 m. At the plume's densest concentration over the Grand Canyon region, 70 particles occupy a volume approximately 7.0×10^4 m $\times$ 1.00×10^5 m $\times$ 1.0×10^3 m. The dilution factor in this case is 200. Although 70% of the original plume pollutant mass transports to the Grand Canyon in the worst instance, the particles disperses through such a great volume due to natural atmospheric processes that one-two-hundredth of the original concentration

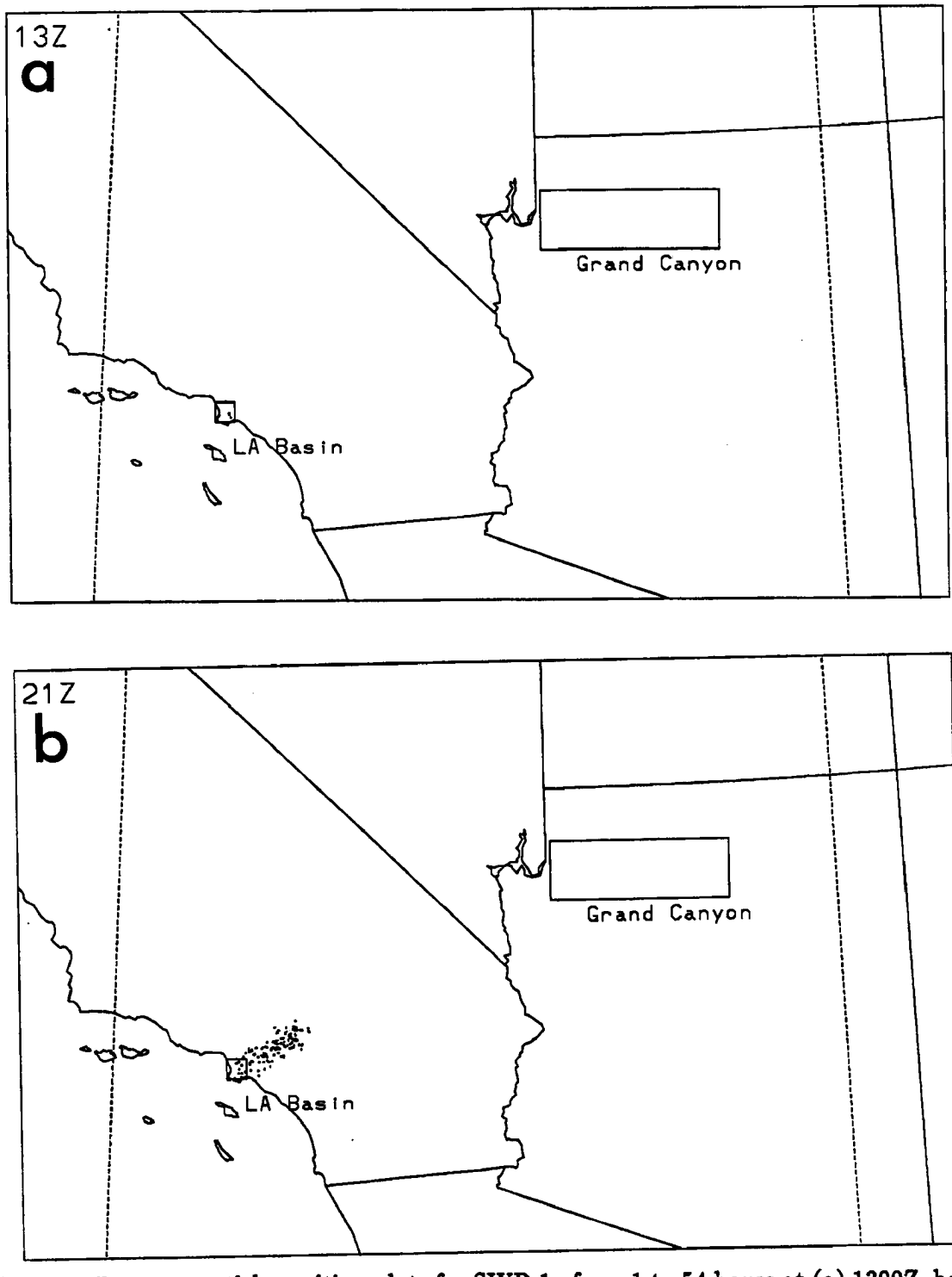

Figure 4.7: $x-y$ particle position plots for SWP-1a from 1 to 54 hours at (a) 1300Z, hour 1; and (b) 2100Z, hour 9. The release area and Grand Canyon region are labeled and shown as boxes at their respective locations.

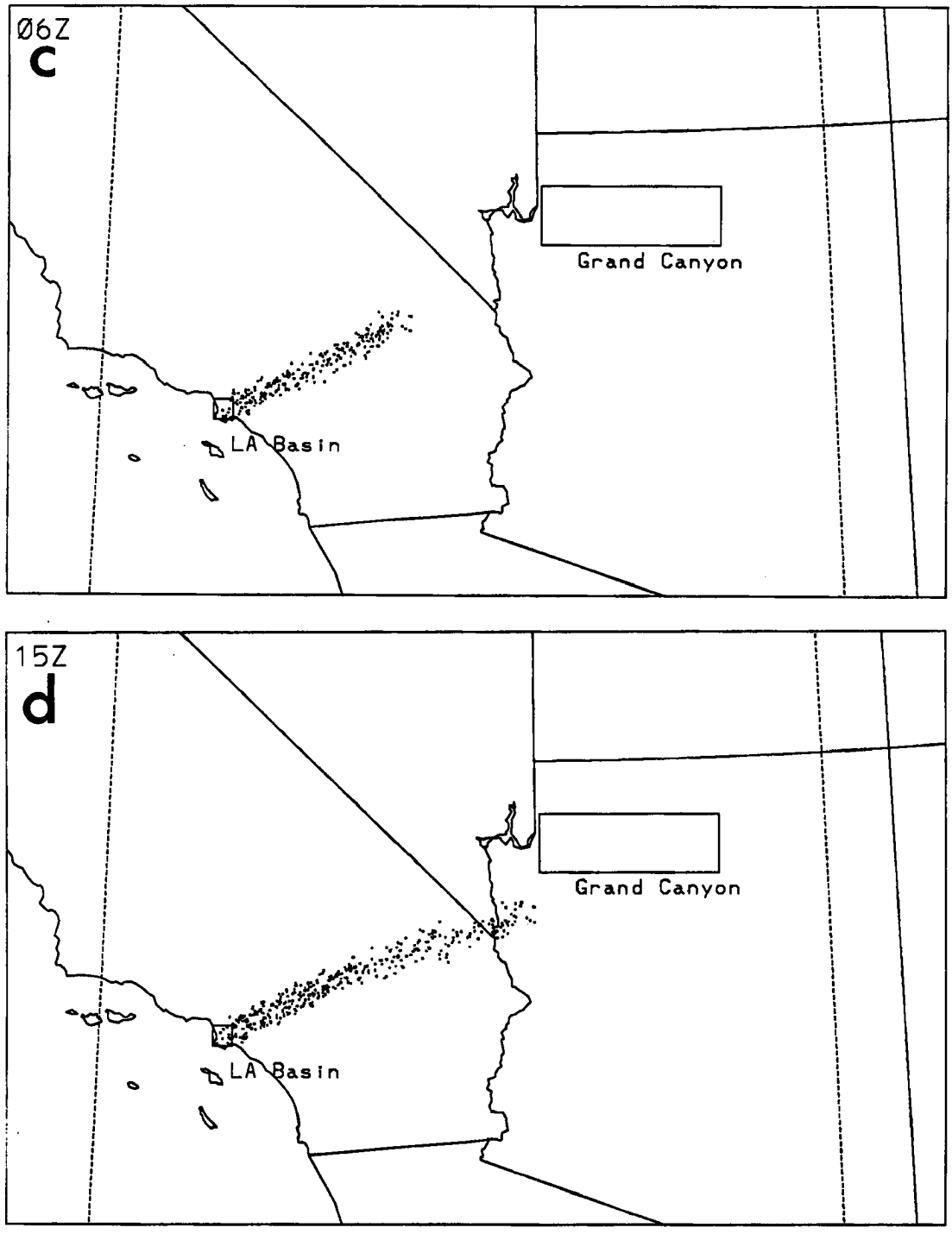

Figure 4.7: (c) 0600Z, hour 18; and (d) 1500Z, hour 27.

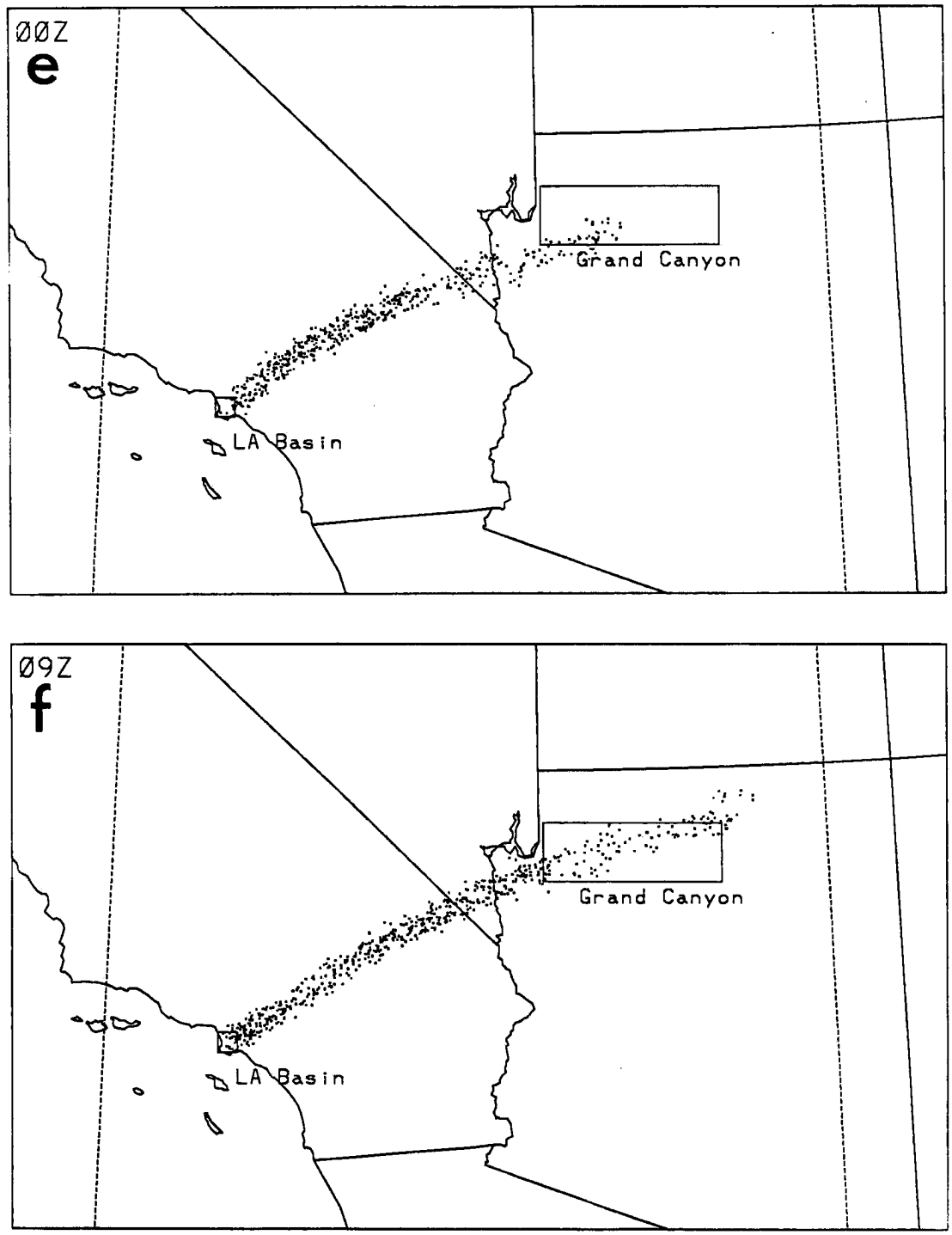

Figure 4.7: (e) 0000Z, hour 36; and (f) 0900Z, hour 45.

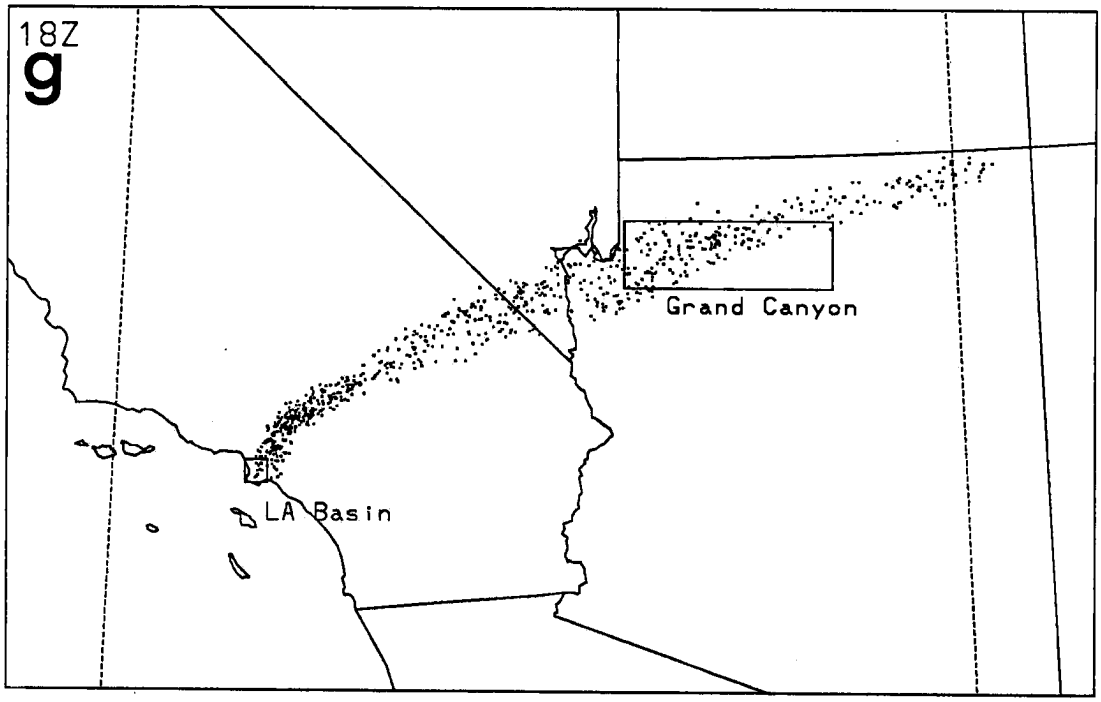

Figure 4.7: (g) 1800Z, hour 54.

is present. A number of details do not enter into this calculation such as wet and dry deposition, chemical conversion processes and, likelihood of entrainment into the Grand Canyon atmosphere (i.e. from above the inversion in the Canyon). These other effects would increase the effective dilution factor further. Note that the dilution factor would have been fifty times less (i.e. four, a worst case) if the pollutants had not mixed through the 1 km deep boundary layer and instead remained within 20 m of the surface. This emphasizes the importance of the growing boundary layer to the dispersion of pollutant plumes.

100 m Release: SWP-1b

SWP-1b releases the same pancake of particles centered at 100 m above the surface over a 20 m depth (90 m – 110 m). Over the 54-hour period many features are the same as SWP-1a. Because this release begins at a higher altitude its particles initially move with the higher speeds present at that level. However, as the boundary layer grows beyond 100 m depth in the early afternoon, the particles rapidly disperse throughout that depth just as the 0-20 m release particles of SWP-1a did. SWP-1b appears very much the same as SWP-1a as depicted in Figure 4.7; its plume meanders with the period of the inertial oscillation, the dilution factor is roughly 200, the primary cause of dilution is boundary layer growth and the horizontal dispersion of the plume is limited. Very few differences with SWP-1a are seen. The plume mixes more quickly to the top of the boundary layer, and its leading edge travels slightly faster than SWP-1a. Vertical shear is also evident.

250 m Release: SWP-1c

Just as with SWP-1a and b, SWP-1c transports its plume of 250 m initial elevation with little horizontal dispersion but with strong vertical mixing. It is also similar in that the plume meanders with the inertial oscillation of approximately 20 hours and the shear layers develop in time. The leading edge of the plume reaches the Grand Canyon area at 37 hours (7 p.m. MST) just as the sun has set and the boundary layer has reduced in depth similar to the plume depiction in Figure 4.7. The leading edge of the plume at 37 hours is travelling between 800 and 1000 m because it has been subject to (at these heights)

to stronger horizontal flow. It is hypothesized that such pollutants would not impact the Grand Canyon due to the stability of the atmosphere during the overnight hours. It would not be until some 5-8 hours later, when the portion of the plume travelling in the lowest levels reaches the Grand Canyon area, that an impact would be felt at the surface.

500 m Release: SPW-1d

SWP-1d's release height caused the particle plume to travel slightly more quickly than the lower level releases SPW-1a through c during stable atmospheric periods. Since this plume was subject to the same boundary layer sequence as all of SWP-1, its characteristics of travel in time were very similar to those of SWP-1a through c (as depicted in Figure 4.7). For brevity those are listed below:

- Extensive mixing during deep boundary layer periods.
- Little or no mixing overnight and prior to boundary layer growth.
- Shearing with height in time.
- Leading edge reaches Grand Canyon region at ~36 hours. This edge is elevated.
- A slight meander with the period equal roughly to an inertial oscillation of 20 hours.
- A dilution factor of approximately 200.

Surface to 500 m Release: SWP-1e

As expected SWP-1e reveals little new information. It contains plume characteristics of each of the previous simulations except for its uniform, random release appearance during stable periods due to the nature of its initial configuration. Refer to the description of SWP-1d for a list of commonalities. During grown boundary layer periods, 1 p.m. – 6 p.m. of each day, its behavior and appearance are essentially similar to the same time periods of SWP-1a through d and is well represented by Figure 4.7.

4.4 SW-2: Simulation Analysis

4.4.1 Meteorological Results

By adding approximate real topography to the model conditions in SW-2, an attempt is made to represent the true fields that would exist over the domain. How the model interpolates the terrain data set to represent actual terrain is depicted in Figures 1.3 and 4.8 for Grids 1 and 2, respectively. Note how the model terrain on Grid 2 is more detailed than that on Grid 1 due to the smaller grid increment on Grid 2.

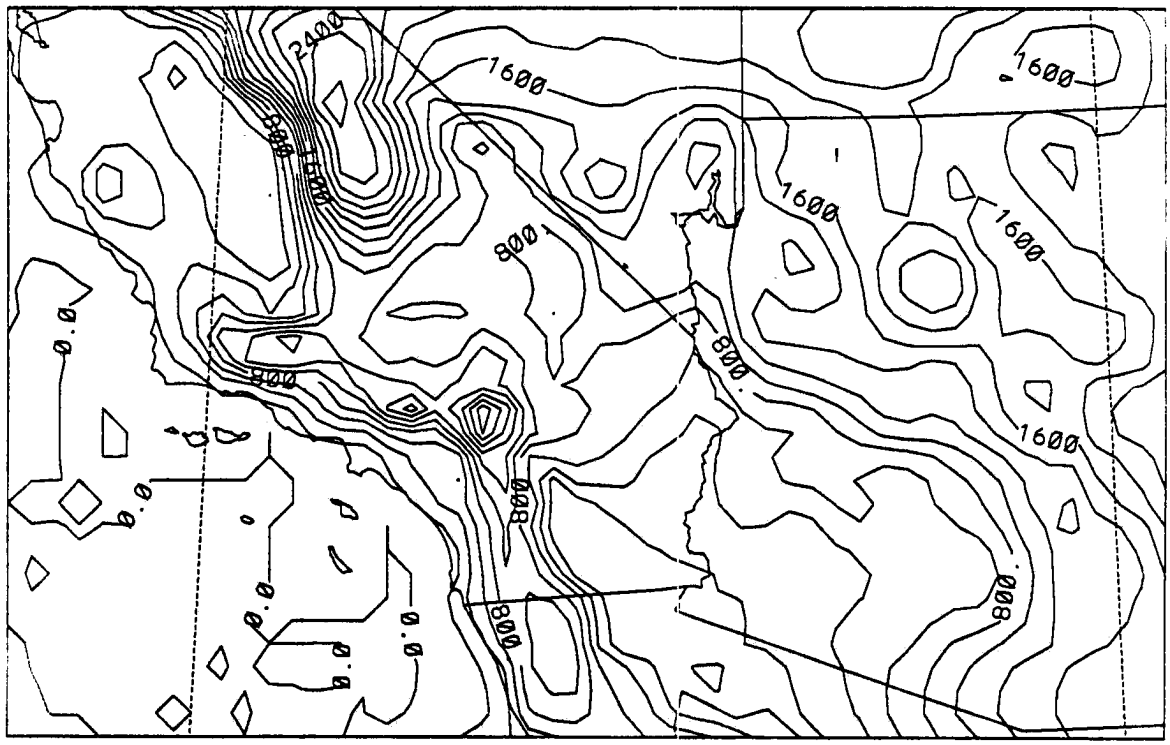

Figure 4.8: Topography on Grid 2 for SW-2. Contour intervals are 200 m. Note the additional terrain detail on Grid 2 compared to Grid 1 (Figure 1.3).

Potential Temperature

Figures 4.9 and 4.10 present vertical cross sections of potential temperature over the 24-hour period from 0080Z to 0800Z the next day (20 hours to 44 hours into the simulation) on Grid 2 at two different horizontal cross sections (see Figure 4.8 for the extent of Grid 2). Figure 4.11 shows the orientation of these cross sections on Grid 2. Note that by

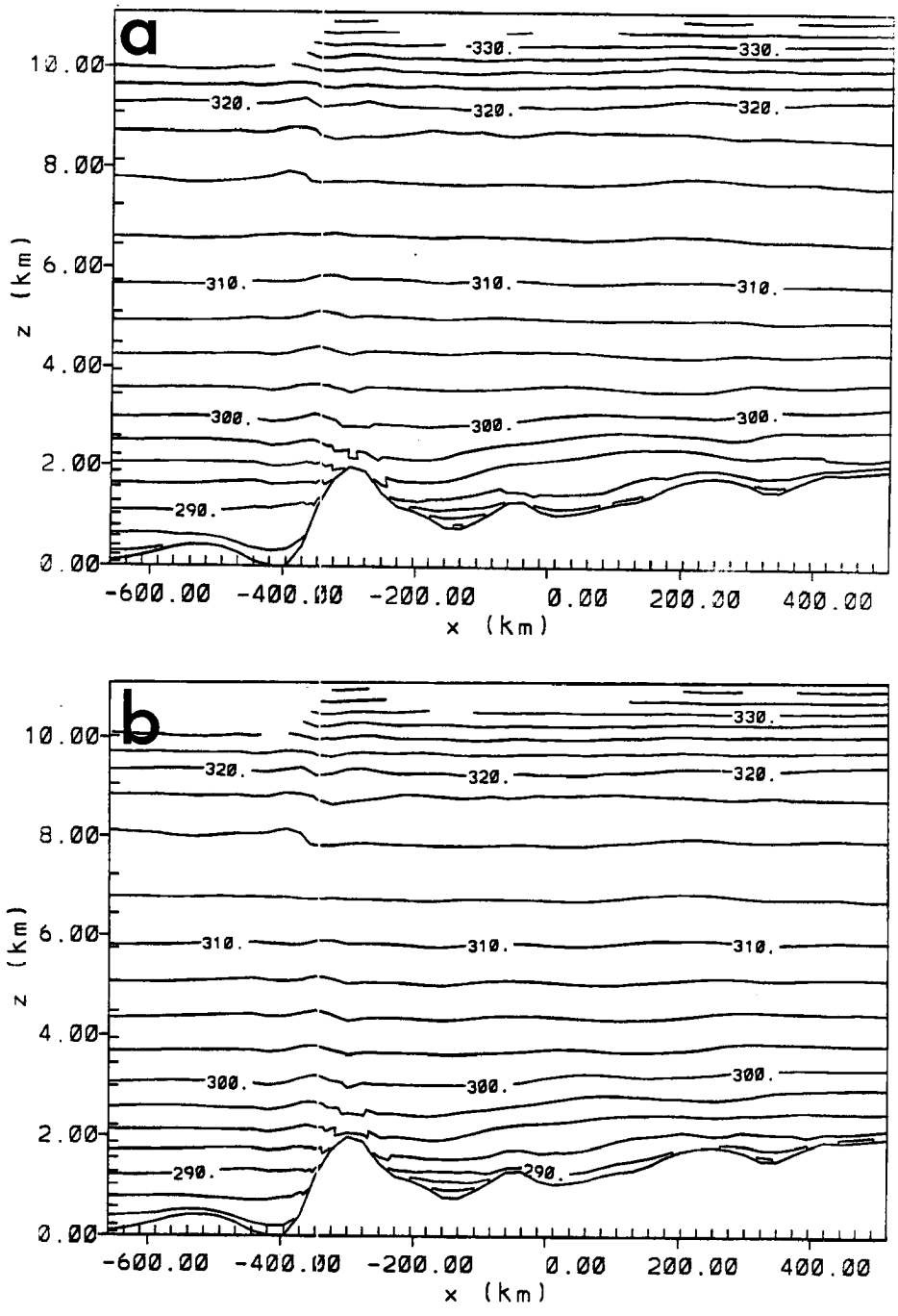

Figure 4.9: A vertical, $x - z$ cross section of potential temperature, θ, for SW-2 at 120 km north of the domain center point transecting the Grand Canyon for a 24 hr period in 4 hour increments at (a) 0800Z, hour 20; and (b) 1200Z, hour 24. Figure 4.9h is 24 hours earlier than 4.9d for comparison.

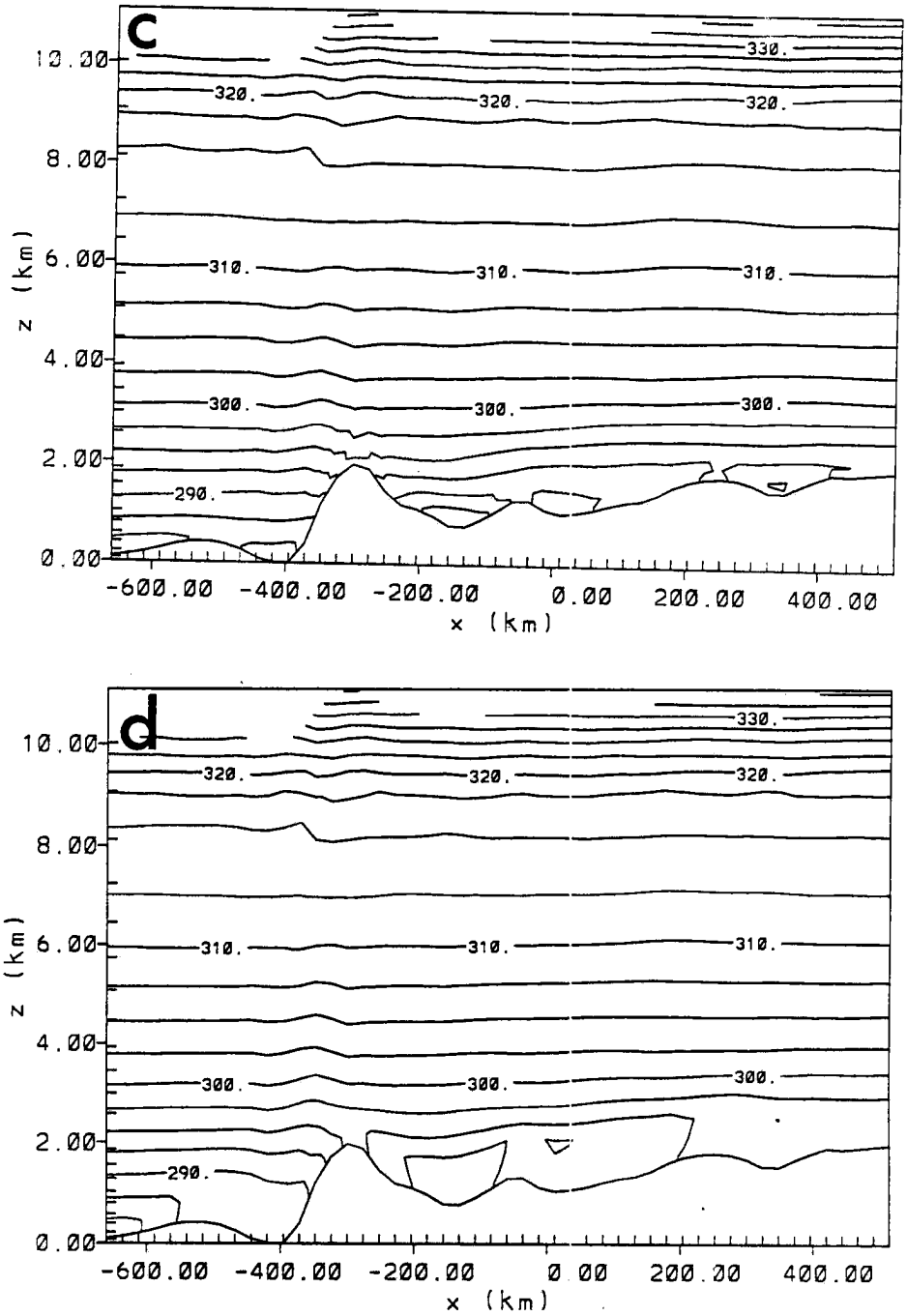

Figure 4.9: (c) 1600Z, hour 28; and (d) 2000Z, hour 32.

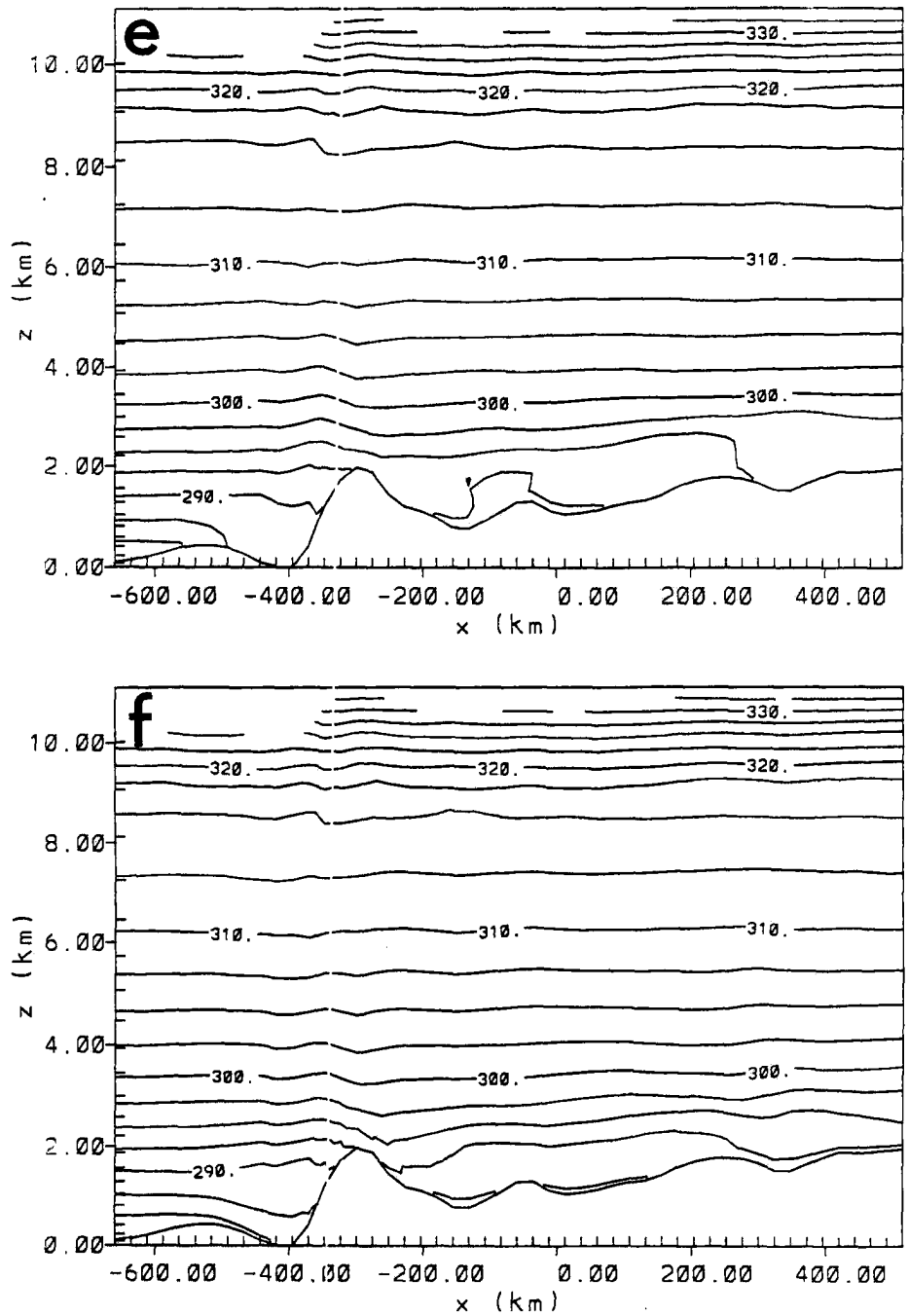

Figure 4.9: (e) 0000Z, hour 36; and (f) 0040Z, hour 40.

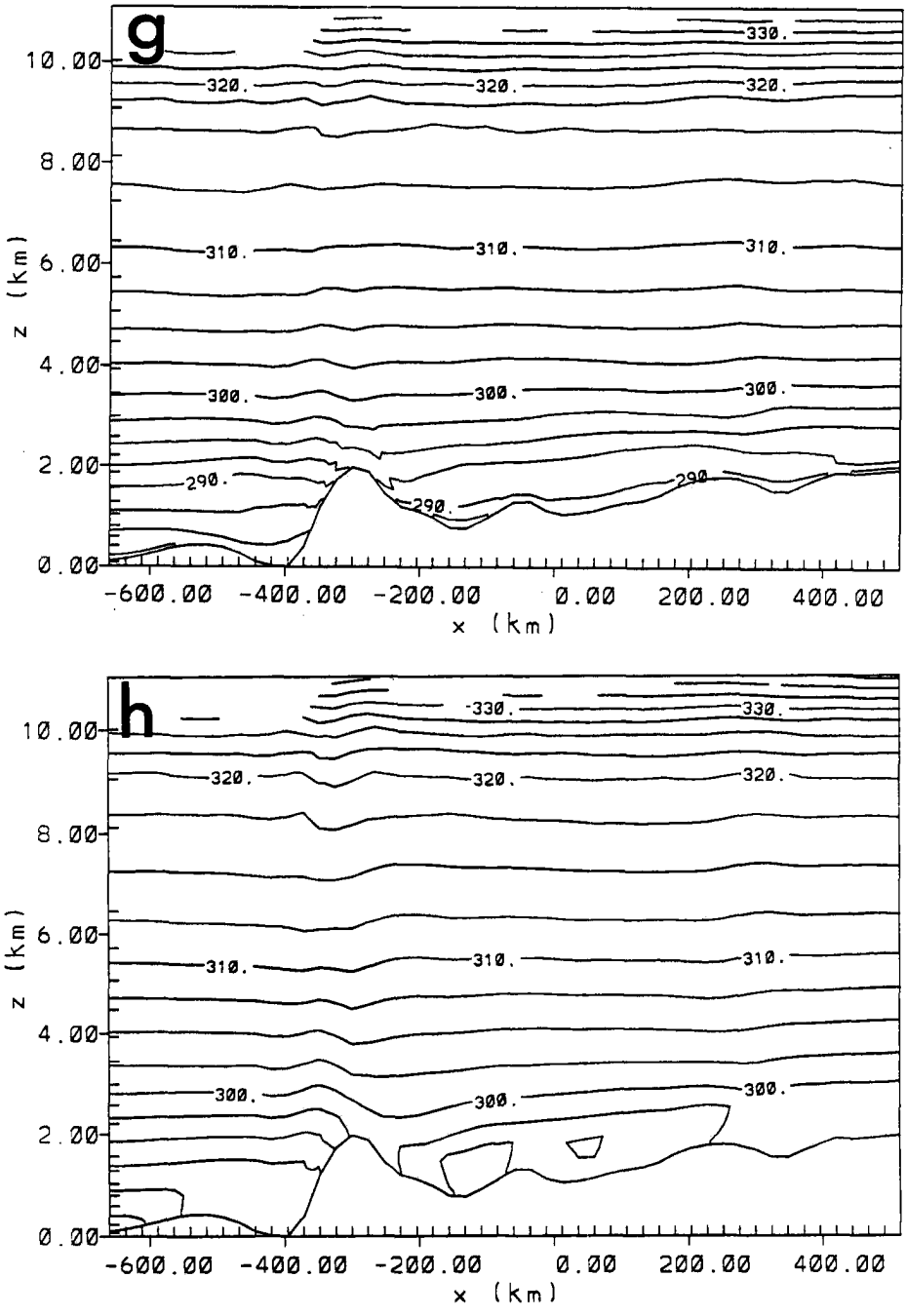

Figure 4.9: (g) 0800Z, hour 44; and (h) 2000Z, hour 8.

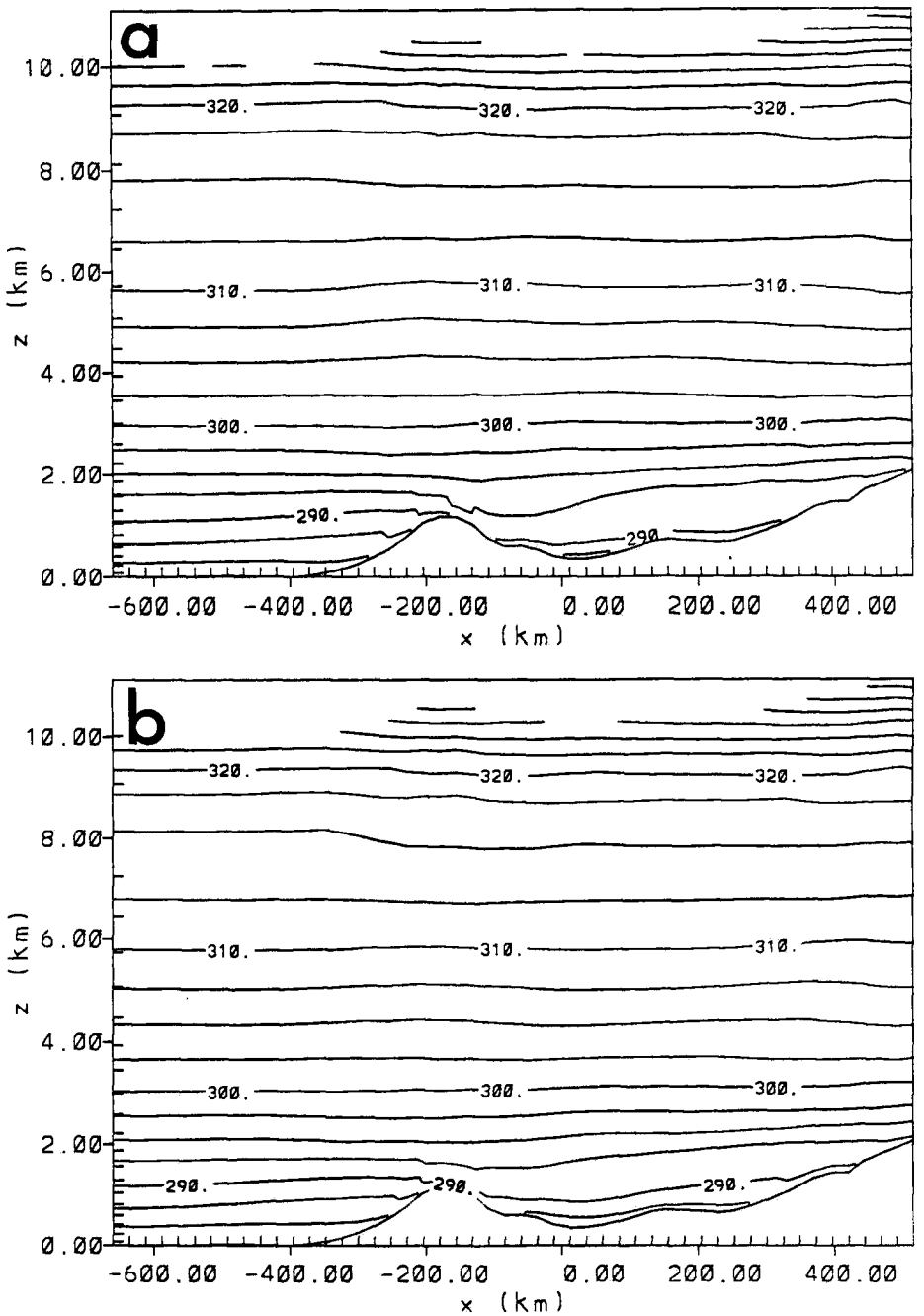

Figure 4.10: A vertical, $x - z$ cross section of potential temperature, θ, for SW-2 at 120 km south of the domain center point transecting the Los Angeles Basin at (a) 0800Z, hour 20; and (b) 1200Z, hour 24. See Figure 4.11 for the cross section locations. The contour interval is 2.0 K, and time interval is 4 hours beginning 20 hours into SW-2 continuing through hour 44.

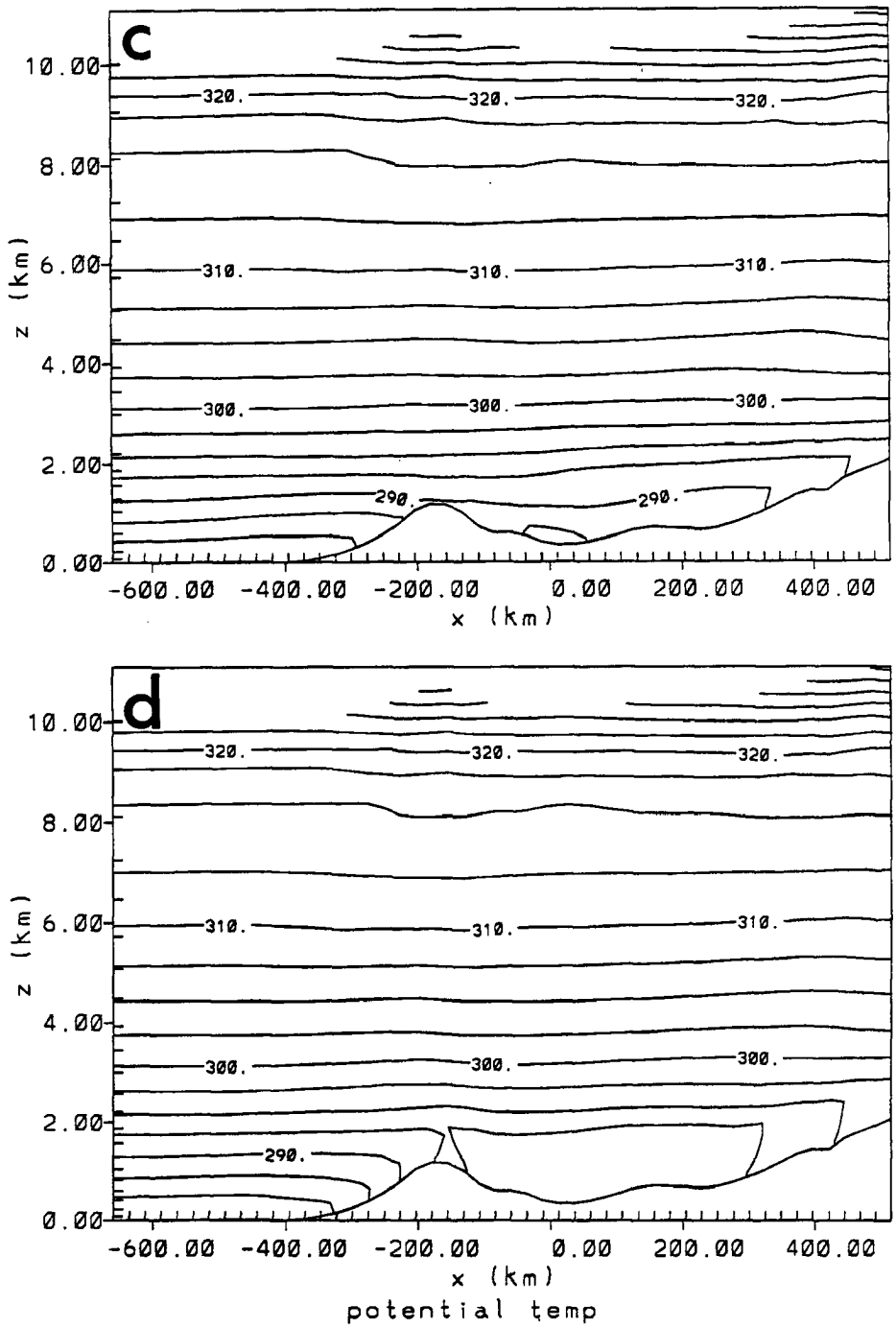

Figure 4.10: (c) 1600Z, hour 28; and (d) 2000Z, hour 32.

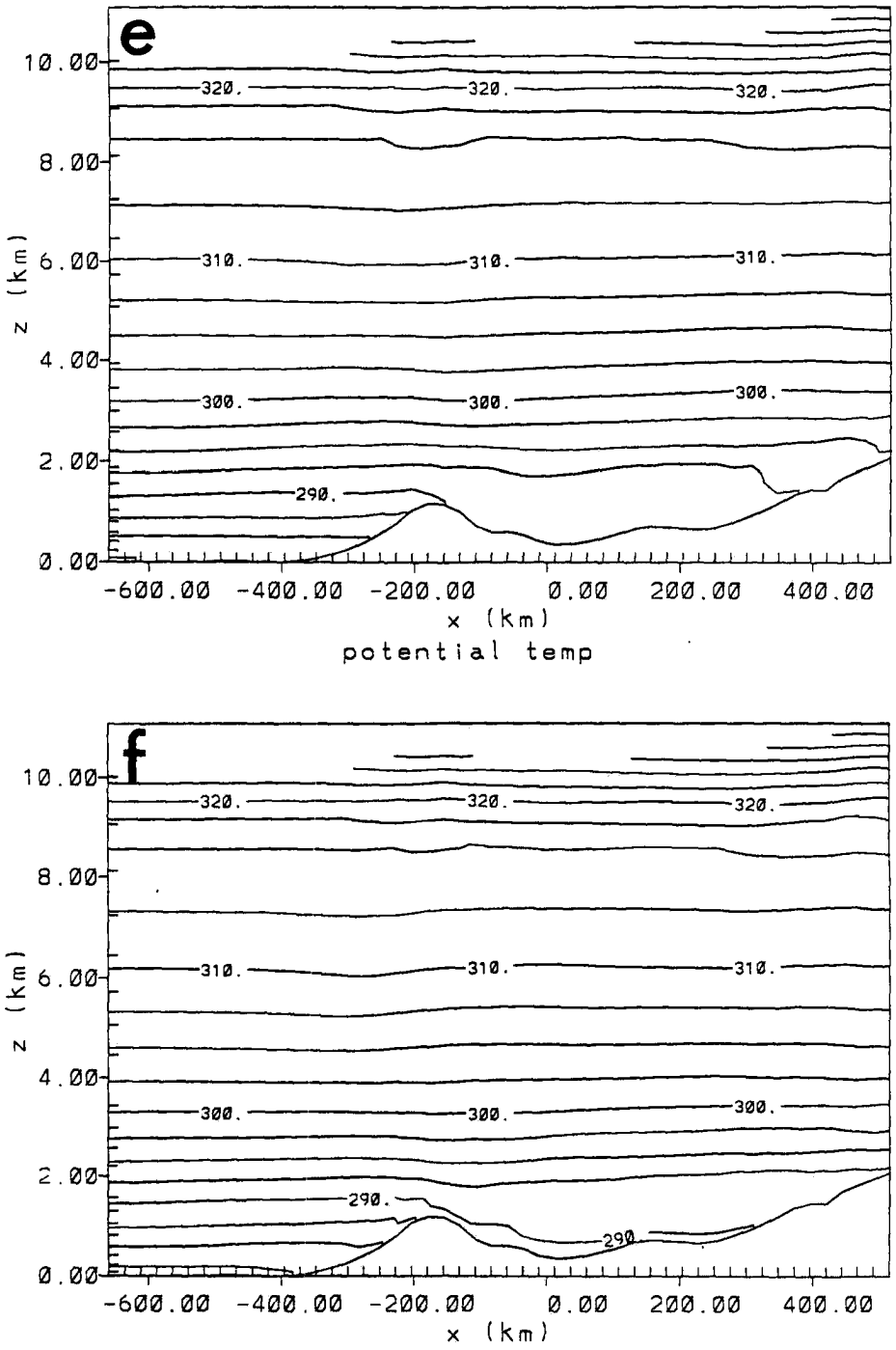

Figure 4.10: (e) 0000Z, hour 36; and (f) 0040Z, hour 40.

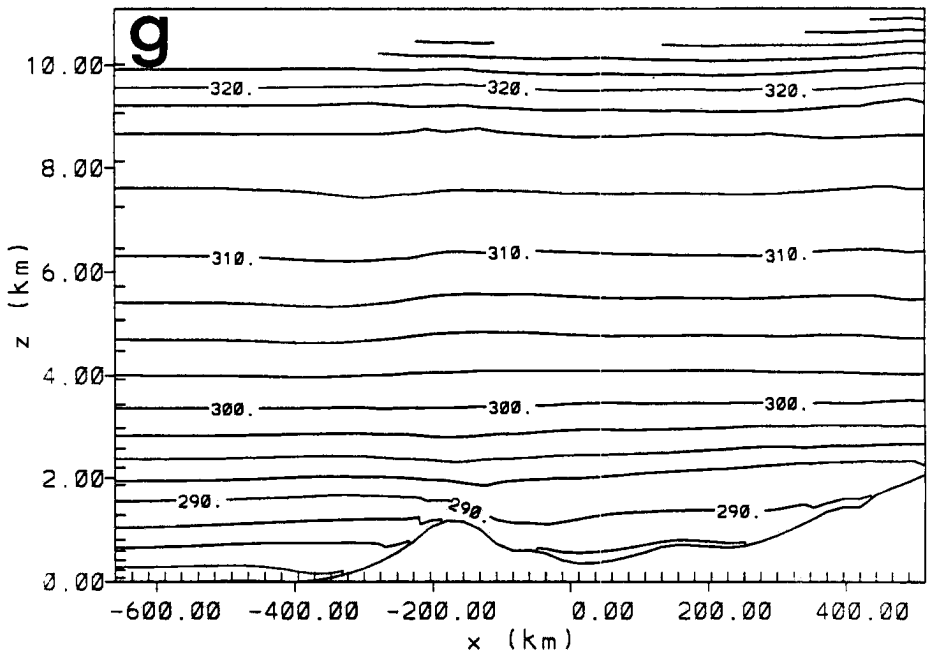

Figure 4.10: (g) 0800Z, hour 44.

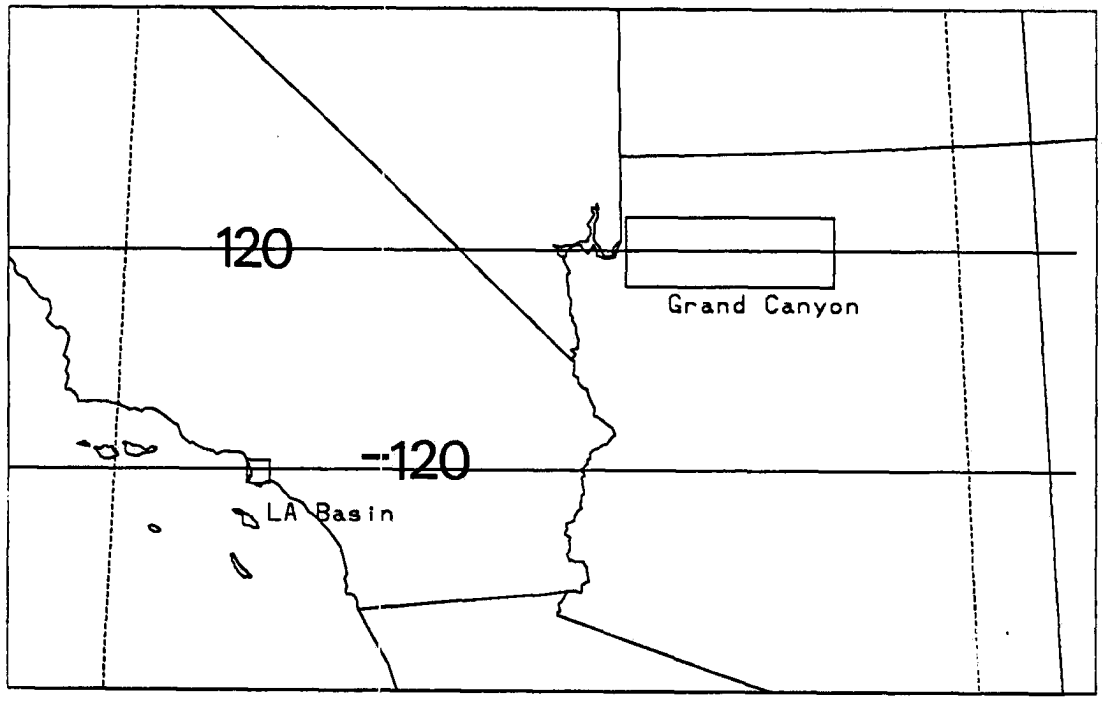

Figure 4.11: The location of the cross sections depicted in Figures 4.9 (upper horizontal line) and 4.10 (lower horizontal line).

1600Z the boundary layer, approximately represented by the area of vertical isentropes, has grown to approximately 500 m on the east side of the mountains. The boundary layer grows to 1 km by 2000Z and is reduced, as would be expected, into the evening and overnight hours (0Z – 12Z, next day). This first 24-hour period (Figure 4.9h) compares very favorably with the potential temperature fields of the next 24-hour period (Figure 4.9d). The effects of the Pacific Ocean on the boundary layer can be seen in the reduced depth of the boundary layer throughout the daytime on the west side of the mountains compared to the high desert (east side of the mountains). For comparison, Figure 4.9h shows the potential temperature field at 2000Z (2 p.m. MST) but 24 hours earlier than the 2000Z isentropes in Figure 4.9d. Differences that exist are primarily where expected, in the lowest 3-4 km of the domain. No direct comparison with observations is strictly valid because the initial conditions were composited, however, the surface temperatures are generally within 4°C of actual surface temperatures during the WHITEX period.

Horizontal Winds

Wind fields are the single most important variable affecting dry, non-reactive pollutant transport Since moisture fields are not modeled with microphysics in this study, the generation of reasonable winds within the simulations is of the greatest importance. Figure 4.12 depicts the time evolution of horizontal wind vectors for the 24-hour, mid-simulation period 0080Z – 0080Z, next day, in 4 hour intervals on Grid 2. These are the near-surface vectors at 73.2 m above the ground on z^* surfaces (terrain-following). At 0000Z (early evening, 6 p.m. MST) the winds have significantly altered from their initial west-southwesterly path. This is in stark contrast to the comparatively uniform field over flat terrain (SW-1, Figures 4.5 and 4.6). The inclusion of real terrain to SW-2 has, as expected, completely changed the windfield evolution. Of course, then, pollutant trajectories are considerably different when released into SW-2's environment, compared to that of SW-1. In the northern portion of Grid 2, the severe terrain of the southern Sierra Nevada mountains have forced impinging winds to diverge to the south causing eventual convergence with west and southwesterlies in south central California north of Los Angeles ($\approx$150 km). This convergence, combined with the relatively high altitude, creates the

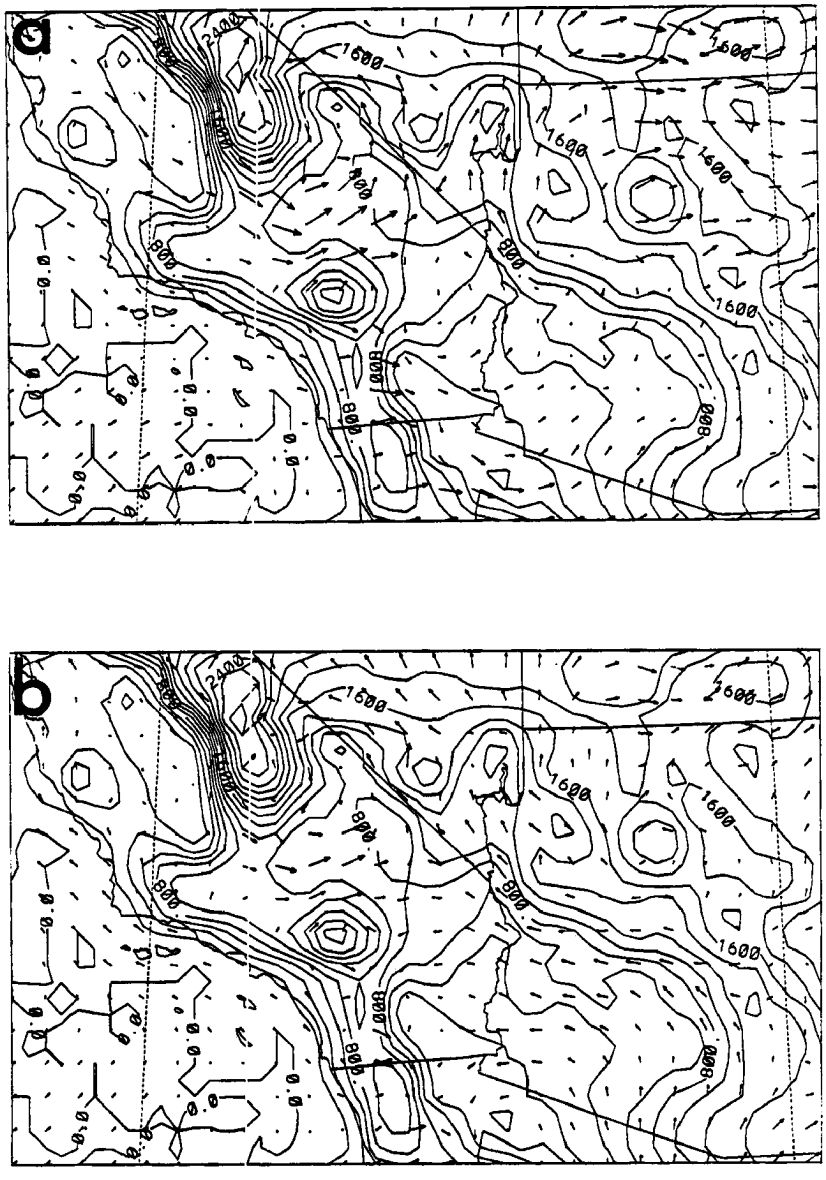

Figure 4.12: The evolution of horizontal wind vectors on Grid 2 for SW-2 at 73.2 m above ground level for the period 20 hours to 44 hours into the simulation (2 a.m. – 2 a.m. MST) in 4 hour intervals at (a) 0800Z, hour 20; and (b) 1200Z, hour 24. Topography is included in 200 m intervals to better show the effects of terrain. The longest vector represents ~9 m s^{-1}.

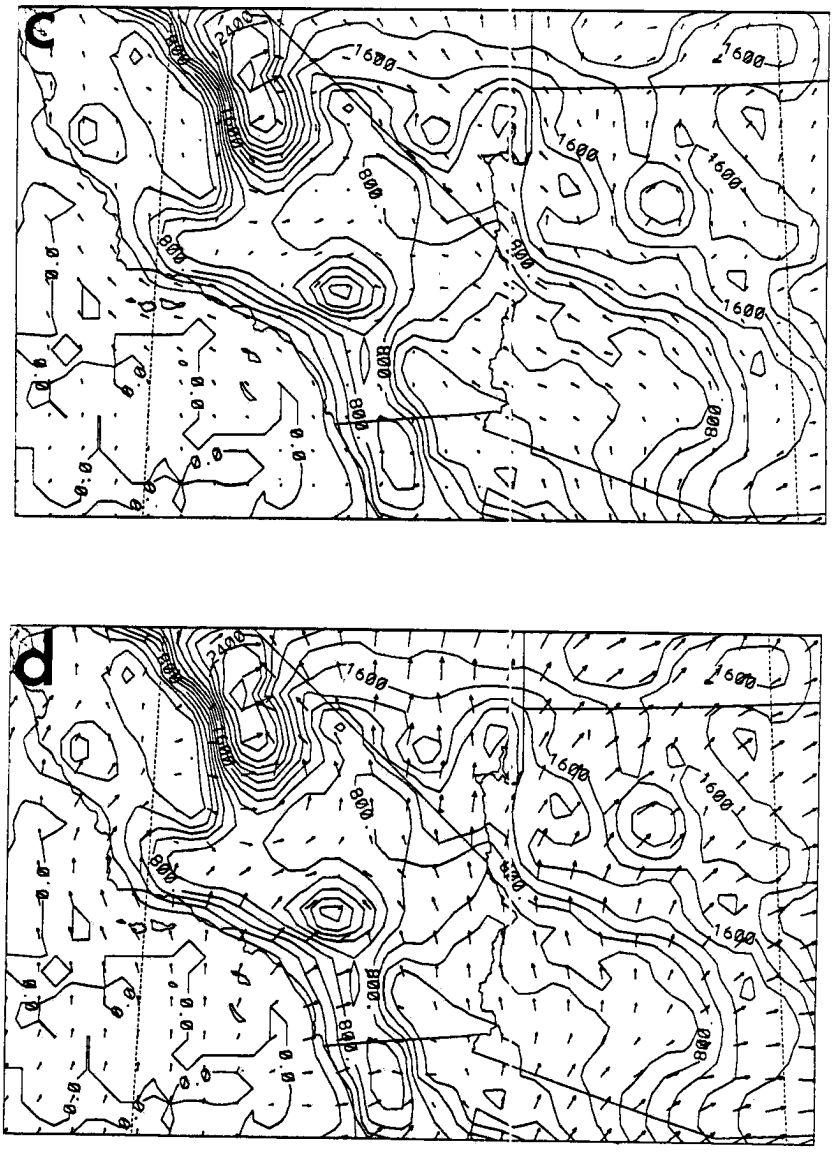

Figure 4.12: (c) 1600Z, hour 28; and (d) 2000Z, hour 32.

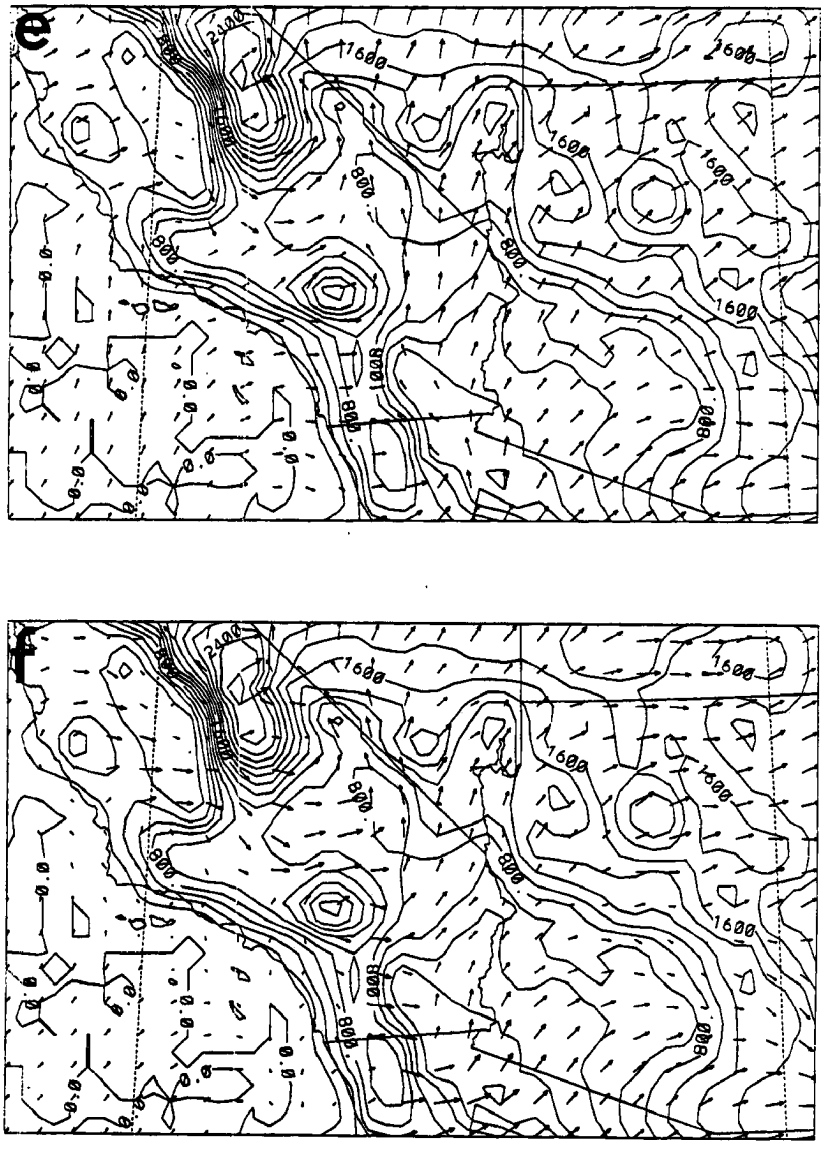

Figure 4.12: (e) 0000Z, hour 36; and (f) 0040Z, hour 40.

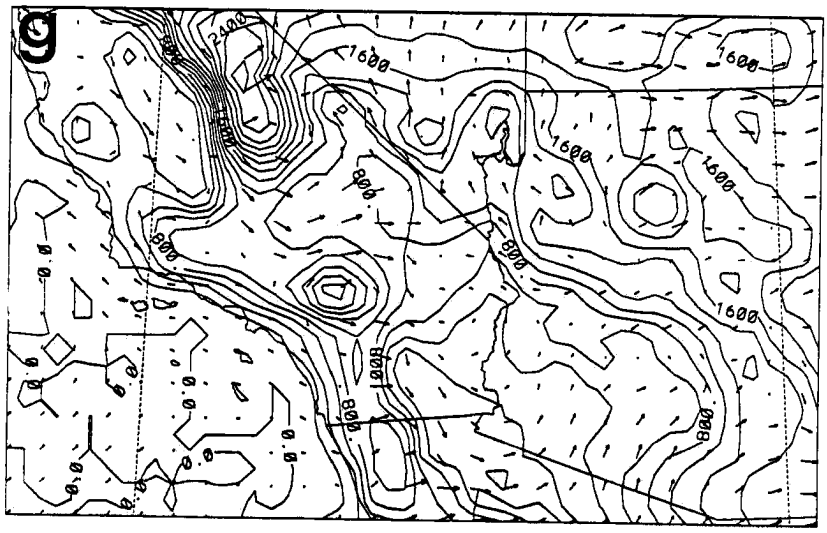

Figure 4.12: (g) 0800Z, hour 44.

strongest winds, 9.8 m s^{-1}, within the domain at this point. To the east of the California mountains winds become northerly and even form a counterclockwise circulation just east of the southern Sierras. Two low-level transport routes appear in the Los Angeles Basin region. The first follows to the northeast through the region representing Cajon Pass. The region does not appear as a 'pass' because of the topography smoothing done within RAMS but is a ridge-like feature. When a fine nest is added over the LA Basin with 8 km grid increment, as in SW-3, such smaller scale features are considerably better represented. The second route goes through Banning Pass. Both routes have been noted as pollutant transport routes in previous studies (Ulrickson and Mass, 1990; McElroy, 1987).

In Southern Arizona the initial southwesterly flow has backed to the southeast, apparently due to low-level terrain forcing by the Mogollon and Colorado Plateaus in central Arizona. This creates a convergence zone in the Mohave desert; a potential location for pollutant accumulation and circulation. Similar turning of the low-level winds occurs as southwesterly initial winds impinge on the Cococino Plateau approaching the Grand Canyon region. Winds become upslope to the elevated land masses. This is noticeable in Northern Arizona where terrain heights vary (compare wind flows to terrain in Figure 4.12).

At the 1 km level the horizontal wind is, as expected, considerably less influenced by terrain than at the 73 m level (see Figure 4.13). Some evidence of an inertial oscillation as was seen in SW-1 appears in SW-2; note the veering of the wind from southwest to west, particularly at upper levels (as shown by vectors above higher terrain). Maximum wind speed is maintained well, remaining consistent between 8 m s^{-1} and 11 m s^{-1} once the model has sufficiently adjusted approximately 6-10 hours into the simulation. Prior to the adjustment to the idealized initial conditions the wind flows, while consistent in direction, are higher in speed by 10-40% over the adjusted fields at 12 hours. Note the consistency between the 1600Z + 2 days (Figure 4.13h) and the 1600Z + 1 (Figure 4.13c) day horizontal wind vectors. This comparison suggests that the model has developed its own consistent solution describing how the atmosphere would react to the given terrain, solar insolation, and idealized initial conditions. Within this regime the pollutant pathways

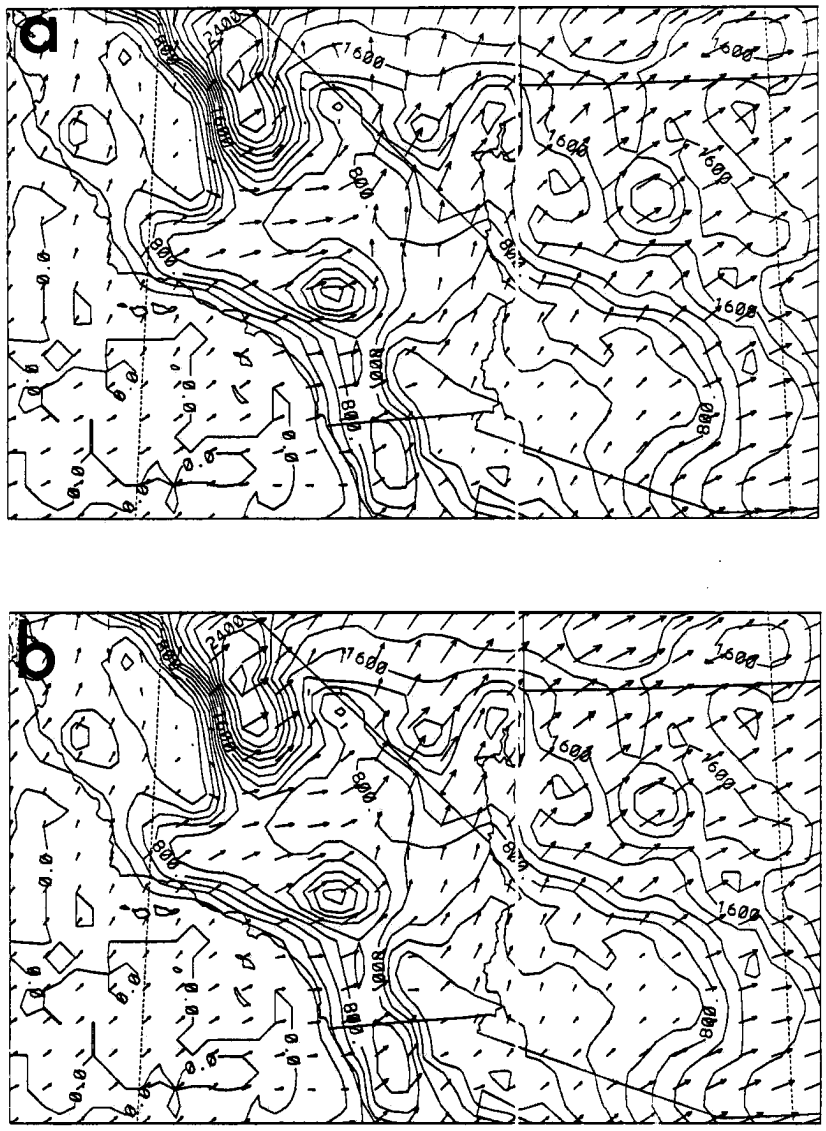

Figure 4.13: Same as Figure 4.12 except for 1033.7 m above ground level at (a) 0800Z, hour 20; and (b) 1200Z, hour 24. The longest vector represents $\sim$10 m s^{-1}.

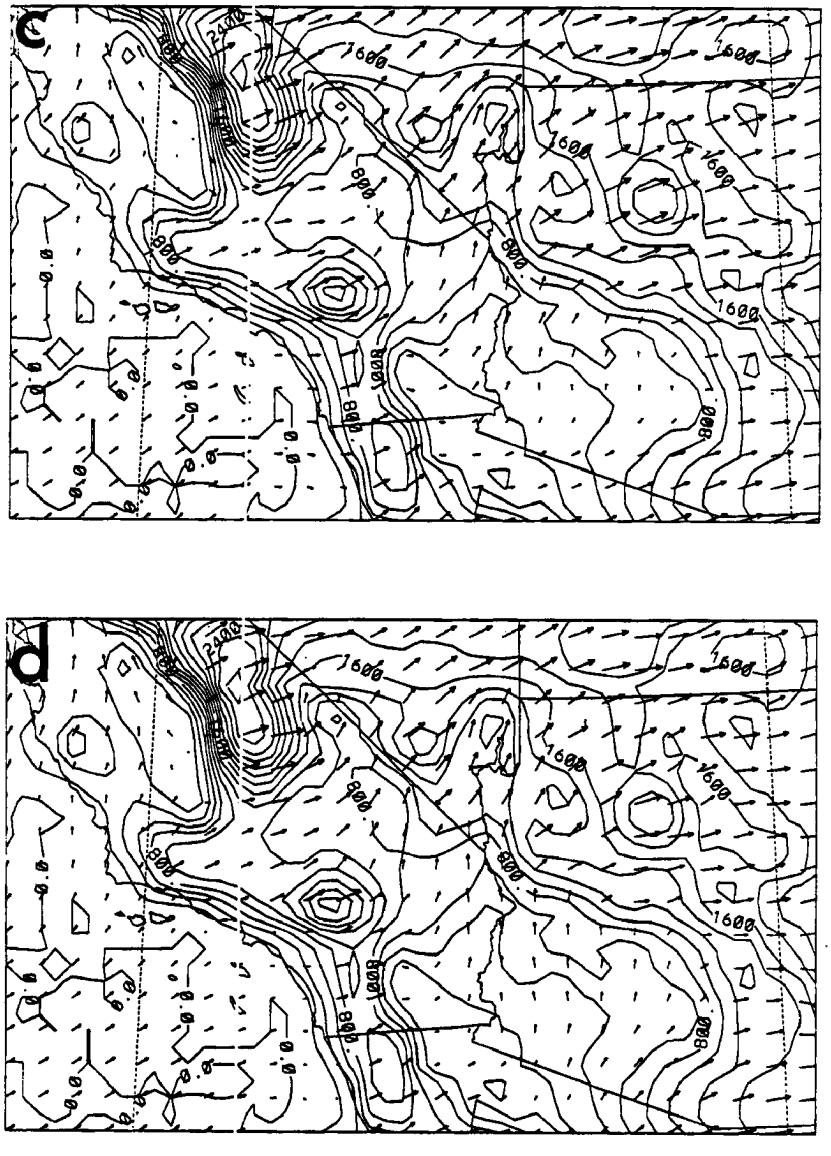

Figure 4.13: (c) 1600Z, hour 28; and (d) 2000Z, hour 32.

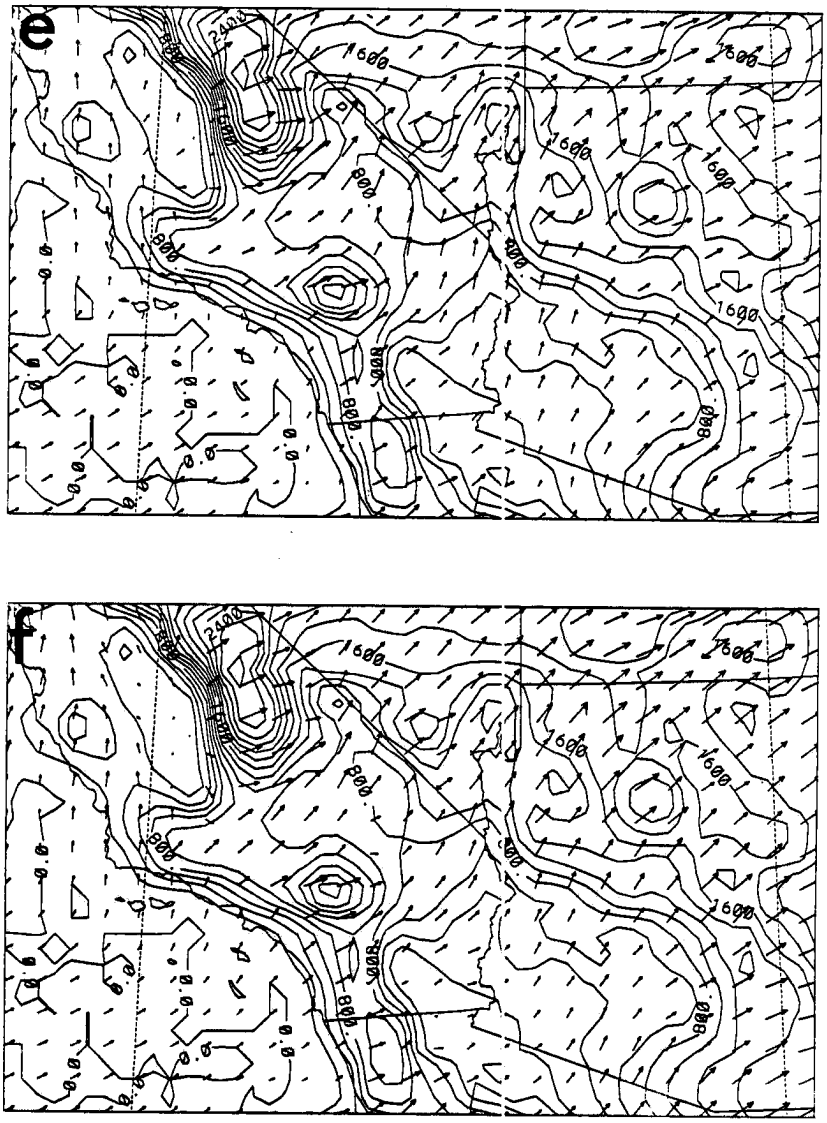

Figure 4.13: (e) 0000Z, hour 36; and (f) 0040Z, hour 40.

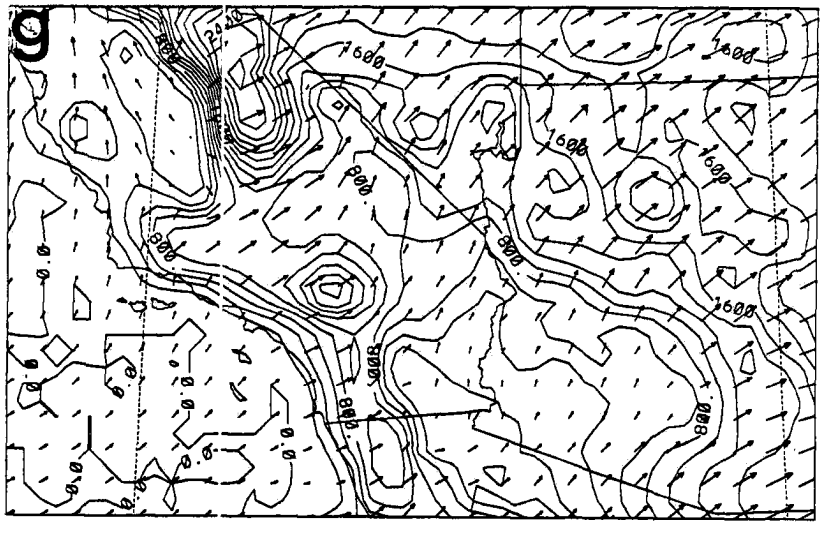

Figure 4.13: (g) 0800Z, hour 44.

to the northeast and east of Los Angeles are much less distinct. At the height of 1 km terrain forcing appears to be limited to large-scale variations in flow. An exception to this can be found over the severe terrain of the southern Sierra Nevadas where wind vectors consistently diverge on the mesoscale.

At 3 km (not shown) the terrain influence is even more limited than at the 1 km level. Model adjustment to terrain effects is limited to approximately a 20% reduction in initial maximum windspeed. After adjusting, windspeed maxima are approximately 13 m s^{-1}. The inertial oscillation of SW-1 and at the 1 km level of SW-2 is further evident at 3 km. Southwesterly-westerly flow is maintained throughout the simulation to varying degrees. This level is far less influential on pollutant transport due to its altitude above any anthropogenic source.

Vertical Wind

Figure 4.14 shows the 24-hour evolution of vertical wind, w, from 20 to 44 hours into the simulation along the LA Basin transect. The simulation is generally characterized by weak vertical motion except in mountainous regions where positive and negative motions peak near 10 cm s^{-1}. As seen in Figure 4.14 the model is able to simulate the upward/downward vertical motion couplet typical of mountain-induced gravity waves. On the mountainside, evidence of upslope flow from solar heating is evident. Pollutants transported into the mountainous area would become subject to strong mixing and be lifted to upper levels. That mountainsides are areas of strong ventilation of Los Angeles pollution has been hypothesized by Ulrickson and Mass (1990a,b), and Segal et al. (1985). Similarly, in the overnight periods, as shown in Figure 4.14a, f, and g shows katabatic mountain drainage flows up to 6 cm s^{-1}. The strength and expanse of such vertical motions emphasizes the differences in dispersion that are expected to occur between the true terrain and flat terrain simulations. One expects increased dispersion and a lessened impact of Los Angeles produced pollution on the Grand Canyon simply due to the existence of complex terrain in the Los Angeles to Grand Canyon corridor.

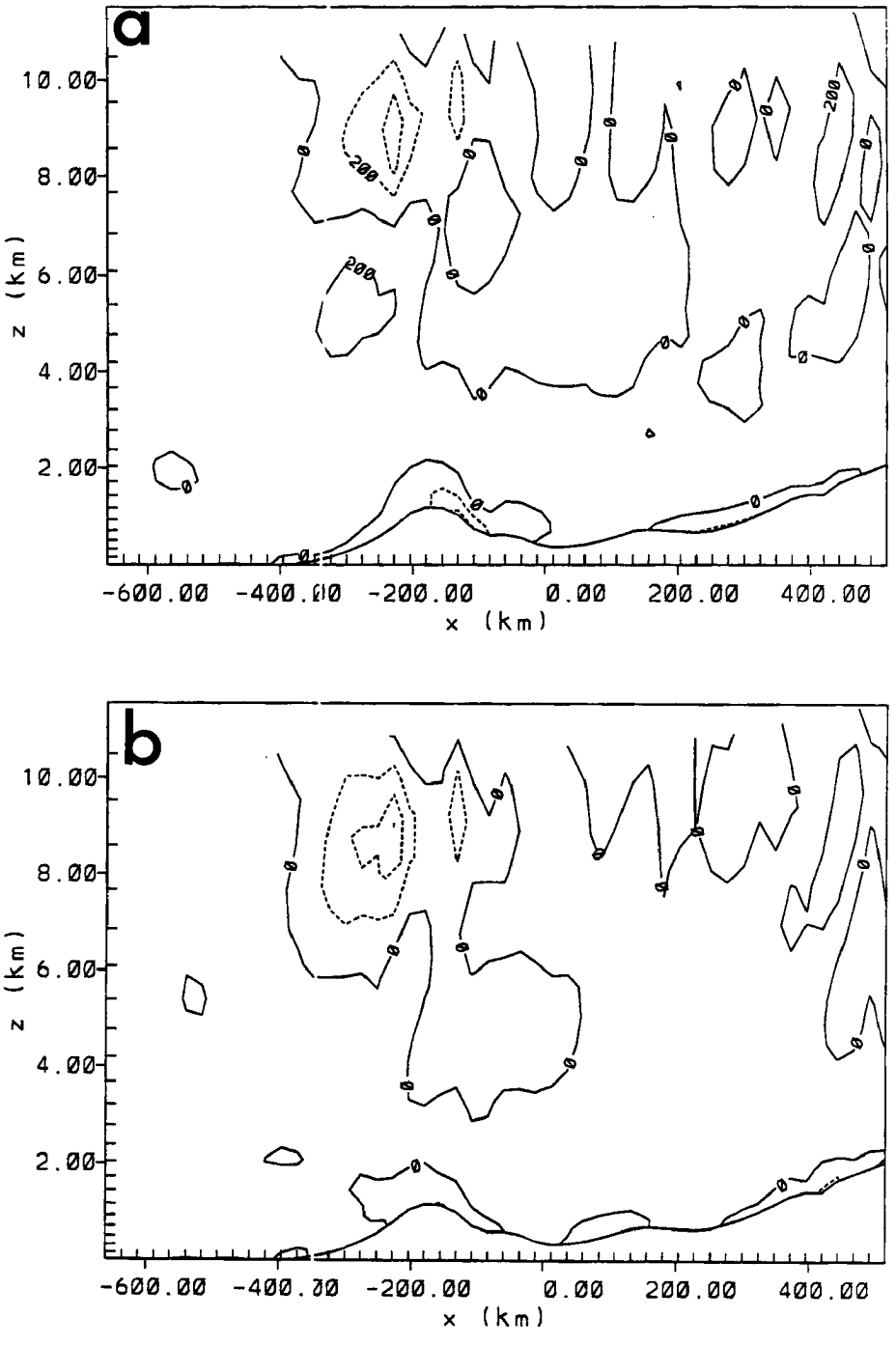

Figure 4.14: The time evolution of vertical motion, w, for SW-2 at the Los Angeles Basin transect for 20 to 44 hours in four hour increments at (a) 0800Z, hour 20; and (b) 1200Z, hour 24. Contours are at 2 cm s^{-1} intervals. This cross section is depicted as the southern horizontal line in Figure 4.11.

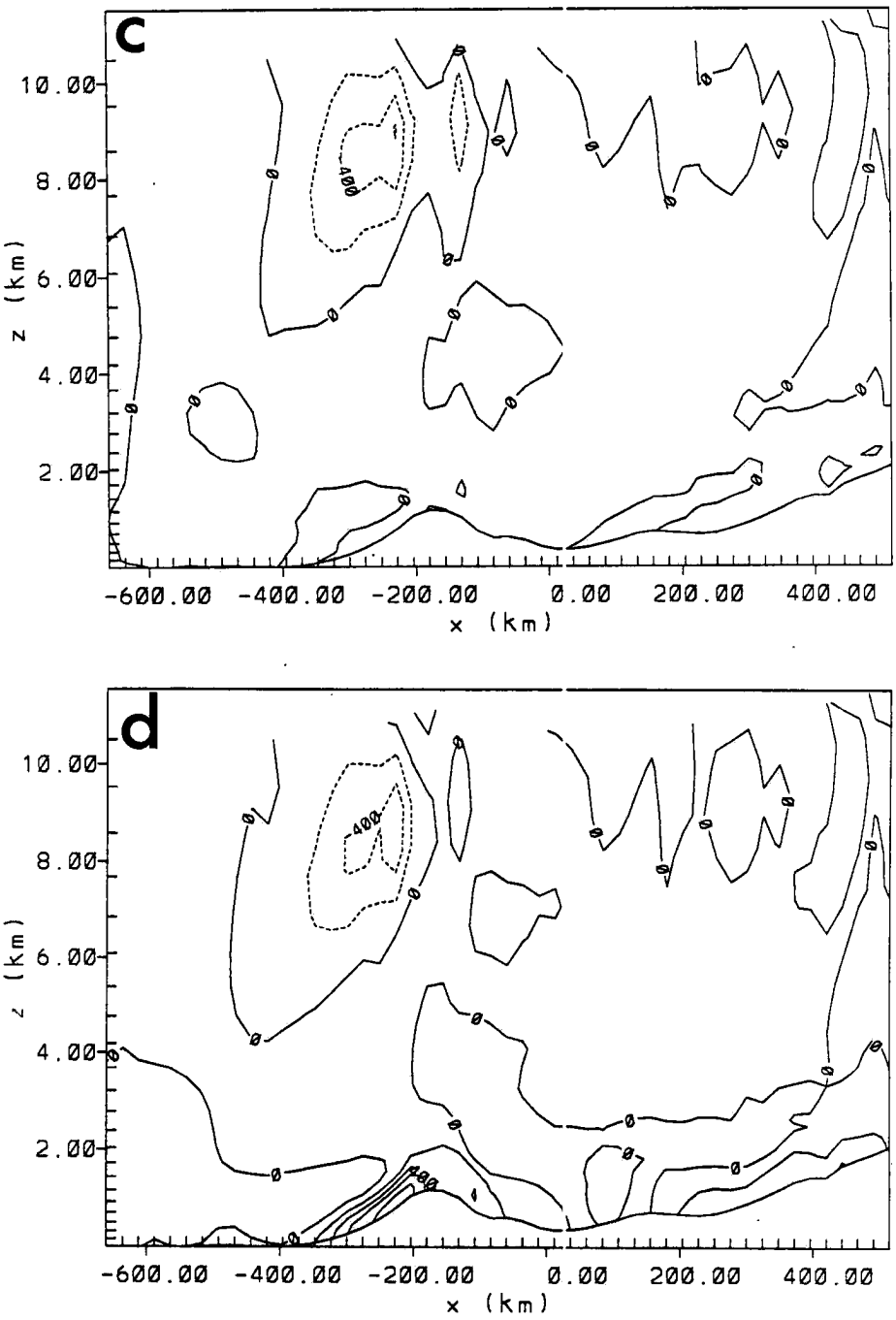

Figure 4.14: (c) 1600Z, hour 28; and (d) 2000Z, hour 32.

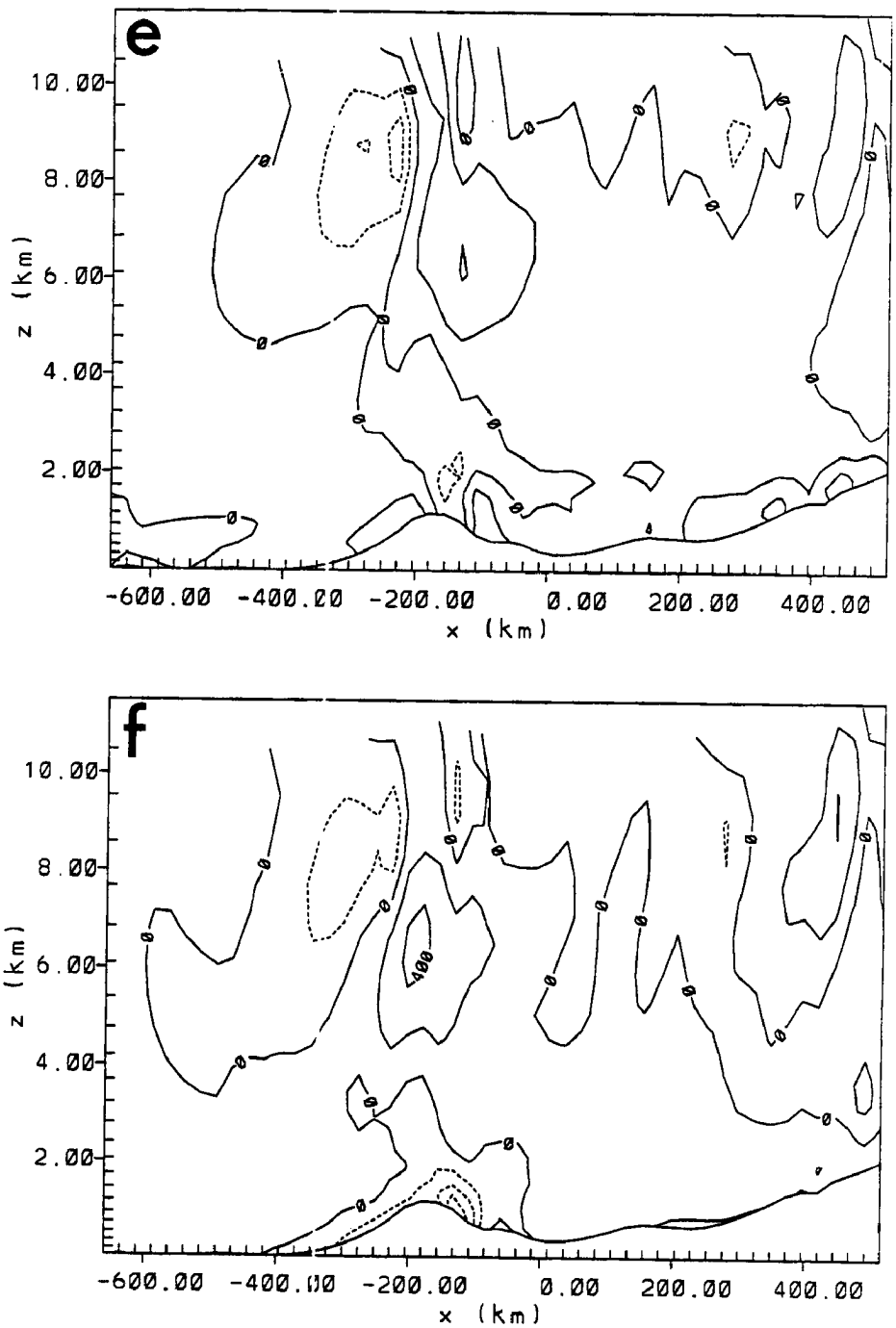

Figure 4.14: (e) 0000Z, hour 36; and (f) 0040Z, hour 40.

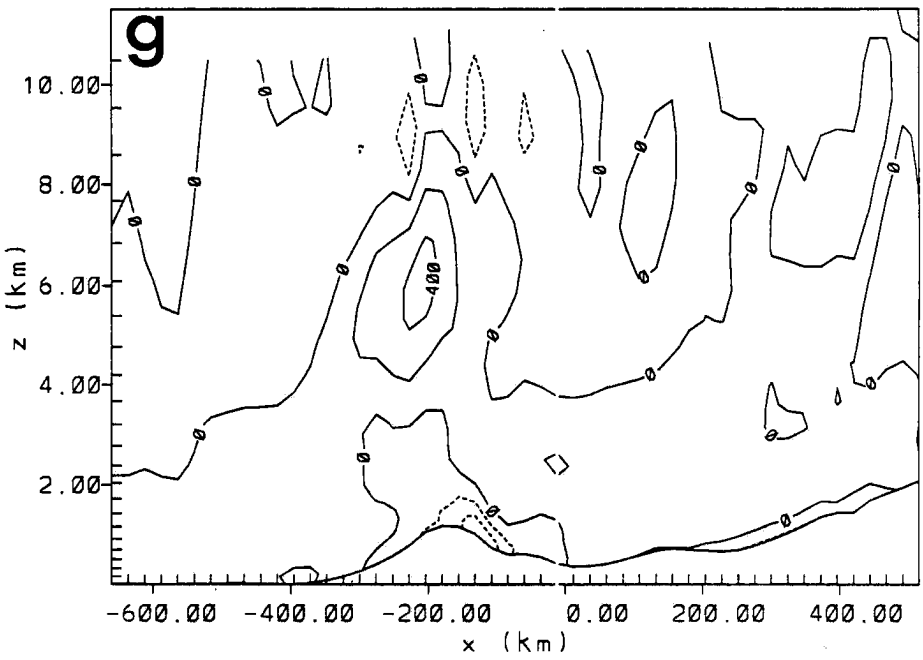

Figure 4.14: (g) 0800Z, hour 44.

4.4.2 LPDM Results: SWP-2

By running with Lagrangian Particle Dispersion Model, using the realistic terrain and more complicated fields of SW-2, numerous insights into the processes effecting pollutants transported out of the Los Angeles Basin are found. In comparison to the relatively simple dispersion characteristics of SWP-1, SWP-2 describes a complicated diurnal cycle of pollutant flow in the Los Angeles–Grand Canyon corridor.

Similar to SWP-1, SWP-2 contains five different types of random volume releases from within the confines of the Los Angeles Basin. The releases are exactly the same in dimension as SWP-1 but are elevated somewhat by the inclusion of terrain in SW-2. As with SWP-1 a rectangular pancake-like volume is the release location for four of the LPDM runs, its dimensions are ~29 km × ~29 km × ~20 m. This rectangular box is centered on release heights of 10 m (surface), 100 m, 250 m, and 500 m. A fifth run was completed which extends from 0 m to 500 m in the vertical (representing a deep volume source). Particle positions were saved every 15 minutes allowing the animation of 210 consecutive files out to 54 hours. The particle release was begun at 45 minutes into the simulation and ended at 54 hours with one particle releasing every 250 seconds. A total of 767 particles were released throughout each simulation.

0–20 m, 100 m, and 250 m Releases: SWP-2a through SWP-2c

SWP-2a through SWP-2c represent continuous releases from close to the surface, 100 m and 250 m, respectively. The animation of particle transport over a 54-hour period reveals numerous atmospheric effects complicating flow out of the LA Basin. Figure 4.15 presents an $x-y$ view of particle transport out of the LA Basin in time based on SWP-2e. Because SWP-2e is a deep release (surface to 500 m) it generically represents the features that exist in SWP-2a through 2c. For brevity, this figure will be referred to in all SWP-2 discussions (a-e).

0–4 hours: During this period the model is still adjusting to terrain feature effects and southwesterlies (as were initialized) exist throughout the domain. Particles

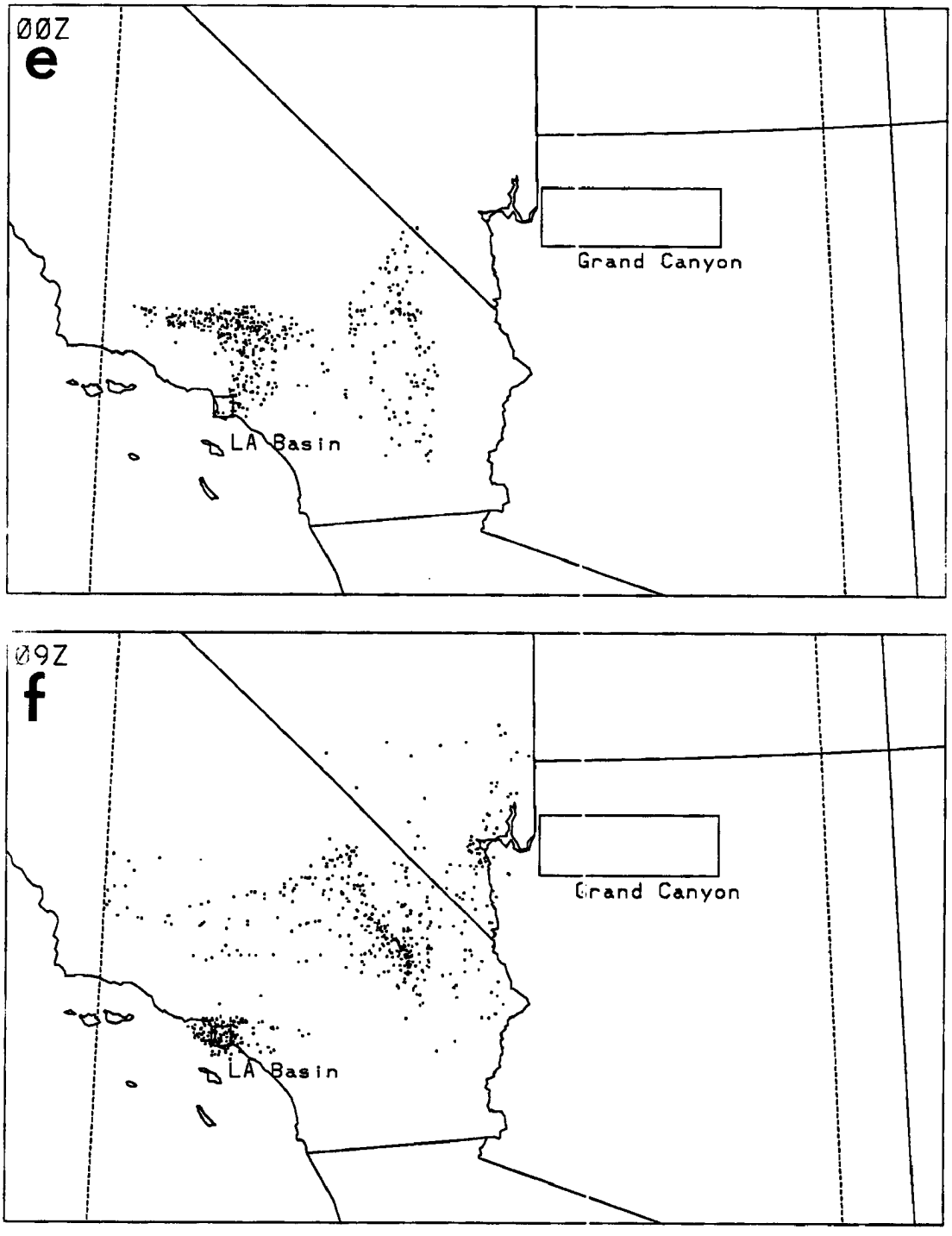

Figure 4.15: (e) 0000Z, hour 36; and (f) 0900Z, hour 45.

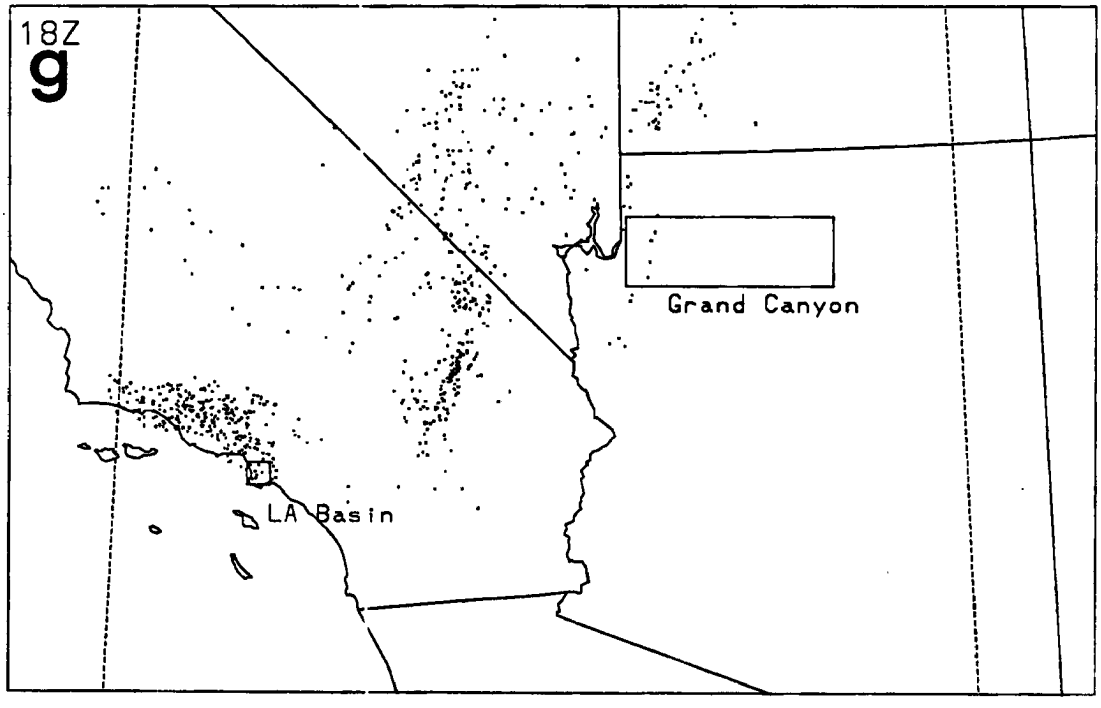

Figure 4.15: (g) 1800Z, hour 54.

are trapped within the LA Basin by weak southwest winds which force particles into the mountains but cannot rise over due to atmospheric stability prior to boundary layer development.

4–12 hours: The boundary layer grows and decays during this period. Mixing reaches its maximum and particles are vertically transported to 800 m or more where higher horizontal winds take particles over the mountains supported by upslope flow to the east of LA into the high Mohave desert. Preferred transport routes are noticeable through Cajon Pass (which the model topography represents as a low ridge) and Banning Pass, while numerous particles are also able to travel over the mountains of San Bernardino National Forest at maximum boundary layer depth.

12–28 hours: During this evening/overnight/early morning period the boundary layer is reduced in depth and the atmosphere becomes quite stable. Because newly released pollutants are, for the most part, trapped within the shallow boundary layer (< 100 m), they reside near the surface and are subject to low-level, terrain-influenced winds. Particles released in the LA Basin are brought by easterly land drainage winds to the west (toward the ocean) *away from* the Grand Canyon. Once reaching the ocean they converge with the southwesterlies prevailing there, unaffected by drainage flows. This convergence contains particles along the mountains to the north of LA in an east-west line. The convergence is weak enough such that the pollutants remain in low levels. The high desert particles are trapped by atmospheric stability as well, being subject to a weak anticyclonic desert circulation near the east side of the San Bernardino National Forest. No particles travel toward or reach the Grand Canyon in the first 28 hours of this simulation.

28–36 hours: Similar to hours 4-12, this period is the daytime of day 2 where the boundary layer grows to nearly 1 km. Strong mixing takes the once-trapped particles to upper levels where stronger winds are able to advect them. Particles that were accumulating to the north of Los Angeles quickly rise

and move over or around the mountains in southwesterly flow. Newly released particles in the LA Basin again (similar to hours 4-12) exit to the Mohave Desert via Cajon and Banning Passes, predominantly. Particles which were trapped in the high desert overnight now begin to move again to the north and east. They do not, however, achieve the Grand Canyon in large numbers. Instead, since model winds have been forced to become south-southwesterly by terrain and atmospheric physics, the particles move north passing to the west of the major vistas of the Grand Canyon. Five of the approximately 100 particles released from the LA Basin during the previous day cross the far western edge of Grand Canyon National Park late in this period. Even so, the height at which they travel, 200-1000 m above ground level, suggests their entrainment in the Canyon is unlikely overnight. By no means, in this specific study, is the Los Angeles influence able to exceed 0.5% of its initial concentration at the far western end of the Grand Canyon National Park. The Grand Canyon's primary vistas are subject to considerably less than 0.5% and are perhaps unaffected.

36-52 hours: This period is quite similar to the 12-28 hour period described earlier, with the exception of those particles which have traveled to the west and north of northern Arizona. While about two-thirds of these particles have become trapped in the shallow overnight boundary layer and travel slowly in the complex mountain flows of eastern California, Nevada, and southern Utah, another third are not trapped by the boundary layer. This third travels at upper levels, where the southwesterlies are consistent and strong. The particles move with this flow off to the northeast. No additional particles affect the Grand Canyon.

SWP-2a through SWP-2c shows that surface LA Basin particles, released to represent approximate worst-case conditions of flow toward the Grand Canyon, are strongly influenced by terrain-induced meteorological flows. Terrain effects are so significant at

these low levels that dilution is increased to 1000-2000 from 100-200 for a no-terrain simulation (see SWP-1 description). This increase in dilution factor is based on the fact that an order of magnitude fewer particles are able to impact the Grand Canyon region in SWP-2a through c. Whereas 70 particles were over GCNP in the worst case of SWP-1, only 7 particles impacted GCNP in the worst case of SWP-2. Different estimates of dilution factors and potential Grand Canyon impact are extended in the SWP-2 discussion. Furthermore, the terrain slope approaching the Colorado Plateau appears to divert initially west-southwesterly winds away from the Grand Canyon causing plume particles to avoid the sensitive northern Arizona/Grand Canyon region. It can be speculated that a meteorological model simulation initialized with low-level westerly winds instead of west-southwesterly winds might bring a greater percentage of particles to the Grand Canyon. Such a simulation would not be representative of the WHITEX period, however.

500 m Release: SWP-2d

SWP-2d had considerably different characteristics than the 'boundary layer releases' SWP-2a through c. The reason for the majority of the difference is that the release level is within the boundary layer for such a short period of time during day 1 of the simulation that its particles are less terrain-influenced. Figure 4.15 still approximately represents SWP-2d, however.

More scrutinizing analysis of the potential temperature fields for SW-2 indicates that the boundary layer on the marine or western side of the mountains (the marine boundary layer) is considerably shallower than the boundary layer elsewhere, especially the high desert (see Figure 4.10) during daylight hours. Since SWP-2d releases its particles within this marine region (on the coast of California), the fact that the marine boundary layer only exceeds 500 m for a short period (approximately 2 hours) compared to SWP-2a through c is significant.

During SWP-2d considerable differences arise in the early portion. During the stable morning period, 0-4 hours of day 1, the particles accumulate in the LA Basin, simply at a higher level than the other releases. In the 4-12 hour period the particles continue to accumulate early, until approximately hour six. At this point the boundary layer has

grown enough to influence some of the particles. The particles in lower levels are taken up in boundary layer flow and are subject to similar mechanisms as described in the previous section; they are transported through Cajon and Banning Passes. Where SWP-2d differs is by the behavior of those particles residing at high levels, above boundary layer effects. By mid-afternoon, model adjusted fields above the boundary layer (the level of SWP-2d's release) are more westerly and not subject to upslope effects. This causes the upper-level SWP-2d particles to travel eastward in more stable, upper-atmosphere layers. These particles travel at this horizontal level eastward into the desert regions by early evening where they accumulate in the lower levels.

Although one might expect the next day to effect the particles of the 500 m release in the same fashion, it does not. The reason for this appears to be the deeper growth of the boundary layer during day 2 (28-36 hours). Because the boundary layer grows to 600-700 m on day 2, the particle transport on day 2 is essentially the same as that described in the previous section (SWP-2a-c) for that period.

What are the implications of these differences? What are their causes? The implications are that during WHITEX pollutants which might have accumulated through stagnation to high levels (i.e. 500 m) prior to the event could be transported in large quantities to the eastern portions of the LA Basin. This has little effect on conclusions about the effect of LA Basin pollutants on the Grand Canyon region, however, because once in the deep boundary layer of the high desert these particles are transported in southerlies such that they, too, pass to the west of Grand Canyon National Park. No additional impact on the Grand Canyon due to their higher release level is found. This may have caused the boundary layer to grow to a lesser extent on day 1 than day 2.

Surface to 500 m Release: SWP-2e

Because SWP-2e releases particles from all levels from the surface to 500 m, its characteristics are a combination of those effects described in the sections for SWP-2a through d (as shown in Figure 4.15. Although SWP-2e reveals no new information on impacts of LA Basin pollutants on the Grand Canyon, it does represent a different scenario than SWP-2a-d. By nature of its configuration, SWP-2e mimics a severe stagnation event

in the LA Basin where pollutants have accumulated under an elevated stable layer to 500 m in significant concentration. In this case, mixing particles to 1000 m or higher represents a dilution factor of 2, whereas the 20 m thick releases (SWP-2a-d) were subject to a dilution factor of 50 by the same mixing. SWP-2e represents another level of conservationism in LA Basin impact assessment which is addressed in the upcoming discussion of SWP-2.

SWP-2: Discussion

It is seen that pollutants released at essentially any level near the surface in the LA Basin in winter conditions are diluted strongly by natural atmospheric processes for this case study. The dilution process prevents the LA Basin plume from reaching the Grand Canyon in large concentrations during this simulated period. The actual impact of what concentration does reach the Grand Canyon during WHITEX is implied to be quite low. Given a dilution factor of 100 (although 200 or higher might more often be found) for a worst case estimate, and an average LA Basin initial concentration of PM-10 (particles less than 10 microns) particles of 60 μg m^{3-1}, the Grand Canyon impact could roughly be 0.6 μg m^{3-1}. With mean PM-10 concentrations from March 1988 to February 1991 of approximately 9 μg m^{3-1} from the National Park Service Fine Particle Network, the LA Basin contribution to Grand Canyon haze is speculated to be at most 6.6% during the February 10-13, 1987 haze period based on this model simulation. Estimates of the potential impact of LA Basin pollutants on the Grand Canyon with different levels of dilution are presented in Table 4.2.

Results are presented for boundary layer growth to 500 and 1000 meters, the 500 meter assumption being an added measure of conservatism representing the case where the model predicted boundary layer growth was too great because cloud effects were not represented in these dry simulations. The worst case surface, wintertime PM-10 measurement in the LA Basin (236 μg m^{-3} San Bernardino County, CARB, 1986), is divided by a given dilution factor to determine the μg m^{-3} estimated concentration impact of the LA Basin at the Grand Canyon. The concentration impact is translated into an estimated percent impact simply by dividing it by a wintertime PM-10 haze condition measurement in the Grand Canyon. For the representative haze Grand Canyon measurement, a value of 50

Table 4.2: Estimates of Los Angeles Basin pollutant impact on Grand Canyon National Park haze conditions during February 10-13, 1987 with differencing levels of dilution. The information presented is based on LPDM results for SW-2 and maximum PM-10 concentrations of pollutants of 236 $\mu g/m^3$ and 50.0 $\mu g/m^3$ for the LA Basin and the Grand Canyon, respectively. The initial number of particles in all cases was 100.

LPDM Run (6)	Initial Release Depth (m)	Final Pollutant Depth	Dilution due to Vertical Mixing	Final # of Particles	Dilution due to Horizontal Dispersion	Total Dilution	Estimated Impact (%)
SWP-2a-d	20	1000	50	5	20	1000	0.46
	20	500	25	5	20	500	0.92
SWP-2e	500	1000	2	5	20	40	11.8
	500	500	1	5	20	20	23.6

$\mu g/m^3$ is used (based on high concentration values in the Grand Canyon, measured by the Western Fire Particle Network, March 1988 – February 1991). For SWP-2e's 500 meter deep release into a 1000 meter boundary layer depth, the total dilution is 40. In this case, the LA Basin impact concentration at the Grand Canyon would be 5.9 $\mu g/m^3$. Using the 50 $\mu g/m^3$ value as representative of typical Grand Canyon haze conditions, the percent impact of the LA Basin release would be 11.8%.

The calculations presented in Table 4.2 are based on a number of conservative assumptions including: (1) the surface maximum concentration value in the LA Basin (236 $\mu g/m^3$) is valid from the surface to 500 m, (2) for the cases where a 500 m final depth is used, the particles did not mix to the model diagnosed boundary layer depth of ~1000 meters, (3) wet and dry deposition processes were ignored, (4) each particle reaching GCNP does become mixed into the Grand Canyon boundary layer and is not transported away aloft, and (5) chemical conversion processes are unimportant. Given these conservatisms and the small magnitude of the estimated percent impact of the LA Basin on Grand Canyon concentration, that LA Basin pollutants might be the primary contributor to WHITEX haze during the February 10-13, 1987 period is unlikely.

4.5 SW-3: Simulation Analysis

As described previously, SW-3 differs from SW-2 by nature of its nest of 8 km grid increment over the LA Basin (see Figure 4.1). This allows greater terrain accuracy (Fig-

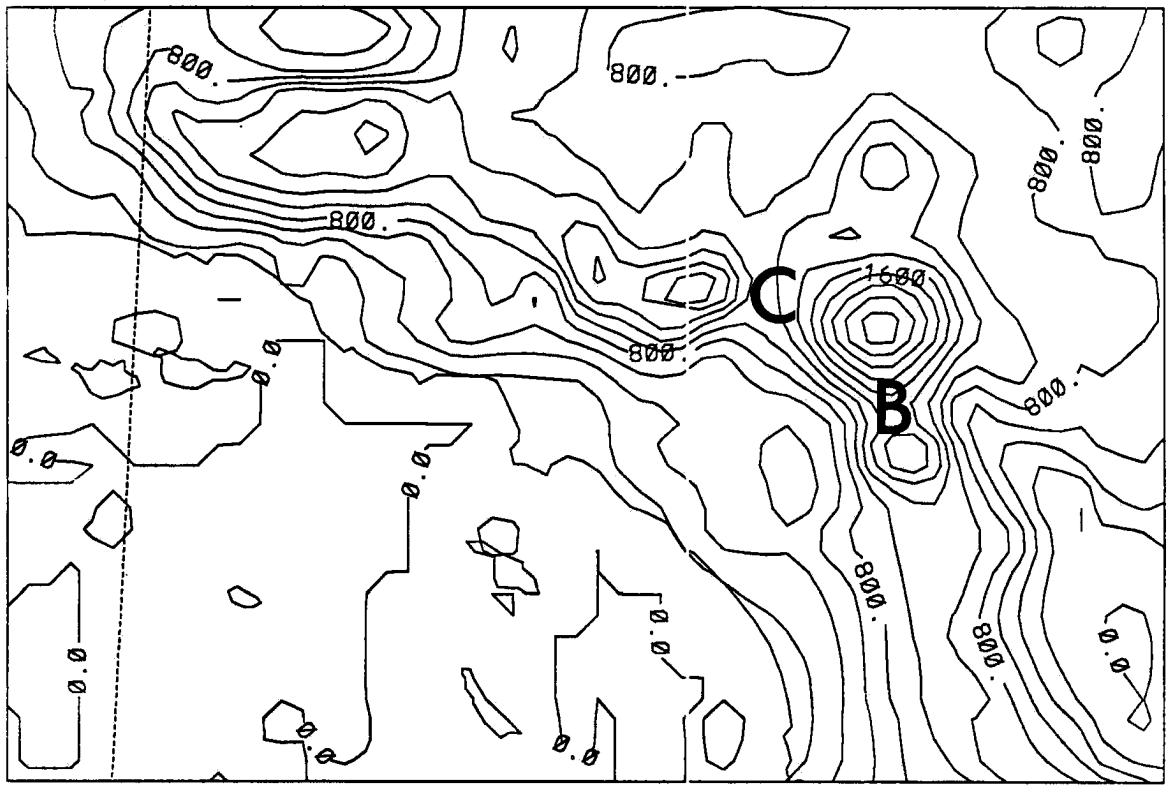

Figure 4.16: The terrain used on Grid 3 of SW-3. Note the greater detail in this plot compared with Figure 4.8 which has 24 km grid increments. Cajon Pass shows up considerably better (marked with a C). Banning Pass is marked with a B.

ure 4.16) and far better resolution of mesoscale meteorological processes. Generally, the inclusion of a fine nest increases the ability of the meteorological model, RAMS, to produce vertical motion. Obviously, this increased motion will affect particle transport as well. A more accurate picture of the terrain combined with the considerably greater atmospheric resolution creates significant changes in atmospheric fields compared to SW-2. These changes will be discussed in the next section. Corresponding changes in particle transport (SWP-3) are discussed directly after the meteorological results.

4.5.1 Meteorological Results: SW-3

Potential Temperature

Figure 4.17 shows the evolution of potential temperature on an $x - z$ plane passing through the northern part of Banning Pass along the LA Basin transect. By comparing this cross section to Figure 4.10 of the SW-2 discussion (which transects the same location) one can see how severely the difference in grid increment (24 km to 8 km) in the fine grid of SW-3 effects terrain depiction. Note the difference in the representation of the mountain centered at -175 km in Figure 4.17 compared to Figure 4.10.

This and other terrain differences induce significant changes in the potential temperature field of SW-3. The primary difference in potential temperature is in the magnitude of the mountain-induced waves. Note the increased amplitude of the wave induced by the mountain in the case of SW-3 throughout the time period of Figure 4.18. The evolution of the boundary layer in SW-3 is very much like that of SW-2. Its depth and location are nearly identical except in locations where nest differences create differing terrain features. SW-3 contains more abrupt changes in boundary depth with distance as shown in the region surrounding the mountain in Figure 4.18. Other cross sections show the same trends as described above although they are not shown here.

Horizontal Wind

The horizontal winds in SW-3 was quite consistent with SW-2, especially outside of the finest nest of SW-3. This is to be expected since outside of Grid 3 the grid increment (and therefore, terrain representation) is identical. A number of changes, however, occur within the bounds of Grid 3, SW-3's finest nest. Figure 4.19 presents horizontal wind vectors of SW-3 for Grid 2 during the 24-hour period from 20 to 44 hours into the simulation at 73.2m. This figure is comparable to Figure 4.12 which shows the same period for SW-2. Many features are quite similar:

- The convergence line to the north of Los Angeles along the San Gabriel mountains.
- The anticyclone circulation to the east of the southern Sierras.

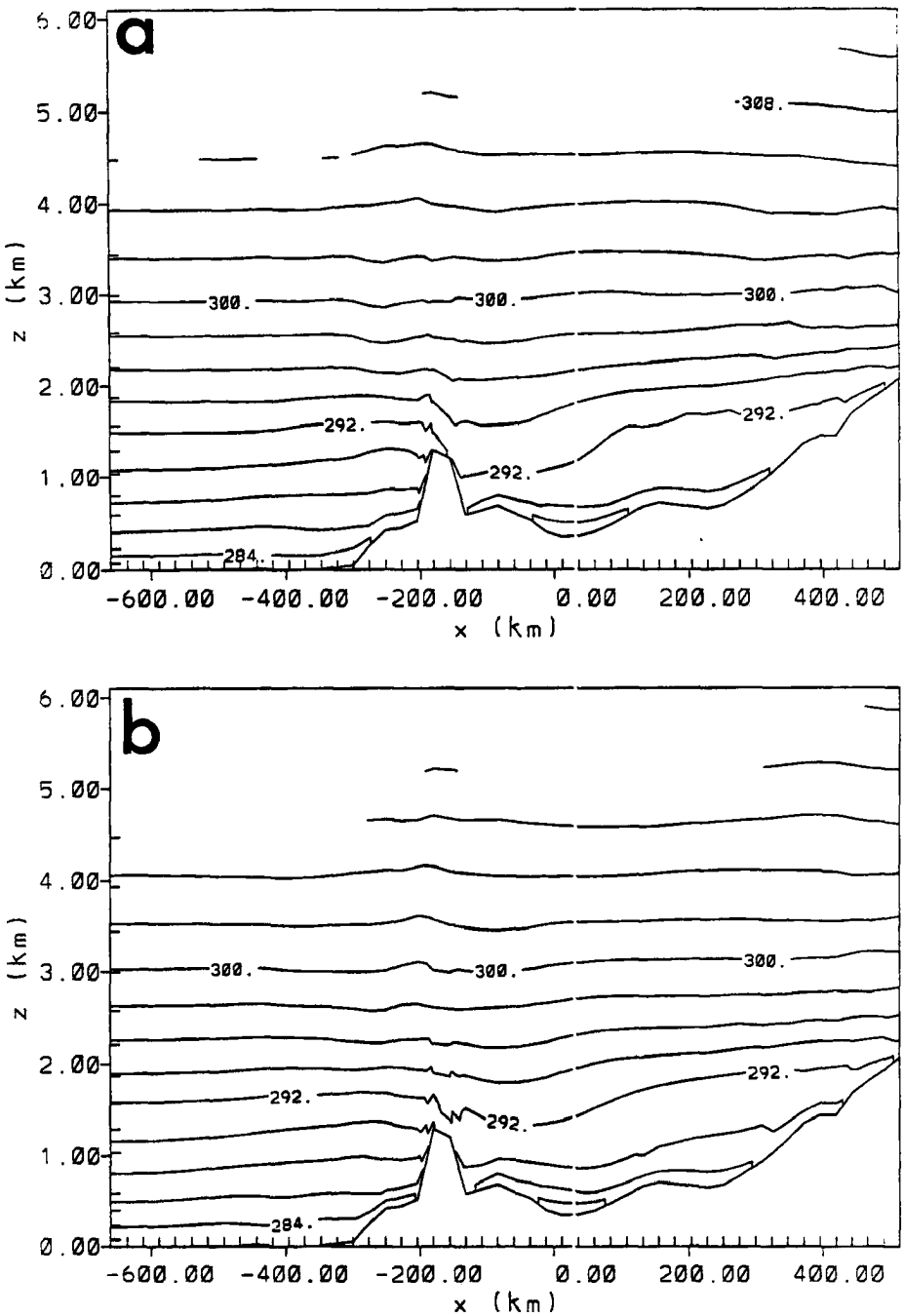

Figure 4.17: The evolution of potential temperature from 20 to 44 hours of the simulation in 4-hour increments on Grid 2 (first nest) for SW-3 on the LA Basin transect. This cross section location is depicted in Figure 4.11.

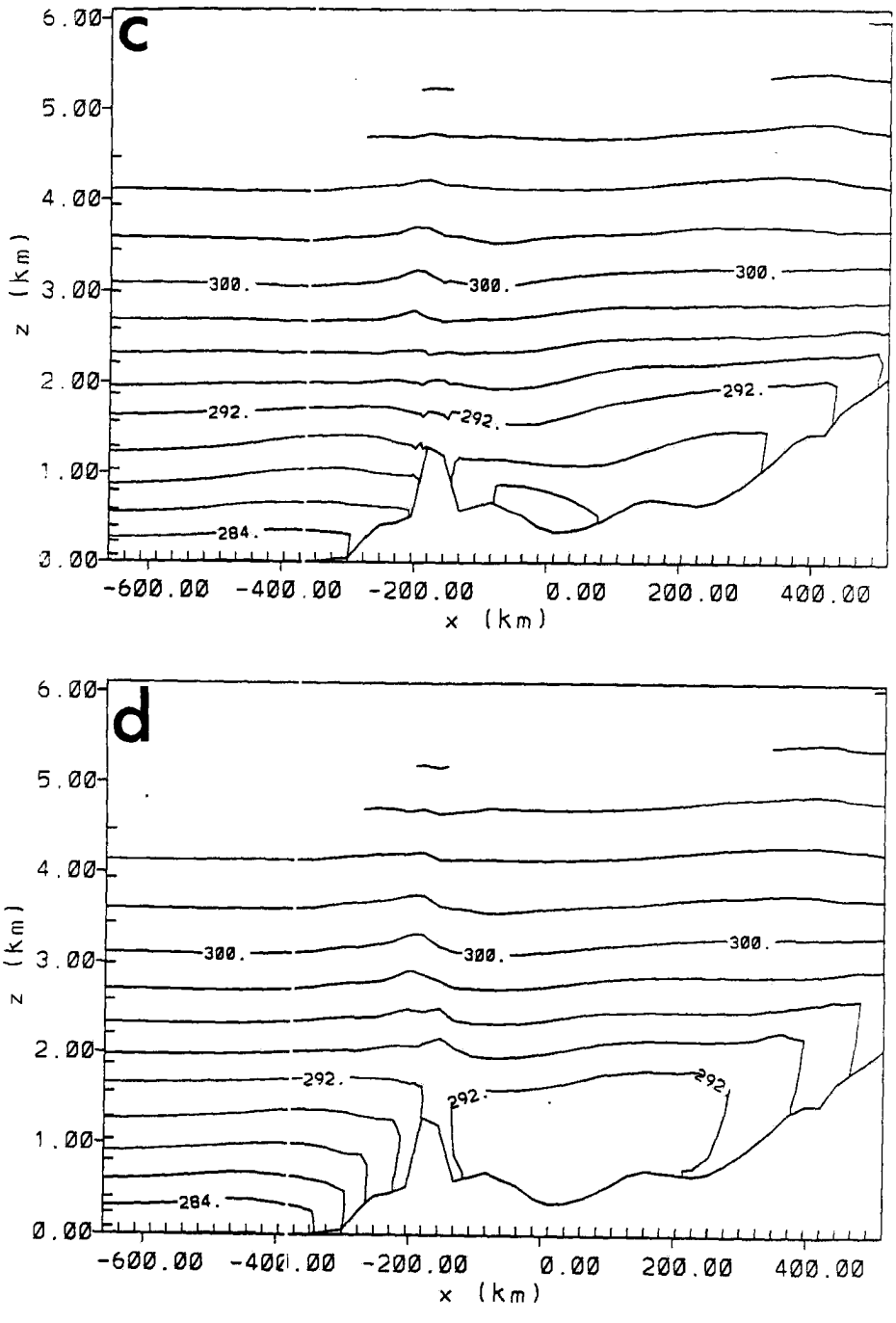

Figure 4.17: (c) 1600Z, hour 28; and (d) 2000Z, hour 32.

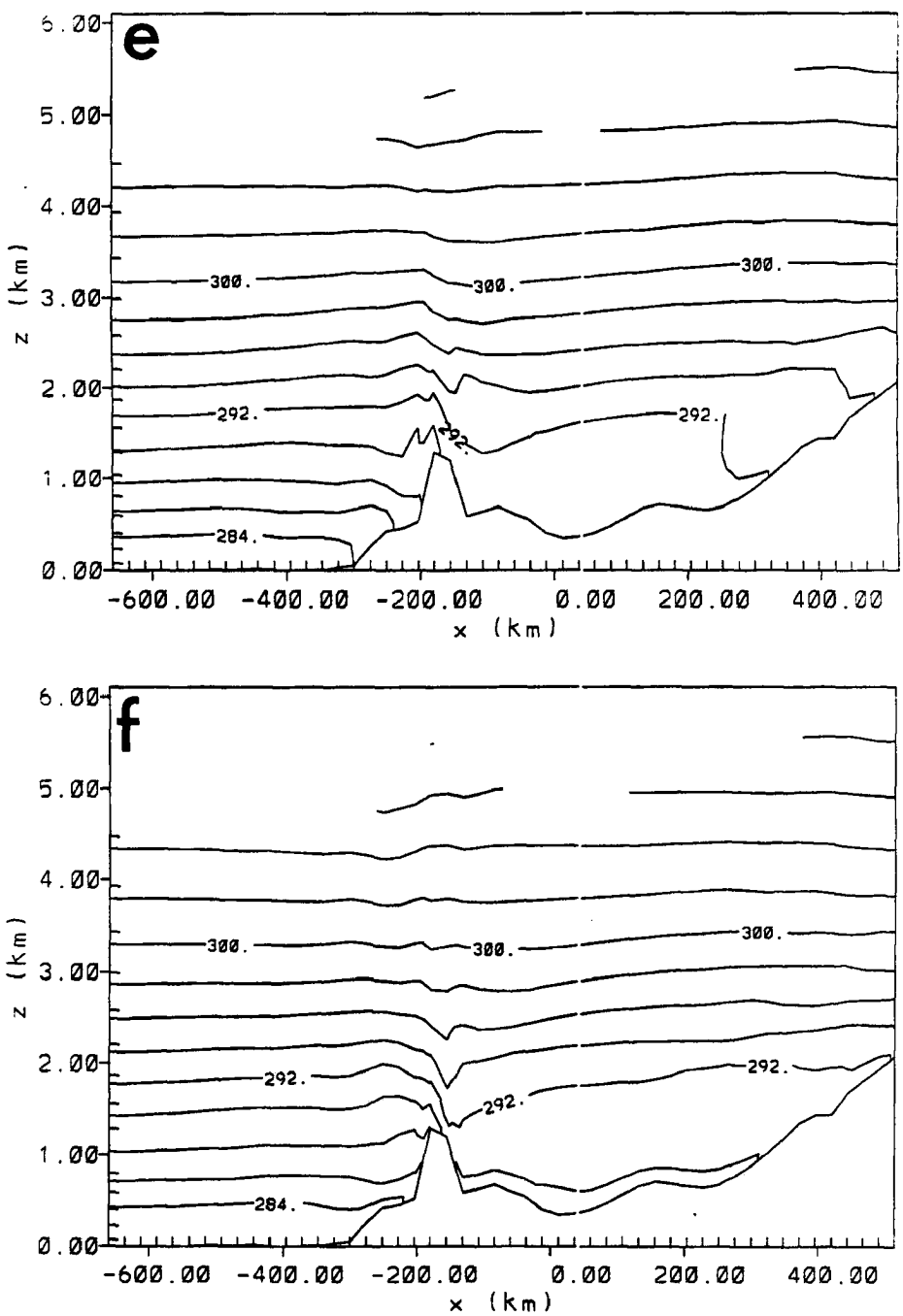

Figure 4.17: (e) 0000Z, hour 36; and (f) 0040Z, hour 40.

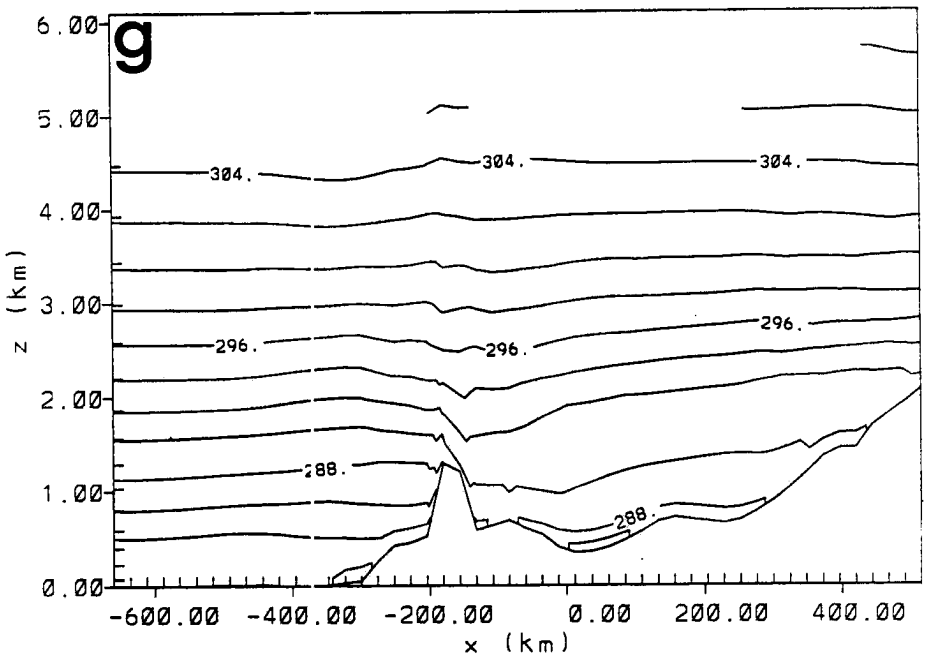

Figure 4.17: (g) 0800Z, hour 44.

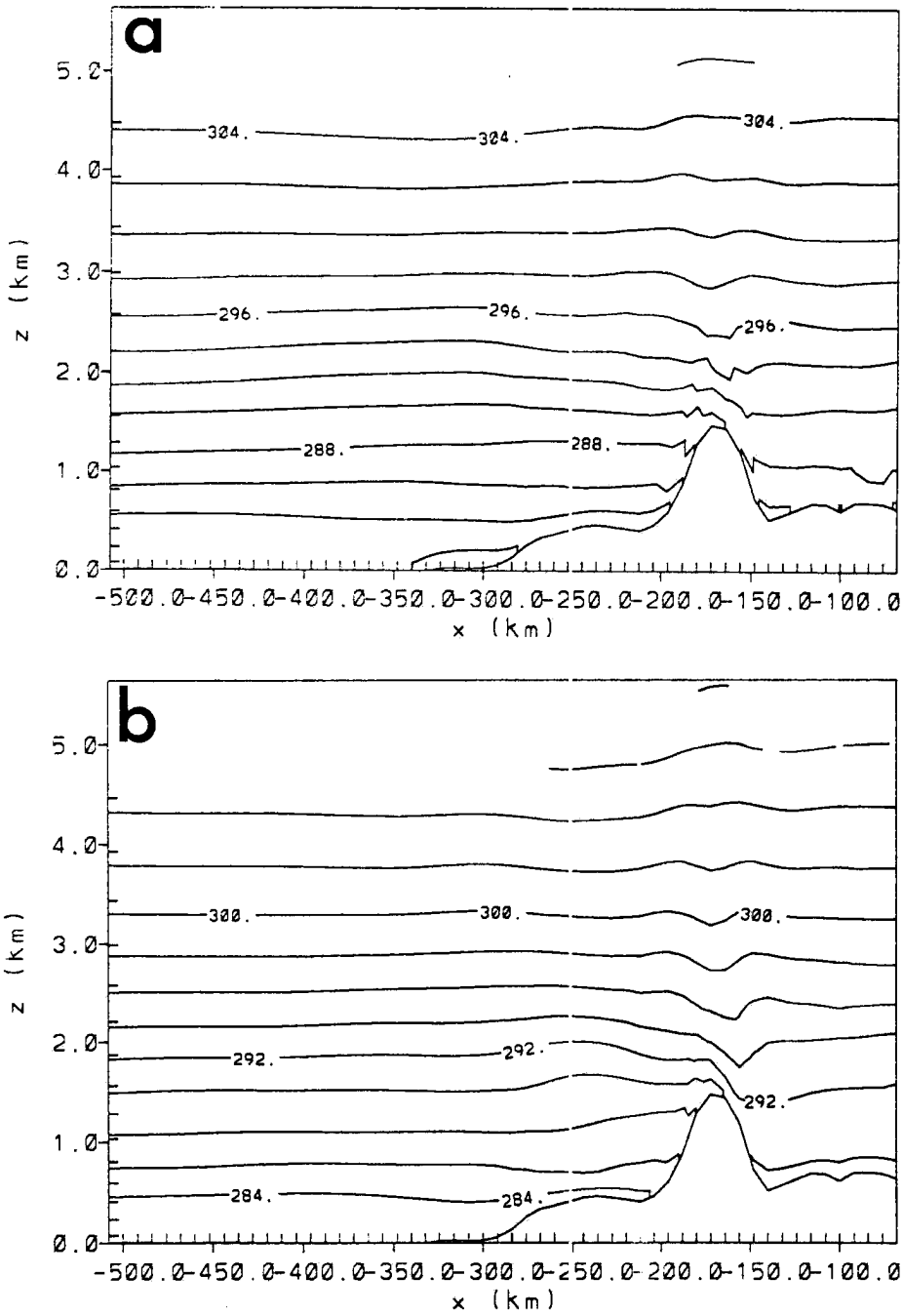

Figure 4.18: The same as Figure 4.17 but for Grid 3 through the LA Basin at (a) 0800Z, hour 20; and (b) 1200Z, hour 24. Note the greater terrain resolution.

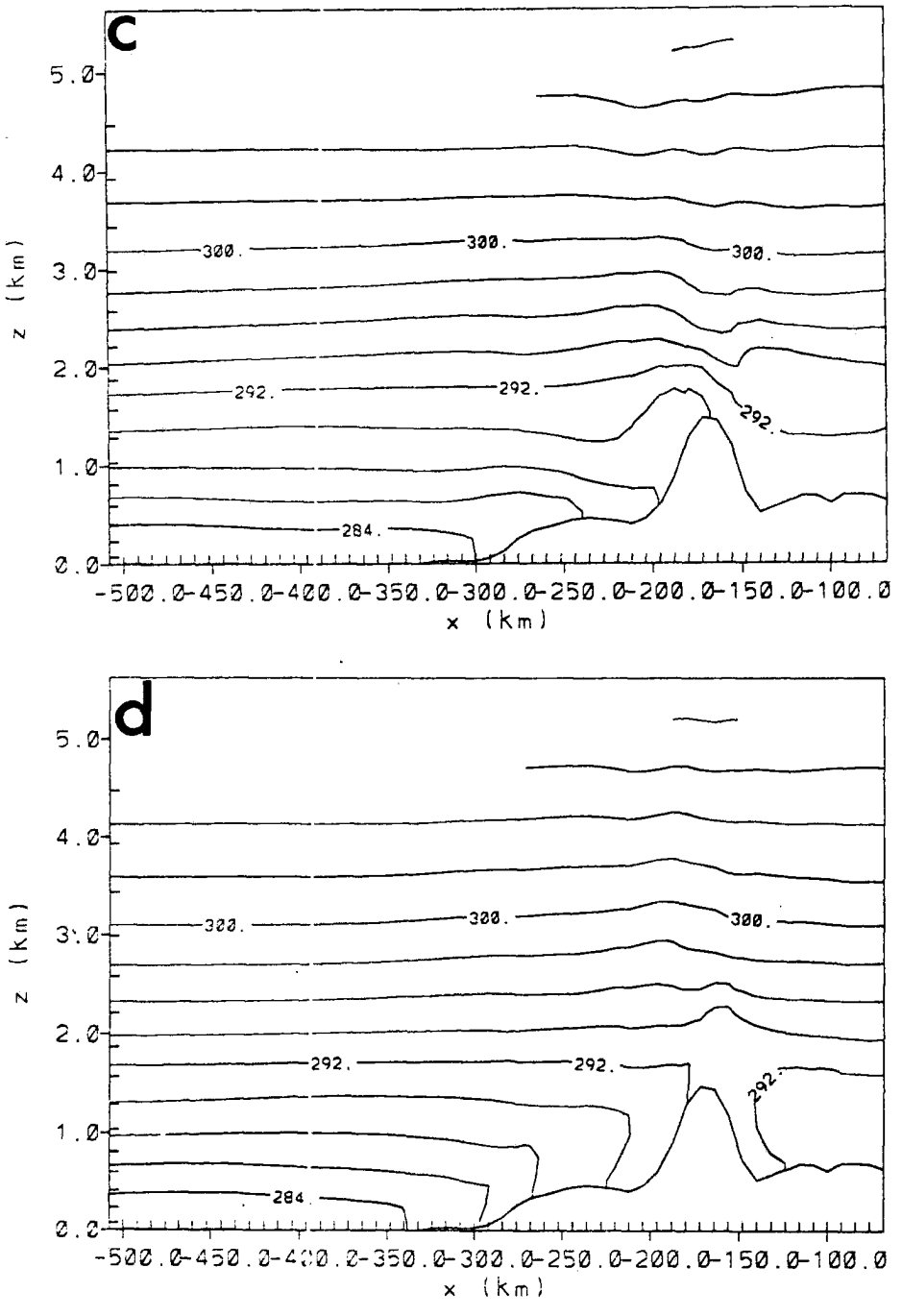

Figure 4.18: (c) 1600Z, hour 28; and (d) 2000Z, hour 32.

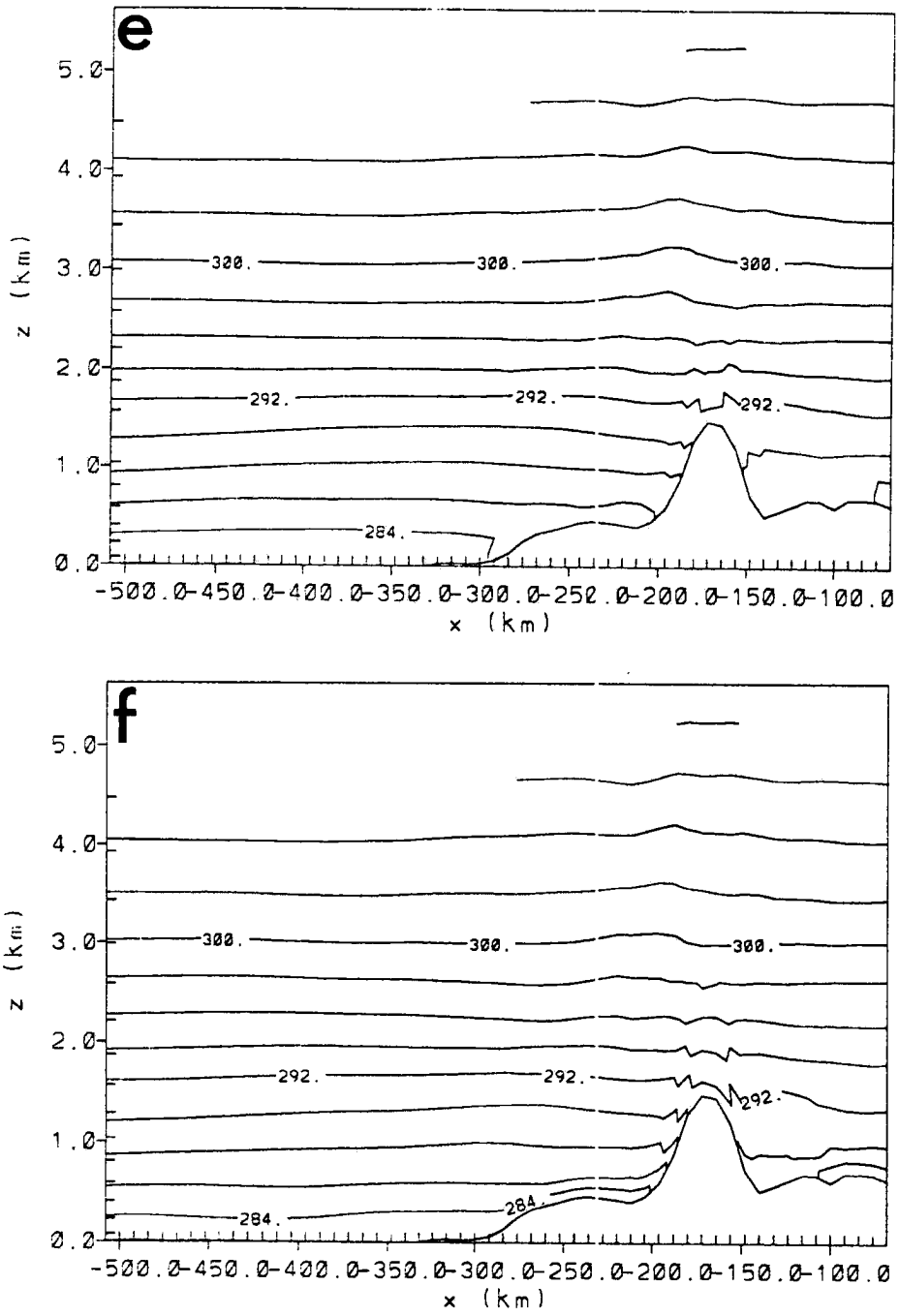

Figure 4.18: (e) 0000Z, hour 36; and (f) 0040Z, hour 40.

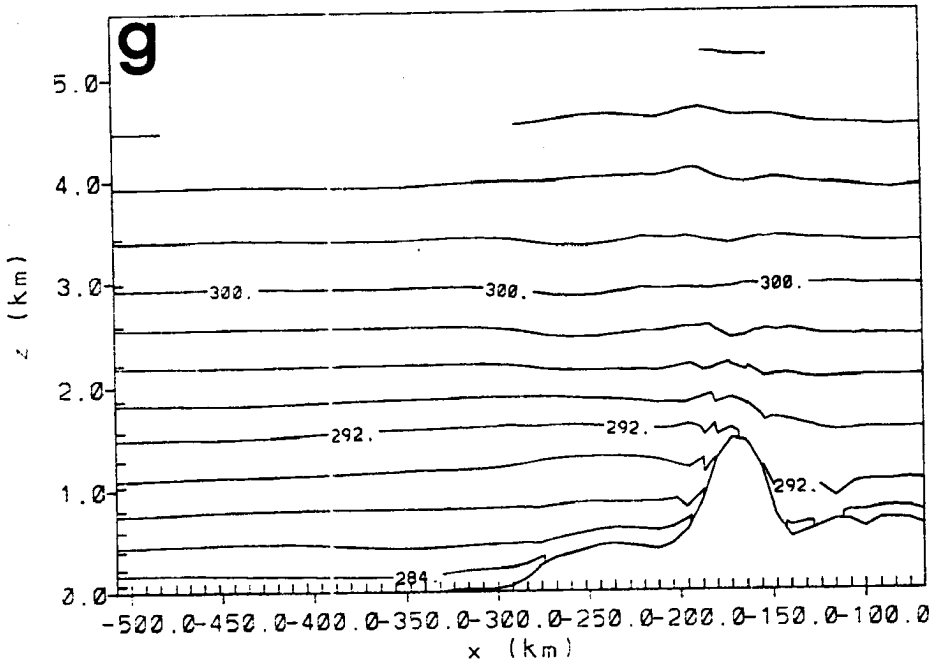

Figure 4.18: (g) 0800Z, hour 44.

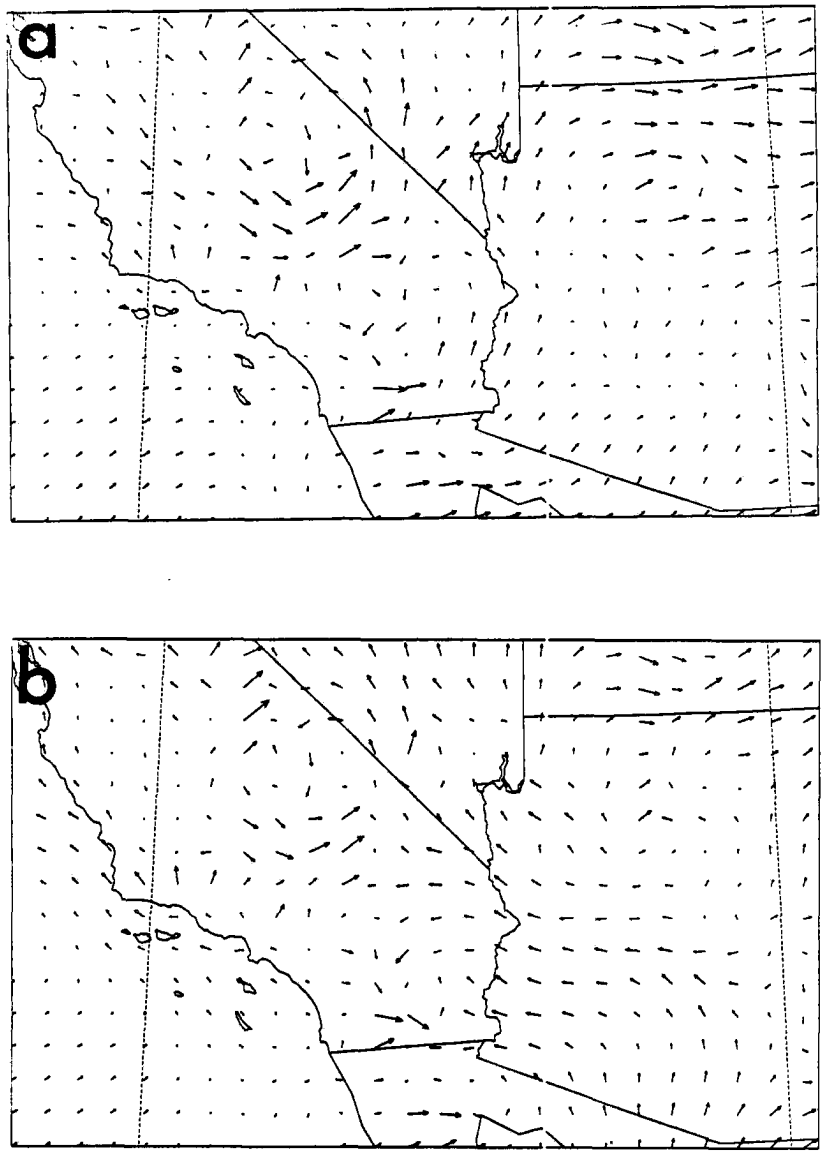

Figure 4.19: Horizontal wind vectors on Grid 2 for SW-3 at 73.2 m for the 24-hour period between 20 and 44 hours of the simulation at (a) 0800Z, hour 20; and (b) 1200Z, hour 24. The longest vector represents $\sim$10 m s^{-1}.

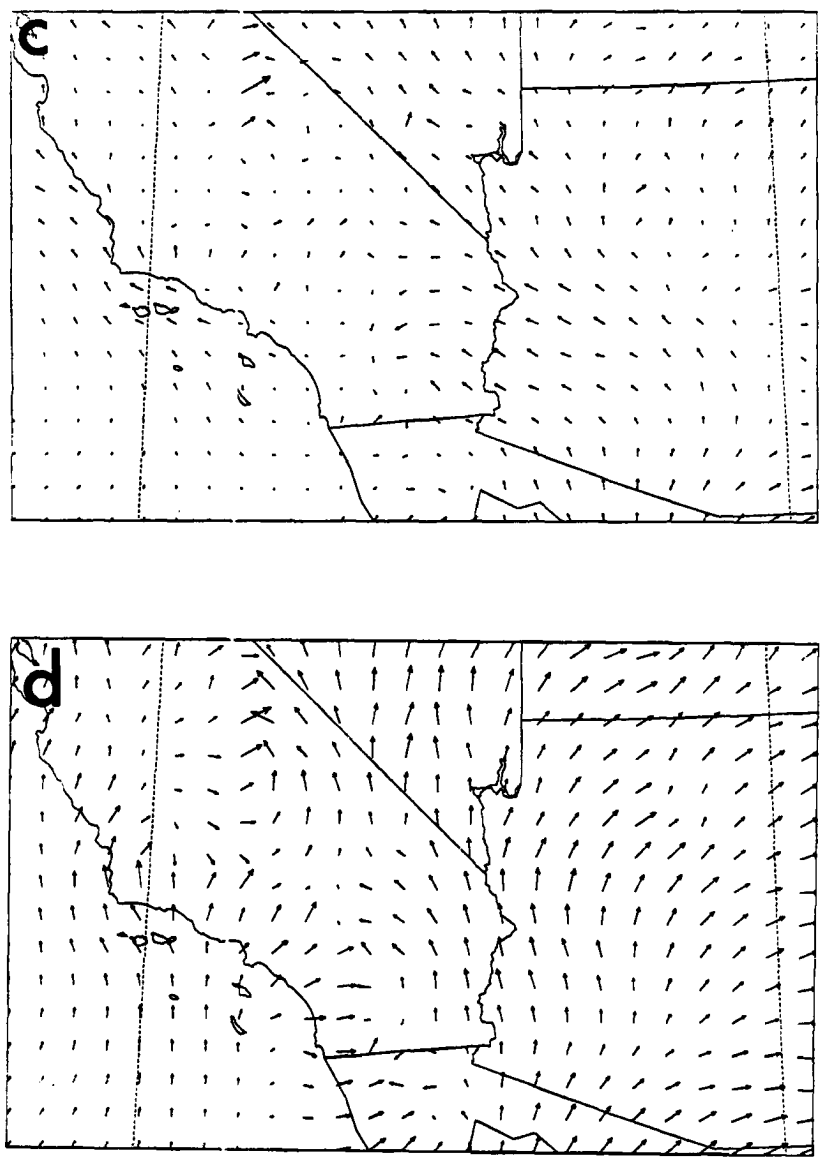

Figure 4.19: (c) 1600Z, hour 28; and (d) 2000Z, hour 32.

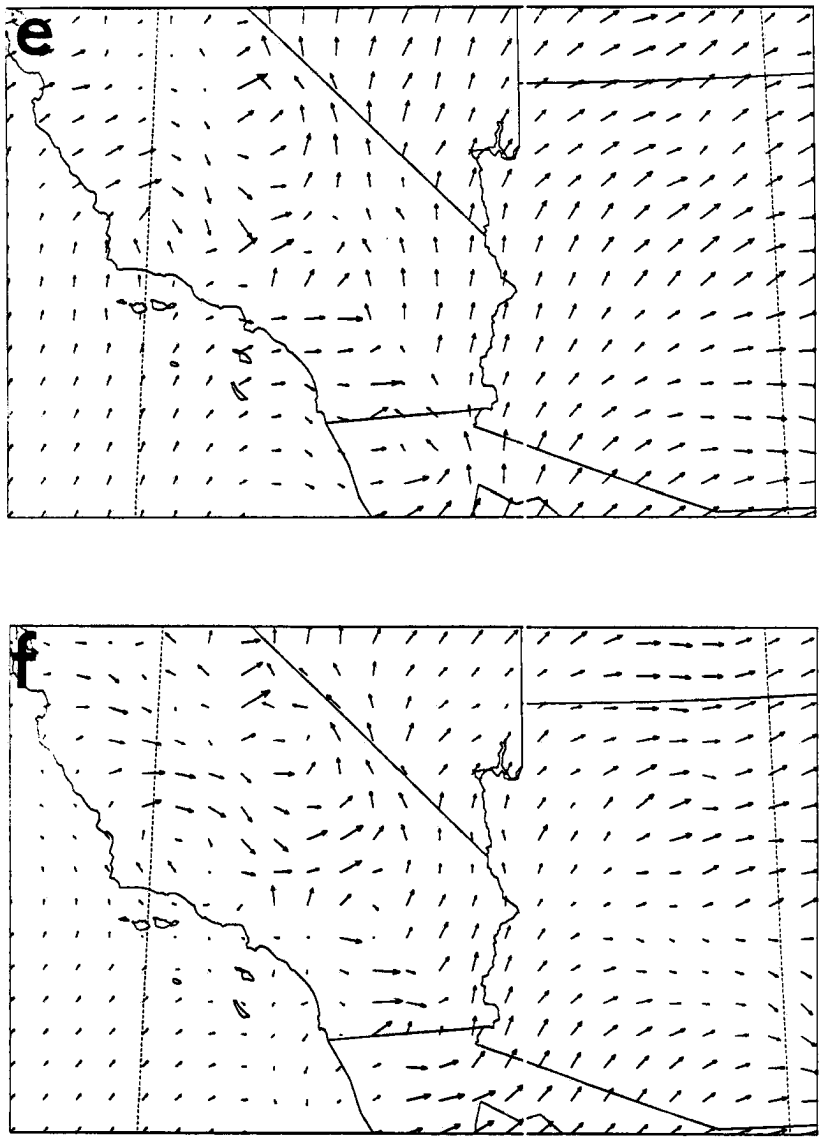

Figure 4.19: (e) 0000Z, hour 36; and (f) 0040Z, hour 40.

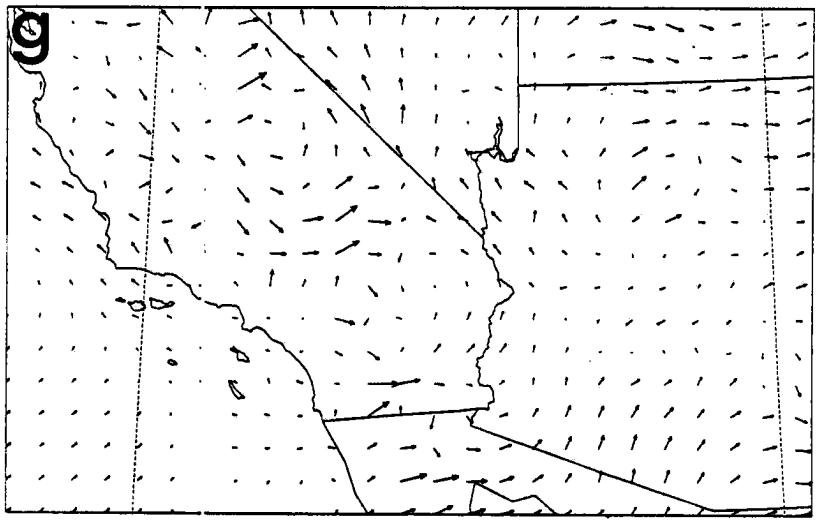

Figure 4.19: (g) 0800Z, hour 44.

- The turning of the wind away from the Colorado Plateau in eastern Arizona.
- The consistency of southwesterly flow over the southwestern part of the Grid 2 domain.
- The maximum windspeed averages only 0.6 m s^{-1} less than that of SW-2 during the 24-hour period (10.2 m s^{-1} for SW-3 vs. 10.8 m s^{-1} for SW-2).

Differences arise for the most part within or near the Grid 3 area. Winds over the ocean back more in SW-3, being more southerly than SW-2 at the similar times.

The strength of the convergence along the San Gabriel mountains increases in SW-3. Divergence of winds around the better resolved mountains of San Bernardino National Forest is considerably more evident, as is convergence into Cajon Pass. Within Grid 3 in the LA Basin over land, windspeeds drop somewhat, approaching 0 m s^{-1} in one location.

At 1033 m (not shown) the horizontal winds in SW-3 are consistently southwest throughout the simulation period of 54. Although not shown, a southerly wind develops along the California/Arizona border and to the west of the Sierras which lasts throughout the simulation. This feature is consistent between SW-3 and SW-2. For the most part, differences (and even these are small) exist over the Grid 3 area. Slight directional differences appear in time reflecting the model's adjustment to the better terrain resolution in Grid 3. For instance, at 1200Z winds in the LA Basin for SW-3 appear to be considerably more diverted by terrain, in this case the San Bernardino National Forest region, than in SW-2. Also, between 1600Z and 2000Z in SW-3, LA Basin winds drop from 3-4 m s^{-1} to 0-2 m s^{-1} whereas in SW-2 winds drop to 2-3 m s^{-1} for the same period.

At approximately 3 km terrain influence drops off considerably. In fact, velocity differences between SW-3 and SW-2 are quite limited and hardly detectable at this height over the simulation period. Over the 24-hour period (20-44 hours of the simulations) the maximum windspeed of SW-3 is 0.17 m s^{-1} higher than SW-2, while vector direction differences are negligible.

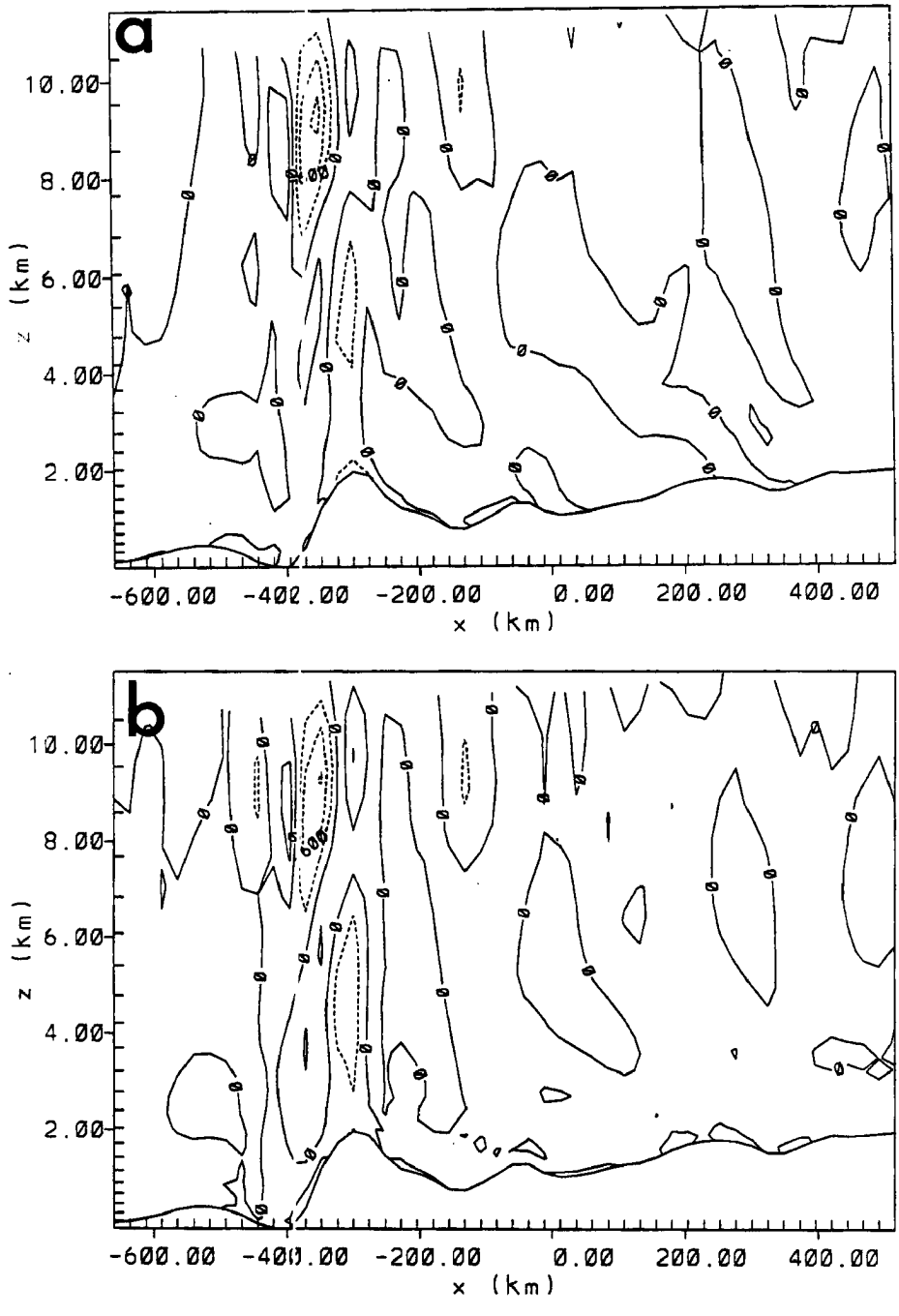

Figure 4.20: Vertical motion for SW-3 at +120 km on Grid 2 for hours 20 to 44 into the simulation in 4 hour increments at (a) 0800Z, hour 20; and (b) 1200Z, hour 24. This passes through the Grand Canyon region. The contour interval is 3 cm s^{-1}.

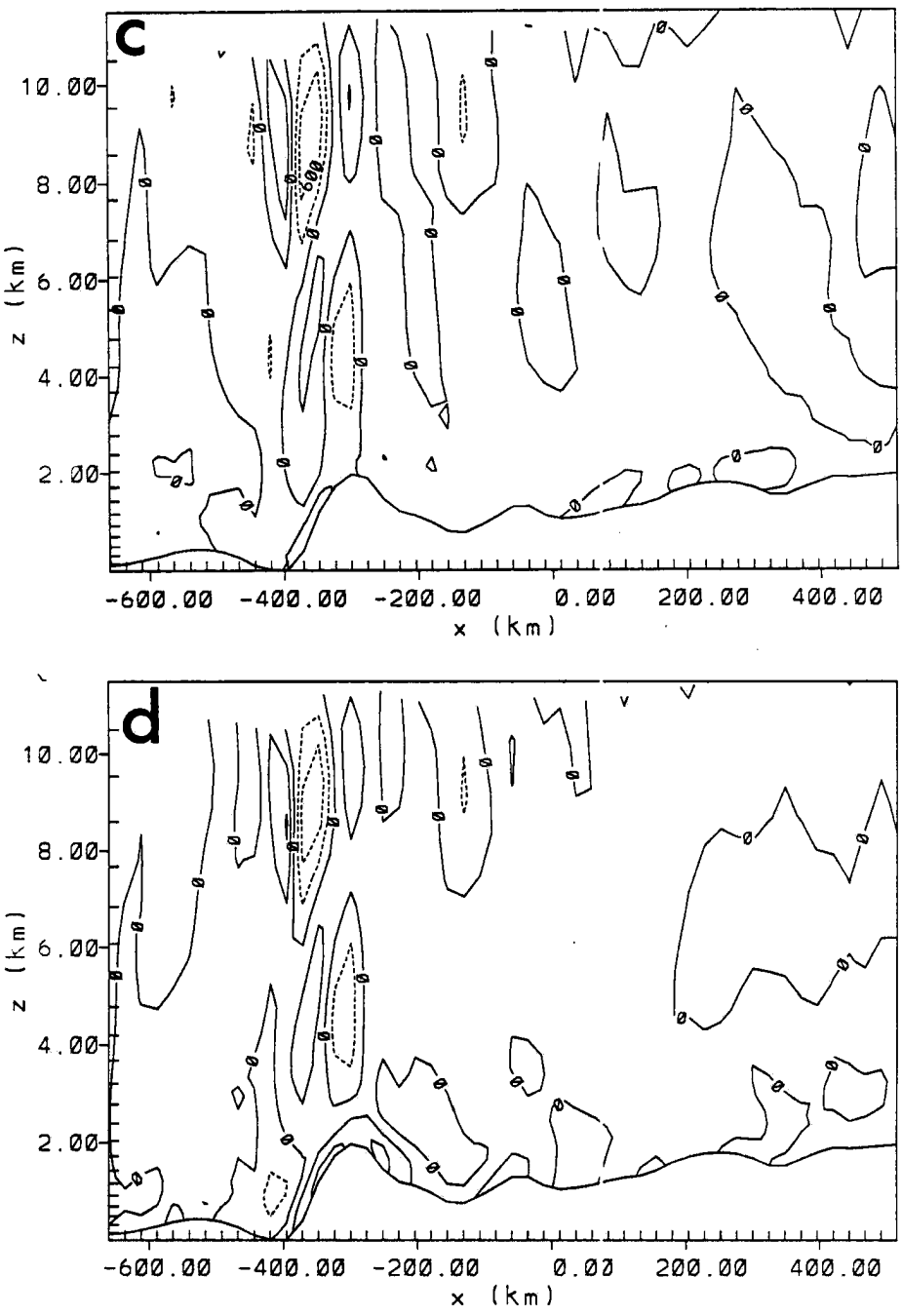

Figure 4.20: (c) 1600Z, hour 28; and (d) 2000Z, hour 32.

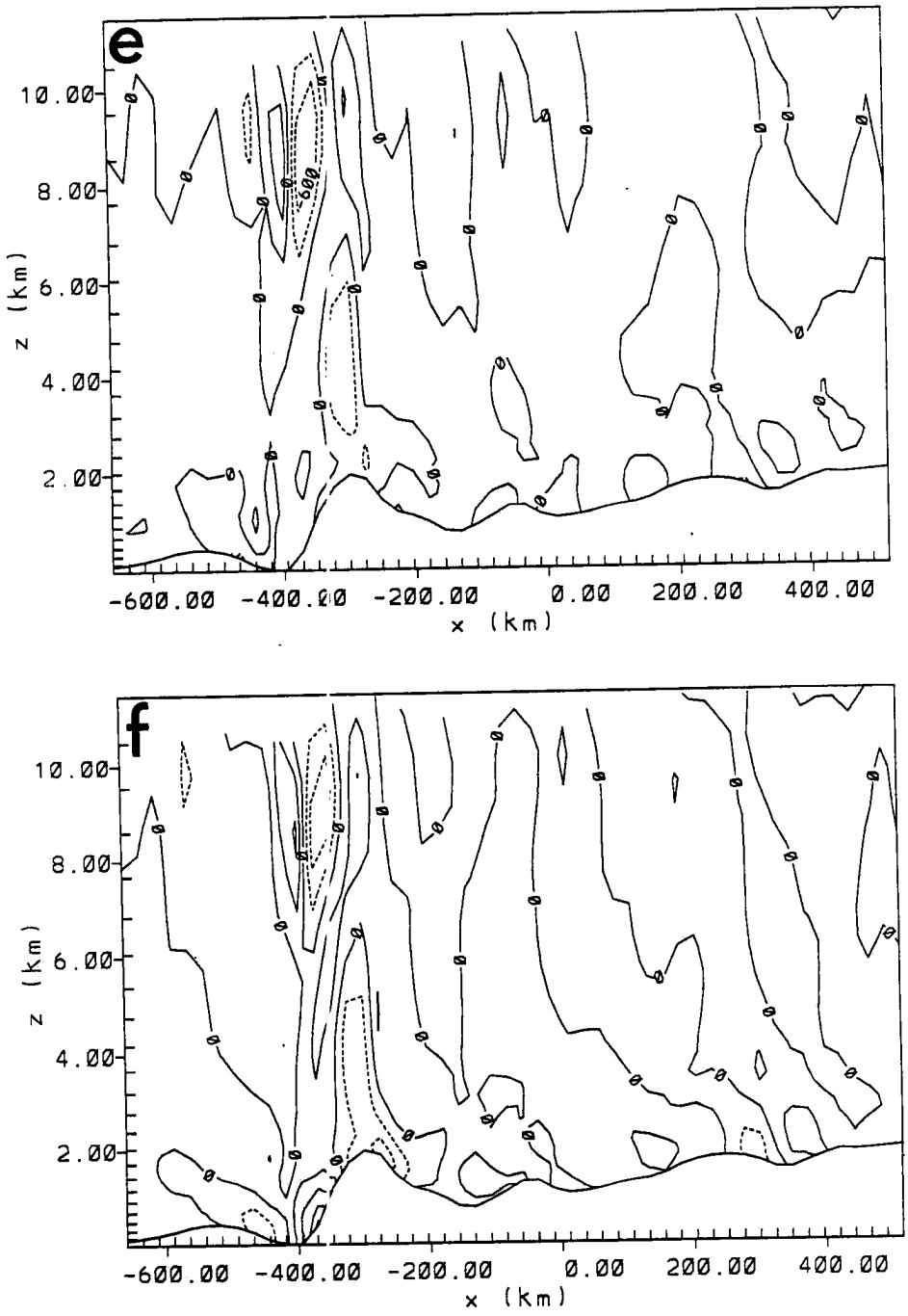

Figure 4.20: (e) 0000Z, hour 36; and (f) 0040Z, hour 40.

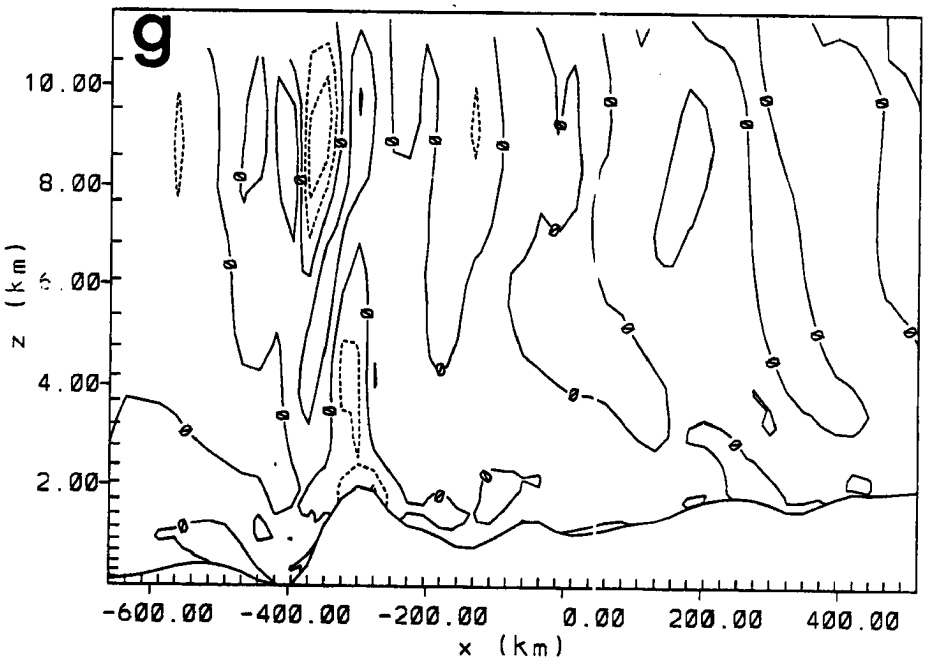

Figure 4.20: (g) 0800Z, hour 44.

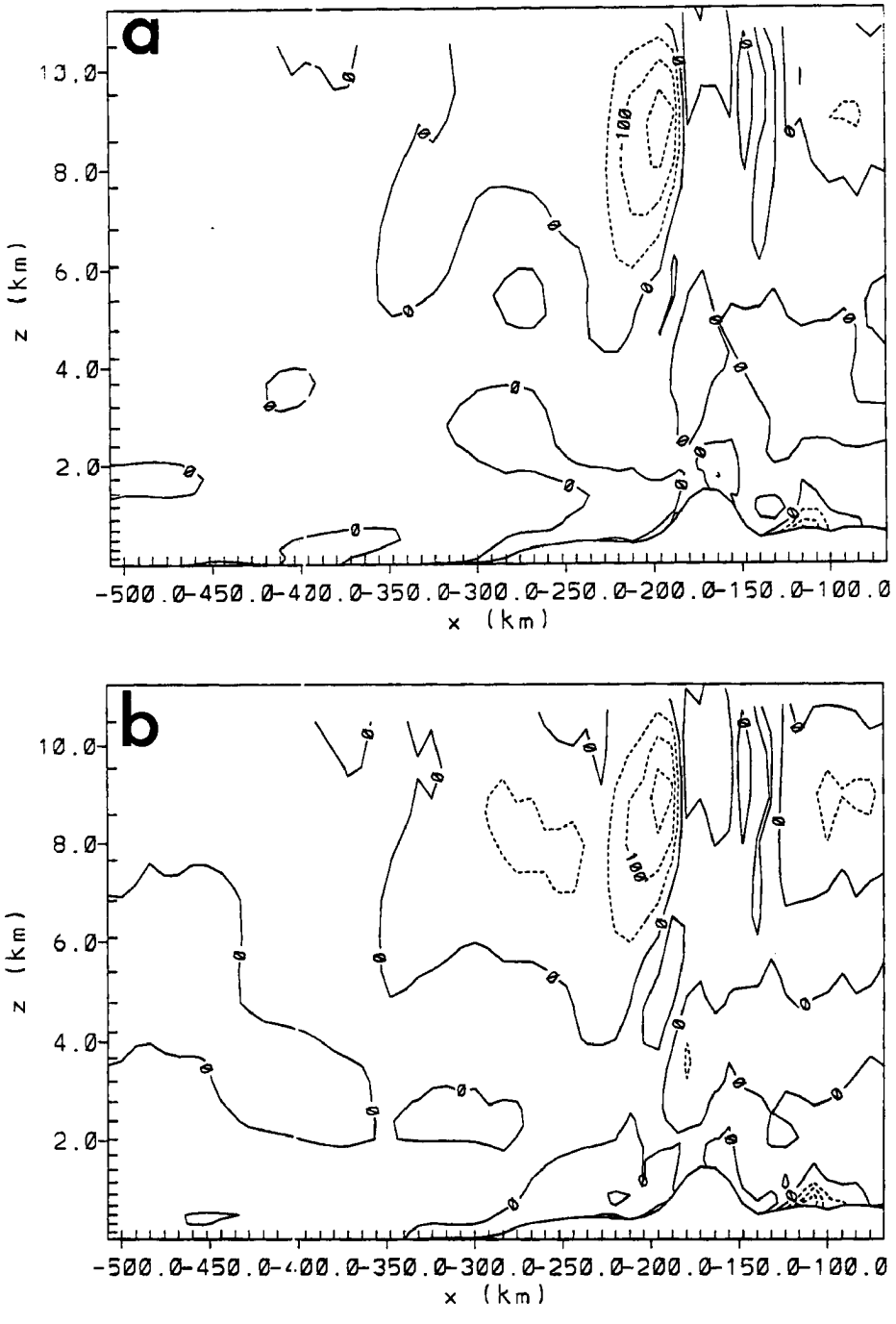

Figure 4.21: Vertical motion for SW-3 at −120 km on Grid 3 for hours 20 to 44 in 4 hour increments at (a) 0800Z, hour 20; and (b) 1200Z, hour 24. This passes through the LA Basin and Banning Pass. The contour interval is 5 cm s^{-1}.

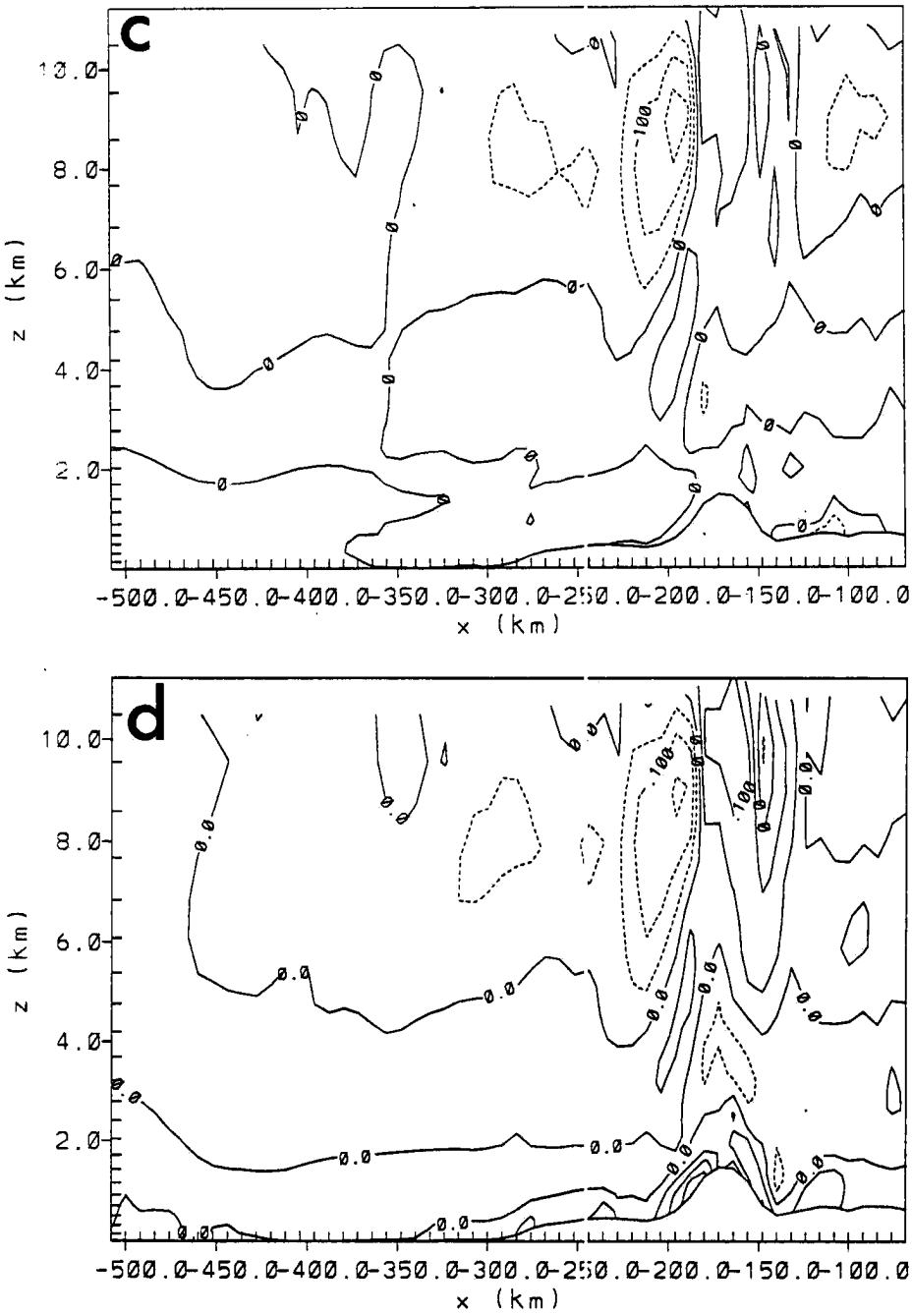

Figure 4.21: (c) 1600Z, hour 28; and (d) 2000Z, hour 32.

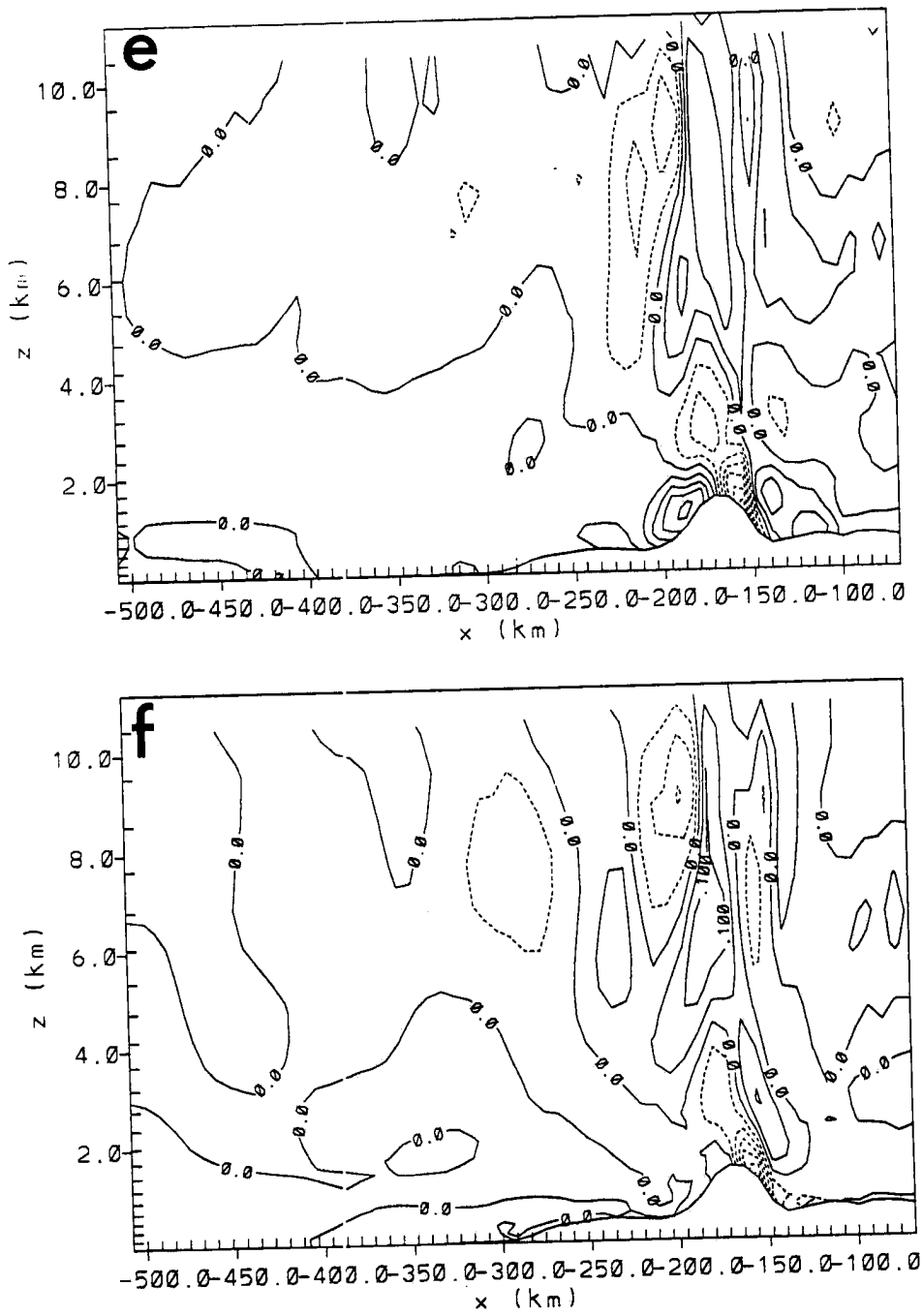

Figure 4.21: (e) 0000Z, hour 36; and (f) 0040Z, hour 40.

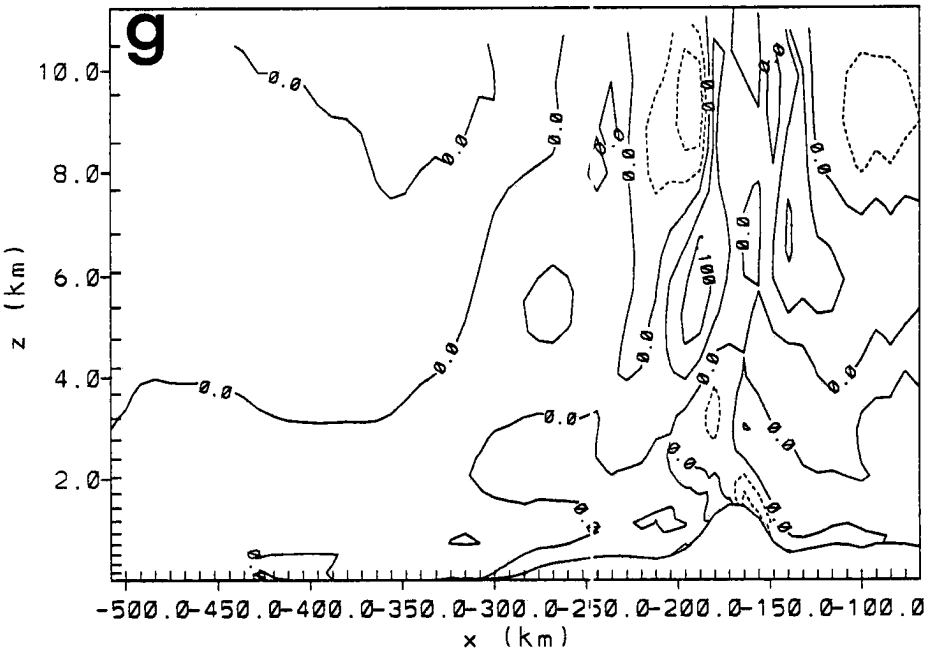

Figure 4.21: (g) 0800Z, hour 44.

Vertical Wind

Vertical wind profiles for SW-3 on Grids 2 and 3 are shown in Figure 4.20.

The additional capability of RAMS to resolve vertical motion with decreasing grid increment can easily be seen by comparing 4.20 and 4.21. Note the strength differences; on Grid 2 the magnitude of the largest vertical motion is 8 cm s^{-1} at 1600Z, on Grid 3 the maximum magnitude at 1600Z is 30 cm s^{-1}. Obviously, such differences are important with respect to pollutant transport. Larger vertical motions not only increase the depth of the boundary layer but bring pollutants to higher levels in the atmosphere subjecting them to higher horizontal windspeeds as well.

Concentrating on Grid 3 (Figure 4.21) because the Grid 2 vertical motion analysis is much the same as that for SW-2, what mesoscale meteorological attributes are better represented by Grid 3 in relation to w? The most noticeable difference is the strength of the mountain-induced downward/upward vertical motion couplet. The finer scale evolution of this feature is evident in time to an extent unresolved in SW-2 on Grid 2. Also easily seen is the diurnal cycle of upslope heating on the mountainside. Note in Figure 4.21 that the morning hours (1200Z and 1600Z) show little or no vertical motion along the mountain, but by 2000Z (2 p.m.) strong upslope ascent of 20 cm s^{-1} has formed on the western slope and upslope caused upward motion of 10 cm s^{-1} on the eastern slope. Toward sundown (sun shining on western slope only) at 0000Z upslope only remains on the western slope having weakened to an ascent of 15 cm s^{-1}. The eastern slope's upslope has reversed and become downslope; perhaps combining with the mountain wave on the eastern side to create strong descent of 30 cm s^{-1}. Overnight the western upslope deteriorates completely; the eastern side downslope is more persistent, lasting until early morning when the eastern side atmosphere has so stabilized that the mountain induced downslope has stopped. Note that the upslope regime lasts only 6 hours during the highest sun during these winter conditions.

4.5.2 LPDM Results: SWP-3

As with SW-1 and SW-2, five simulations of particle transport were completed for SW-3, SWP-3a through SWP-3e. The five runs of SWP-3 were identical in configuration

to the previous LPDM runs with an area release of 20 m depth for a) surface, b) 100 m, c) 250 m, d) 500 m, and a volume release e) extending from the surface to 500 m. Since these runs are exactly similar to the previous LPDM runs in configuration, the influence of increased terrain and meteorological resolution of SW-3 is shown by this analysis.

Because of the higher resolution on Grid 3 of SW-3 mesoscale motions were better represented. The resulting fields were more complex and contained distinctly stronger vertical motions than SW-2. Particle model analysis of SWP-2 revealed the importance of vertical motion to particle transport, particularly in reference to boundary layer mixing. The meteorological differences between SW-3 and SW-2 manifest themselves as particle transport details in SWP-3. More specifically the particle simulations of SW-3, SWP-3a-e, vary in large part by the vertical placement of particles in time compared to those of SWP-2. This, in turn, creates minor differences in horizontal position generally, with major differences on occasion. As with the SWP-2 discussion for briefly only one figure representing the time evolution of the surface to 500 m release (in this case, SWP-3e) will be referred to throughout the upcoming discussion (Figure 4.22). In essence, the SWP-3 set of simulations maintains the general patterns of SWP-2. For this reason, as with the earlier descriptions, only differences will be emphasized, and the set of five simulations are grouped together in the discussion.

The animation of the 54-hour period of continuous particle surface release for the LA Basin reveals the numerous effects of Grid 3 on particle positions in time. Many of the main features seen in SWP-2 are found in SWP-3a, as seen in Figure 4.22. The following were repeated in a general sense: 1) trapping of pollutants in the LA Basin and the high desert during stable atmospheric periods with low wind flow, 2) katabatic flows transporting pollutants *westward* to converge with southwesterly winds over and near the ocean, 3) mixing of particles deep within the boundary layer of Los Angeles allowing transport through passes and over mountains, 4) mixing of particles in the deep, high desert boundary layer to the point where they are caught in stronger, southerly winds at higher altitudes, and 5) the lack of significant numbers of particles crossing Grand Canyon National Park boundaries.

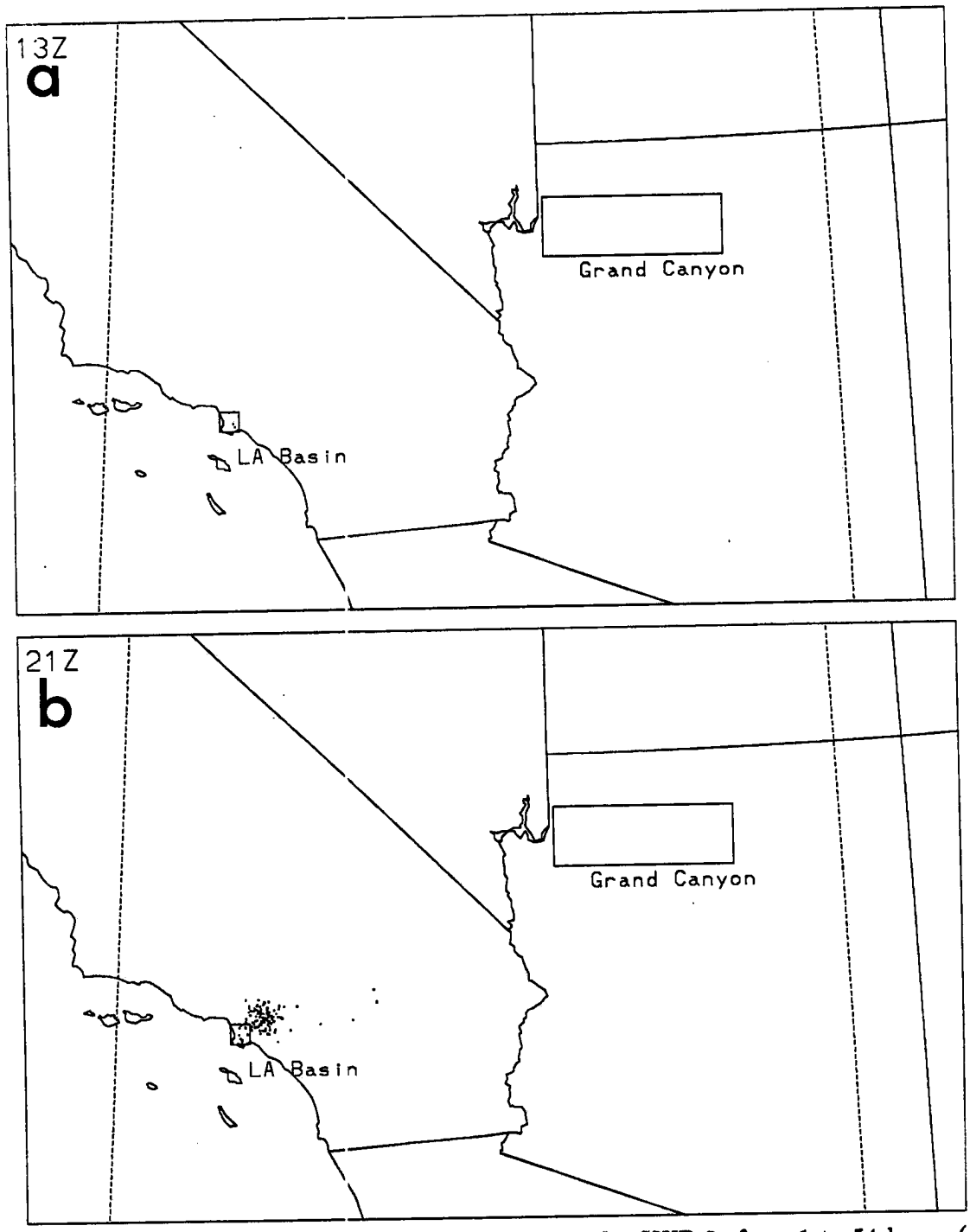

Figure 4.22: The time evolution of particle positions for SWP-3e from 1 to 54 hours (a) 1300Z, hour 1; and (b) 2100Z, hour 9. Note the greater detail compared to Figure 4.15.

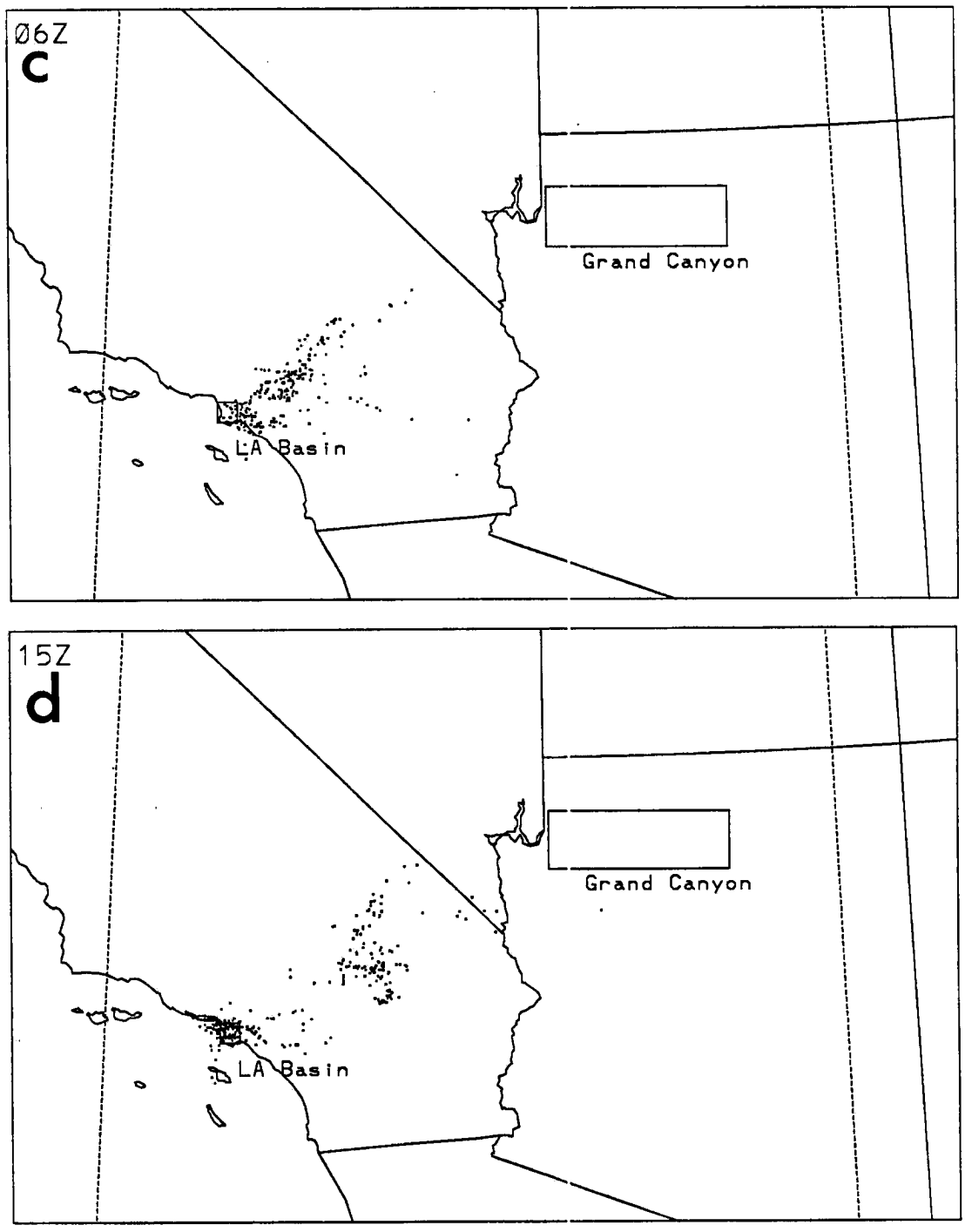

Figure 4.22: (c) 0600Z, hour 18; and (d) 1500Z, hour 27.

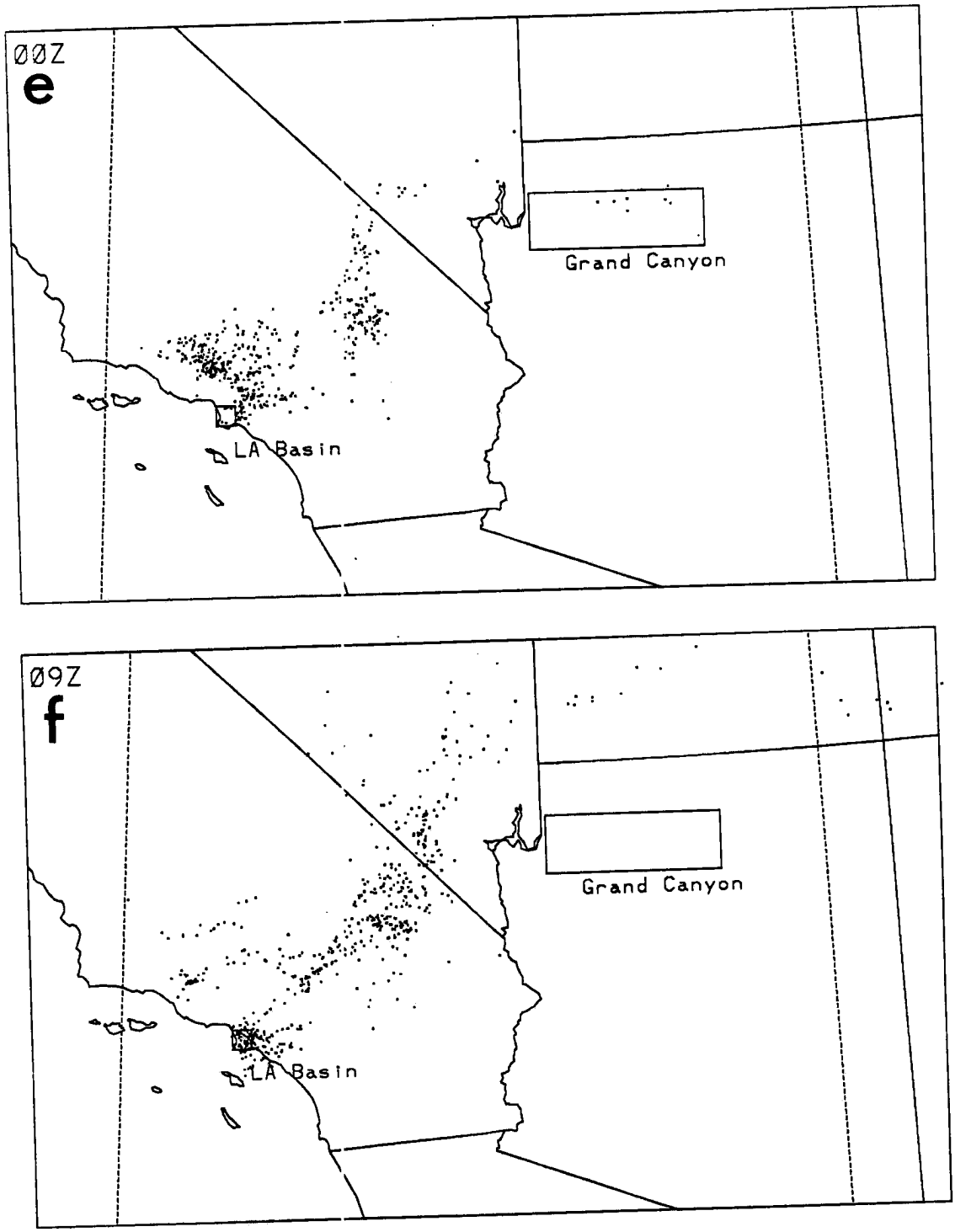

Figure 4.22: (e) 0000Z, hour 36; and (f) 0900Z, hour 45.

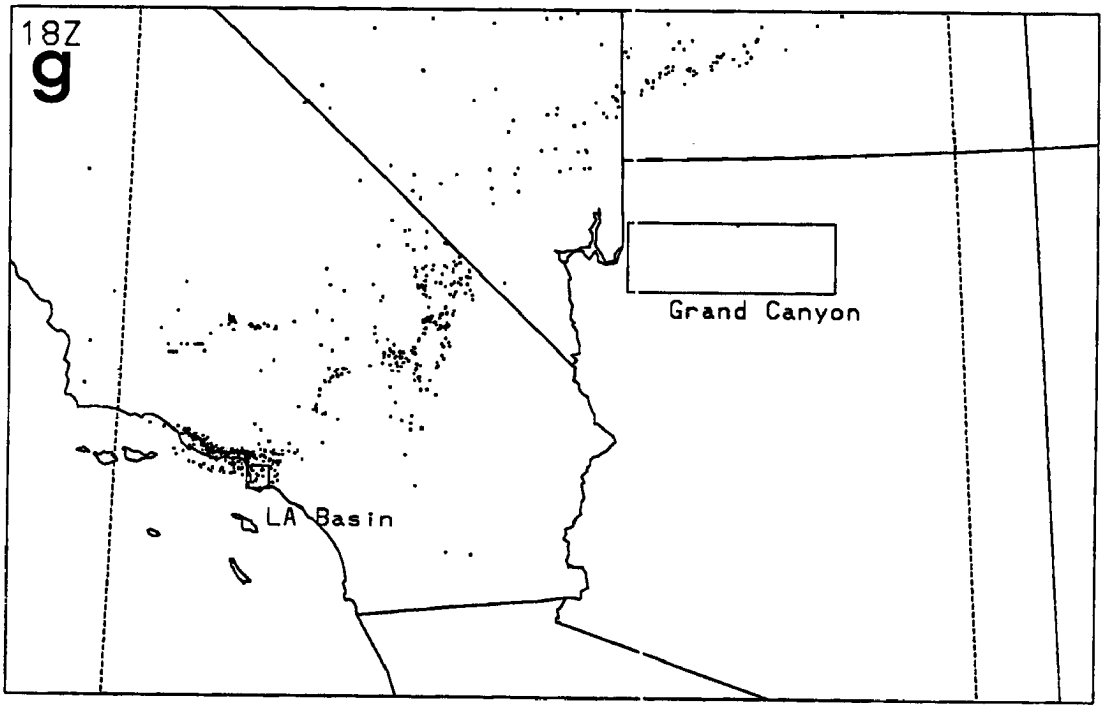

Figure 4.22: (g) 1800Z, hour 54.